AEDC-TR-82-10

1981 Calibration of the AEDC-PWT Aerodynamic Wind Tunnel (4T) at Mach Numbers from 0.1 to 1.3

Wallace Luchuk, Charles F. Anderson, and Melvin L. Homan
Calspan Field Services, Inc.

August 1982

Final Report for Period March 18 – 24, 1981

Approved for public release; distribution unlimited.

ARNOLD ENGINEERING DEVELOPMENT CENTER
ARNOLD AIR FORCE STATION, TENNESSEE
AIR FORCE SYSTEMS COMMAND
UNITED STATES AIR FORCE

NOTICES

When U. S. Government drawings, specifications, or other data are used for any purpose other than a definitely related Government procurement operation, the Government thereby incurs no responsibility nor any obligation whatsoever, and the fact that the government may have formulated, furnished, or in any way supplied the said drawings, specifications, or other data, is not to be regarded by implication or otherwise, or in any manner licensing the holder or any other person or corporation, or conveying any rights or permission to manufacture, use, or sell any patented invention that may in any way be related thereto.

Qualified users may obtain copies of this report from the Defense Technical Information Center.

References to named commercial products in this report are not to be considered in any sense as an endorsement of the product by the United States Air Force or the Government.

This report has been reviewed by the Office of Public Affairs (PA) and is releasable to the National Technical Information Service (NTIS). At NTIS, it will be available to the general public, including foreign nations.

APPROVAL STATEMENT

This report has been reviewed and approved.

P. G. BRYANT
Directorate of Aerospace Flight Dynamics Test
Deputy for Operations

Approved for publication:

FOR THE COMMANDER

JOHN M. RAMPY
Director of Aerospace Flight Dynamics Test
Deputy for Operations

REPORT DOCUMENTATION PAGE		READ INSTRUCTIONS BEFORE COMPLETING FORM
1. REPORT NUMBER AEDC-TR-82-10	2. GOVT ACCESSION NO.	3. RECIPIENT'S CATALOG NUMBER
4. TITLE (and Subtitle) 1981 CALIBRATION OF THE AEDC-PWT AERODYNAMIC WIND TUNNEL (4T) AT MACH NUMBERS FROM 0.1 TO 1.3		5. TYPE OF REPORT & PERIOD COVERED Final Report - March 18-24, 1981 6. PERFORMING ORG. REPORT NUMBER
7. AUTHOR(s) Wallace Luchuk, Charles F. Anderson, and Melvin L. Homan, Calspan Field Services, Inc.		8. CONTRACT OR GRANT NUMBER(s)
9. PERFORMING ORGANIZATION NAME AND ADDRESS Arnold Engineering Development Center/DOF Air Force Systems Command Arnold Air Force Station, TN 37389		10. PROGRAM ELEMENT, PROJECT, TASK AREA & WORK UNIT NUMBERS Program Element 65807F
11. CONTROLLING OFFICE NAME AND ADDRESS Arnold Engineering Development Center/DOS Air Force Systems Command Arnold Air Force Station, TN 37389		12. REPORT DATE August 1982 13. NUMBER OF PAGES 85
14. MONITORING AGENCY NAME & ADDRESS (if different from Controlling Office)		15. SECURITY CLASS. (of this report) UNCLASSIFIED 15a. DECLASSIFICATION/DOWNGRADING SCHEDULE N/A

16. DISTRIBUTION STATEMENT (of this Report)

Approved for public release; distribution unlimited.

17. DISTRIBUTION STATEMENT (of the abstract entered in Block 20, if different from Report)

18. SUPPLEMENTARY NOTES

Available in Defense Technical Information Center (DTIC).

19. KEY WORDS (Continue on reverse side if necessary and identify by block number)

calibration	least squares method
transonic wind tunnel	air flow
pressure transducers	honeycomb structures
static pressure	porosity

20. ABSTRACT (Continue on reverse side if necessary and identify by block number)

The Propulsion Wind Tunnel facility Aerodynamic Wind Tunnel (4T) has been recalibrated. Measurements of the tunnel centerline Mach number distributions and tunnel calibration parameter have been obtained over a Mach number range from 0.1 to 1.3. The bulk of the Mach number measurements was made at a total pressure of 1,200 psfa, with other measurements taken at pressures ranging from 600 to 3,100 at selected Mach numbers. Data were obtained

20. ABSTRACT (Continued)

for tunnel wall porosities of 4, 5, and 6 percent over the entire Mach number range and for wall porosities ranging from 1 to 7 percent at selected transonic Mach numbers. Results of previously obtained flow angularity measurements in the test section made over a Mach number range of 0.4 to 1.3 are presented. Effects of honeycomb geometry and asymmetric wall porosity on the mean flow angles and on the standard deviations in flow angles are also presented.

PREFACE

The work reported herein was conducted by the Arnold Engineering Development Center (AEDC), Air Force Systems Command (AFSC), under Program Element 65807F, Control Number 9T02. The program sponsor and user was AEDC/DOFO. The project monitor was Lt. Ron Hill, AEDC/DOFO. The results were obtained by Calspan Field Services, Inc., operating contractor for the aerospace flight dynamics testing effort at the AEDC, AFSC, Arnold Air Force Station, Tennessee. The test was conducted in the Aerodynamic Wind Tunnel (4T) during the period from 18 March to 24 March, 1981, under AEDC Project Number C355PB, PWT Test No. TC 709.

CONTENTS

ILLUSTRATIONS

Figure

Figure | Page

TABLES

APPENDIXES

1.0 INTRODUCTION

1.1 OBJECTIVES OF THE TEST PROGRAM

Wind tunnels require periodic calibrations as do other measurement systems. The frequency of wind tunnel calibrations is normally on the order of years unless there are indications in the test data that make the test flow conditions suspect.

The Aerodynamic Wind Tunnel (4T) of the Propulsion Wind Tunnel Facility (PWT) was put into operation in 1968. The tunnel Mach number was calibrated initially and after each major modification, as indicated by Refs. 1-4. Partial Mach number calibrations were also performed as part of various test programs; however, the last complete calibration with the sonic nozzle was performed in October 1969. During the interval since the last complete calibration there have been no apparent anomalies in the test data to suggest that a Mach number recalibration was necessary, yet there were a number of factors that prompted the subject calibration program. There have been a number of modifications in the stilling chamber (primarily the installation of a honeycomb) which have substantially reduced the test section flow angularity. These stilling chamber modifications could possibly have affected the test section Mach number distributions. Also, there have been significant improvements in tunnel instrumentation since 1969, and uncertainties in the measurement of tunnel operating parameters have been reduced. As a result of these more precise measurements, recent calibrations of the Propulsion Wind Tunnel (16T) have revealed a slight variation of the tunnel calibration parameter, DM, with unit Reynolds number (Ref. 5). A brief check for Reynolds number effects was included in a tunnel wall effects investigation, which indicated that there might be a similar Reynolds number effect in Tunnel 4T. Most of the previous complete calibration was obtained at a tunnel total pressure of 2,000 psfa; however, the increase in electrical power costs in recent years has caused most testing to be done at a total pressure of 1,200 psfa for Mach numbers 0.6 and above.

Considering these factors, it was decided to do a new Mach number calibration at a total pressure of 1,200 psfa for Mach numbers 0.6 and above. A check calibration was also done at a total pressure of 2,000 psfa for Mach numbers below 0.60. The effects of total pressure (Reynolds number) were investigated at selected Mach numbers. Data were also obtained on the effects of a new reflecting schlieren plate, installed on the north wall, on tunnel Mach number distributions.

Some previously unpublished flow angularity measurements in the test section that were obtained after the installation of a "one-piece" honeycomb in the stilling chamber are included in this report to present a more complete picture of the Tunnel 4T flow quality. In addition, a brief investigation of the effects of asymmetrical porosity distributions on flow angles is described.

2.0 APPARATUS

2.1 TEST FACILITY

The AEDC Aerodynamic Wind Tunnel (4T) is a closed-loop continuous flow, variable-density tunnel in which the Mach number can be varied from 0.1 to 1.3 and can be set at discrete Mach numbers of 1.6 and 1.96 by placing nozzle inserts over the permanent sonic nozzle. At all Mach numbers, the stagnation pressure can be varied from 300 to 3,400 psfa. The test section is 4-ft square and 12.5 ft long with perforated, variable-porosity (0.5- to 10-percent open) walls. It is completely enclosed in a plenum chamber from which air can be evacuated, allowing part of the tunnel airflow to be removed through the perforated walls of the test section. The model support system consists of a sector and sting attachment which has a pitch angle capability of -8 to 27 deg with respect to the tunnel centerline and a roll capability of -180 to 180 deg about the sting centerline. A more complete description of the tunnel may be found in Ref 6.

2.2 CALIBRATION EQUIPMENT

A centerline pipe extending through the nozzle and test region was used to determine the centerline Mach number distribution. The centerline pipe is supported by forward swept support struts attached to the nozzle walls at the upstream end and by the model support system at the downstream end. A pre-tension load of 11,000 lb was applied to the pipe by spring washers at the forward support struts. The centerline pipe has 100 orifices; however, only 67 orifices were used during the current calibration because only 100 pressure readout channels were available and some channels had to be reserved for other measurements. Details of the static pipe and test installation are presented in Figs. 1 and 2; orifice locations are listed in Table 1.

2.3 SCHLIEREN PLATE

A reflective plate with a Scotchgard®-coated surface used with a multiple slit schlieren system being developed for Tunnel 4T was installed on the north wall of the test section to determine the effects of the plate on the tunnel calibration and flow quality. Details of the plate are shown in Fig. 3.

2.4 PRESSURE INSTRUMENTATION

The centerline and wall static pressure measurements were obtained with 15-psi differential pressure transducers referenced to atmospheric pressure and recorded by a digital pressure measurement system. The tunnel total, plenum, and diffuser pressures were measured by precision absolute pressure transducers. Both the tunnel reference pressure system and the digital pressure system were recalibrated and the system uncertainties evaluated immediately after the tunnel calibration test.

2.5 FLOW ANGULARITY PROBE

A sensitive flow angularity probe has been in use at PWT for a several years. This probe consists of a 3-in.-span cruciform wing-body model installed on a 0.16-in.-diam, five-component force balance. The probe and balance are shown in Figs. 4 and 5. The design criterion for an ideal wind tunnel flow angularity probe is to provide full balance loading at a small angle of attack. In this way the maximum sensitivity and resolution of the force balance can be used. Although the present probe used an existing force balance with a substantial mismatch between the model's maximum normal force at 2-deg angle of attack and the balance's maximum normal force capability, the sensitivity of the probe was excellent (± 0.008 deg). To align the probe with the tunnel centerline to within ± 0.05 deg, a laser optical alignment device was built and used. The model was made of magnesium, which gave a model-balance natural frequency of about 180 Hz and permitted the determination of the dynamic variation in flow angularity of up to about 100 Hz. The high natural frequency and the very fast response of the force balance permitted taking flow angularity measurements while the probe was in motion traversing the test section (in a manner similar to the technique reported in Ref. 7). The five-component force balance had load ratings as follows: normal force and side force, ± 6.5 lb; pitching and yawing moments ± 3.25 in.-lb; and rolling moment ± 3.25 in.-lb. The sign convention used for the flow angularity measurements is presented in Appendix A.

2.6 CAPTIVE TRAJECTORY SYSTEM

The flow angularity probe was mounted on the Captive Trajectory Support (CTS), an electromechanical support system which provides six degrees of freedom of motion. This system provides horizontal and vertical translations of ± 15 in. from the tunnel centerline, an axial translation of 36 in., pitch and yaw angles of ± 45 deg from an axis parallel to the tunnel centerline, and a roll angle variation of ± 360 deg about the CTS head axis. This system was used with the flow angularity probe to scan various cross sections of the test section. A photograph of the flow angularity probe installed on the CTS is presented in Fig. 6. Further details on the CTS and its use in supporting the flow angularity probe and in providing lateral traverses may be found in Refs. 6 and 7.

3.0 PROCEDURE

3.1 CENTERLINE MACH NUMBER TEST PROCEDURE

The centerline Mach number calibration was conducted over a Mach number range from 0.1 to 1.3. Primary emphasis was placed on obtaining calibrations at the normal operating total pressures of 2,000 psfa for Mach numbers less than 0.60 and at 1,200 psfa for Mach numbers equal to or greater than 0.60. The effects of Reynolds number on the tunnel calibrations were evaluated at Mach numbers above 0.6 by varying total pressure at selected Mach numbers. The tunnel wall porosity was varied one percent above and below the standard Tunnel 4T porosity schedules (see Appendix B) and additionally at selected Mach numbers. The tunnel top and bottom wall angles were set to 0 deg (walls parallel) for the entire centerline Mach number calibration program, since previous experience had shown that the small improvement in the Mach number distribution (reported in Ref. 2) did not warrant the extra test time (and costs) required to conduct testing at the optimum wall angle.

At subsonic Mach numbers, the tunnel pressure ratio was adjusted to give the desired Mach number over the test region. At supersonic Mach numbers, the pressure ratio was set at a value above a preestablished minimum and the Mach number was controlled by plenum chamber suction. Figure 7 presents the minimum pressure ratio (λ) as a function of Mach number. The minimum pressure ratios shown in Fig. 7 are higher than those presented in Ref. 2 because the location of the diffuser static pressure orifice ring has been moved upstream since the calibration reported in Ref. 2.

The test procedure for obtaining an average centerline Mach number was to set the tunnel conditions and to take five consecutive data points. The average Mach number was determined for each data point over the designated test section length, then these five average Mach numbers were again averaged to give the final average.

It should be noted that the previous calibrations considered the test section to extend downstream to Station 140. However, experience has shown that test models rarely extend aft to Station 130. Therefore, the test region was assumed to extend from Station 72 to Station 130 only, and the centerline Mach numbers were averaged over this distance. Another reason for reducing the rear extent of the test section is that if the tunnel is operated at other than the optimum pressure ratio at Mach numbers between 0.85 and 1.00, there will be a significant expansion or compression after Tunnel Station 134 (similar to that presented in Ref. 5).

3.2 FLOW ANGULARITY TEST PROCEDURE

The flow angularity tests consisted of calibration of the probe and measurement of the flow angularities. The data reduction associated with the calibrations of the probe was done "online" so that the determination of the probe characteristics and the various checks on its performance were completed before test section flow angle measurements were started. Calibration of the probe is essentially the same as reported in Ref. 7 for a single plane probe. However, both planes of the 3-in.-span probe were calibrated in the vertical plane of the wind tunnel so that the local flow angle (in the vertical plane) as determined from the two calibrations of the probe (upwash and sidewash planes) could be compared. These two local flow angles at the calibration location were called NUP and NUY for pitch and yaw planes of the probe, respectively. Probe calibrations consisted of performing pitch traverses in both the upright and inverted positions for the upwash plane of the probe and at ±90 deg roll positions for the sidewash plane of the probe at each Mach number.

Flow angularity measurements were taken over 28- by 28-in. cross sections of the test section at grid points spaced 2 in. apart. This was done by a series of 15 horizontal traverses spaced 2 in. apart in the vertical plane of the tunnel. Fifteen data points were taken at 2-in. invervals during these traverses while the probe was moving at approximately 1-½ in./sec. The probe was stopped at the end (or beginning) of each horizontal traverse and a new set of readings of the tunnel operating conditions was obtained. The tunnel operating conditions were assumed to be constant during the horizontal traverses between the end points. This procedure permitted the scanning of the 28- by 28-in. cross section in about 6 min with 225 values of upwash and sidewash angles being obtained.

The calibration data were reduced by a linear least-squares fit to the normal-force coefficient (and side-force coefficient) versus pitch angle data for both the upright and inverted traverses. The fitted linear coefficients were then used to obtain the sensitivity C_{N_α} (or C_{Y_β}), the zero shifts or asymmetry of the probe, C_{N_0} (or C_{Y_0}). and the local flow angle, NUP (or NUY). The procedure is illustrated in Appendix C. The results of a typical calibration are presented in Fig. 8. Figure 8a presents the force coefficient slopes, C_{N_α} (CNALFA) and C_{Y_β} (CYBETA), as a function of Mach number. Noteworthy is the excellent agreement between the pitch and yaw characteristics. Presented in Fig. 8b is the RMS value of the residuals of the least-squares fits of lines to both the C_N and C_Y data converted to equivalent angles. The RMS value of the residuals which represent the resolution of the probe was excellent. Improved resolution could be achieved if the probe and balance were better matched (or used at much higher dynamic pressures). The resolution of the probe from Fig. 8b was about ±0.008 deg over the entire Mach number range. Another significant characteristic of the probe is presented in Fig. 8c, where the asymmetries have been converted to equivalent angles by dividing the asymmetry in coefficient form (C_{N_0} or C_{Y_0}) by

its respective coefficient slope (C_{N_α} or C_{Y_β}). The asymmetries, indicative of misalignment of the fins with respect to the body or a slight bend in the body itself, are acceptably small when one considers the small size of the probe, and should be independent of Mach number. One last check on the efficiency of the probe is presented in Fig. 8d, where the local flow angles in the vertical plans as determined by the calibrations of the pitch (or upwash) plane of the probe, NUP, and as determined by the calibrations of the yaw (or sidewash) plane of the probe, (NUY), are plotted as a function of Mach number. These two measured angles show reasonable agreement with each other.

3.3 FLOW QUALITY CRITERIA

Desirable standards for the test section Mach number flow quality were considered to be a gradient in Mach number of less than one-half percent over a length of 48 in. (or equal to the test section height), a spatial uniformity in Mach number of less than one-half percent over the test section length, a mean flow angle of under 0.1 deg in both the horizontal and vertical planes, and a uniformity in flow angle of less than ± 0.05 deg over the entire test section. Some of these standards are rather severe; however, they should satisfy the most demanding test program a user could request. As it turns out, most of these standards were met, as will be shown in the subsequent presentation of the test results.

A flow quality standard for Mach number uniformity was suggested in an earlier calibration study and included in Ref. 8. This suggested standard proposed a standard deviation of 0.0025M for subsonic flow and 0.005M for supersonic flow. The standard considered here for Mach number uniformity coincides with that of the earlier study for supersonic flow and is twice that of the earlier study for subsonic flow.

3.4 DATA REDUCTION AND UNCERTAINTIES

3.4.1 Data Reduction

The plenum chamber Mach number was computed using the isentropic relationship between the plenum chamber pressure (PC) and the tunnel total pressure (PT)

$$MC = \sqrt{\left(\frac{2}{\gamma-1}\right)\left[\left(\frac{PC}{PT}\right)^{\frac{-\gamma-1}{\gamma}} - 1\right]} \qquad (1)$$

The local Mach number on the calibration pipe (MBX) was also computed using the isentropic relationship between the local static pressure (PLX) and PT

$$MBX = \sqrt{\left(\frac{2}{\gamma-1}\right)\left[\left(\frac{PLX}{PT}\right)^{\frac{-\gamma-1}{\gamma}} - 1\right]} \tag{2}$$

The average Mach number in the test section was calculated from

$$MA = \frac{1}{n} \sum_{X=72}^{X=130} MBX$$

The tunnel calibration factor is defined as:

$$DM = MA - MC$$

The upwash and sidewash angles are determined from the following equations:

$$UPWASH = \frac{C_{N_0} - C_N}{C_{N_\alpha}} - \alpha_i \tag{3}$$

$$SIDEWASH = \frac{C_{Y_0} - C_Y}{C_{Y_\beta}} - \beta_i$$

3.4.2 Uncertainty of Measurements

Uncertainties (combinations of systematic and random errors) of the basic tunnel instrumentation were estimated from repeat calibration of the systems against secondary standards whose uncertainties are traceable to the National Bureau of Standards calibration equipment. The instrument uncertainties, for a 95-percent confidence level, were combined using the Taylor series method of error propagation described in Ref. 9 to determine the uncertainties of the tunnel parameters MC, MAV, and DM which are shown in Fig. 9.

The uncertainties presented in Fig. 9 are those associated with the tunnel instrumentation system and do not include axial variations of the Mach number along the tunnel centerline or the errors introduced through tunnel total pressure variations during the data acquisition cycle.

Uncertainty in flow angle measurements has been estimated to be approximately ±0.05 deg, most of the error being in model alignment with the tunnel axis.

4.0 RESULTS AND DISCUSSION

4.1 CENTERLINE MACH NUMBER DISTRIBUTIONS

Some of the centerline Mach number measurements are presented in Figs. 10 and 11 in which the local Mach number on the calibration pipe is plotted versus axial station with other tunnel variables as parameters. The Mach number distributions for fixed values of the wall porosities are shown in Fig. 10. The Mach number distributions for various tunnel total pressures are shown in Fig. 11.

Least-squares lines were fitted to the data of Figs. 10 and 11 using only the data corresponding to the range of tunnel stations from 72 to 130. The results of these fits are presented in Table 2 in which MLXO is the intercept and represents the Mach number at station X = 0; DML/DX is the Mach number gradient, and SIGMAM is the standard deviation of the fit. These fits were done to determine if gradients (however small) were present in the distribution. In the past, standard deviations were obtained about the mean test section Mach number and no consideration was given to the effect of gradients on the standard deviations. In most cases the gradients were found to be small and the differences between the two types of standard deviations were negligible.

Some of the results in Table 2 are presented in Figs. 12, 13, and 14. The centerline Mach number gradients, DML/DX versus MC for constant porosities, are shown in Fig. 12. The standard deviation (SIGMAM) as a function of porosity for constant Mach numbers is presented in Fig. 13. A standard deviation of one-half percent of the free-stream Mach number is plotted as a constant dashed line when it is within the scale of the graph. As seen in Fig. 13, there is little effect of porosity on the standard deviations at Mach numbers up to about 0.8, but there is a great effect of porosity at the higher Mach numbers. Also, it appears that the optimum porosity with respect to SIGMAM is about 5 percent at the higher Mach numbers. The standard deviation (SIGMAM) versus Mach number for constant values of porosity is shown in Fig. 14. Also shown in Fig. 14 is a line which represents one-half percent of the local Mach number. Figure 14 shows that in virtually all of the test conditions, the nonuniformity as represented by SIGMAM is within one-half percent of the Mach number. An interesting thing to note in Fig. 14 is the dip in all the curves that occurs around Mach number 1.0. This dip indicates that the centerline Mach number distributions tend to become more uniform at M = 1.0. This effect appears to be more pronounced at the lower porosities. No explanation for this effect can be offered at this time.

The Mach number gradients for the two porosity schedules (Appendix B) are presented as a function of Mach number in Fig. 15. Dashed lines indicating gradients of ± ½ percent change in Mach number over a 48-in. model length are also plotted in Fig. 15. It is evident from Fig. 15 that the Mach number gradients are within these standards except at the extreme Mach numbers.

The standard deviations in centerline Mach number are presented in Fig. 16 for the two operating porosity schedules. A line representing a standard deviation in Mach number of one-half percent is also plotted. Examination of Fig. 16 shows that the standard deviation at all operating porosities is within ± ½ percent, except at M = 0.10. The results presented in Figs. 15 and 16 reveal that the uniformity of the flow for most operating conditions is excellent. Further improvements in the Mach number distributions do not seem warranted, except at M = 1.30. The data of Figs. 12 through 13 also show that there is considerable latitude for operating off the existing porosity schedules and still maintaining good quality air flow. Finally, the data presented in Fig. 11 show that there are little effects of total pressure (or Reynolds number) on the centerline Mach number distributions. The subsonic variations in SIGMAM with total pressure presented in Fig. 13 *probably* reflect a pressure measurement uncertainty rather than a variation attributable to total pressure because there appears to be a systematic reduction in SIGMAM with increasing total pressure. The supersonic variations in SIGMAM with total pressure probably indicate a worsening of the distributions because no systematic variation with the pressure is evident.

4.2 TUNNEL CALIBRATION PARAMETER, DM

Another aspect of the calibration of the transonic wind tunnel is determining the tunnel calibration factor (DM) defined in Section 3.4.1. During normal tunnel operations, the plenum chamber Mach number (MC) is computed first and then DM is determined from the calibration equation (Table 3) for the specific operating conditions. Finally the free-stream Mach number is calculated from MA = MC + DM. So the determination and description of the variation of DM with all of the tunnel variables is an essential part of the tunnel calibration. A list of the tunnel operating variables includes MC, the wall porosity (τ), the test section wall angle (θ_w), the tunnel total pressure (PT), the tunnel pressure ratio (λ), and the diffuser flap position. Past tunnel calibrations and wall interference studies have shown that the wall angle should always be set at 0 deg. Therefore, the effects of θ_w were not studied during this program. Also, λ (which is the major factor in setting Mach numbers), PT, and flap setting have been demonstrated to have little effect on the Mach number distributions. The effects of flap setting can be seen only aft of Station 130 (Ref. 3). The variables, MC and τ, have the most pronounced influence on the Mach number distributions and DM. Their effects are presented in Fig. 17 where the values of DM (averaged for each run) are plotted versus MC for constant porosities.

Once the values of DM were obtained, the next problem was to determine a mathematical expression which satisfactory describes DM as a function of MC and τ. Previous calibrations (Ref. 2 and 3) have used fifth-power polynomials in both MC and τ and their cross-products whose exponents add up to five or less. Examination of the test data indicated a high degree of linearity of DM with τ at each Mach number. Examination of Fig. 17 shows that there could be as many as nine inflection points in the data, thus suggesting a tenth-power polynomial in MC. Various polynomials up to and including a tenth-power polynomial were fitted to the test data by the method of Ref. 10. None of the selected polynomials produced a fit with a standard error of estimate (RMS value of the residuals) which are considered acceptable. Therefore, it was decided to use the same fifth-order polynomial of Refs. 2 and 3 to divide the data into two Mach number ranges. One set of data covered the Mach number range from 0.10 to 0.95, and the second set covered the Mach number range from 0.95 to 1.30. The results of the two fits are presented in Table 3 and are plotted along with the test data in Fig. 17.

The effect of tunnel total pressure on the calibration parameter DM was examined but the results were not definitive, although there appeared to be a small effect below a Mach number of 0.60. Further, more precise measurements need to be taken to establish a firm relationship between PT and DM below Mach number 0.60.

4.3 FLOW ANGULARITY MEASUREMENTS

Flow angularity measurements using a winged model on a force balance have been made in Tunnel 4T since 1975 (Ref. 7). The winged model has evolved to the cruciform shape shown in Figs. 4 and 5 and the balance that was used approaches the limit regarding smallness and load ratings.

The first test to determine the flow angularity characteristics over a substantial cross section of the tunnel was done in 1977 after a honeycomb was first installed in the stilling chamber. These results showed that the standard deviation in both upwash and sidewash angles over a 28- by 28-in. cross section was about ± 0.15 deg. However, the detailed measurements (taken over a 2-in. grid spacing) showed that there was a high quality core flow (with a standard deviation of about ± 0.05 deg) in the center of the tunnel and a pattern of flow angle perturbations about this core which resembled the pattern of honeycomb panels in the stilling chamber. It appeared that the honeycomb panels produced a very uniform test section flow, but the support framing and panel edge treatment caused substantial disturbances in the test section airflow. Some typical measurements of the flow angularity in the test section at Station 108, at a Mach number of 1.20 and a total pressure of 2,001 psfa are presented in Fig. 18. In Fig. 18, the upwash and sidewash vectors have been added vectorially to give a resultant vector at each grid point. This was done to give a better pictorial representation of the flow angularity. The arrow in the legend represents one degree

of sidewash. Note the uniform core between vertical distances of ± 8 in. and lateral distances of ± 10 in. from the centerline. A photograph of a portion of the built-up honeycomb which shows the framing arrangement and the honeycomb panels is shown in Fig. 19. Note the resemblance between the flow angularity perturbations of Fig. 19 and the panel geometry of Fig. 19.

Late in 1980, a new "one-piece" honeycomb was made and installed in place of the "built-up" honeycomb. The new honeycomb was made up of an 8- by 8-ft central piece surrounded by circular arc segments to make up the 14-ft-diam circle of the stilling chamber. The new honeycomb was 6 in. thick with ¼-in. hexagonal cells. The cell wall thickness was only 0.003 in., thus providing a blockage of less than 5 percent. The honeycomb segments were bonded together using a core splice adhesive type FM41 manufactured by the American Cynamid Co. The bonding reduced the blockage at the panel boundaries from more than 1 in. for the built-up honeycomb to ¼ in. or 1 cell width. The new honeycomb was attached to the stilling chamber structure only along its circumference. A photograph of the "one-piece" honeycomb under construction is presented in Fig. 20, and the installed honeycomb is evident in the background of Fig. 2b. Periodic inspections of the newly installed "one-piece" honeycomb have indicated no mechanical or structural faults. The installation appears to be totally sound with no apparent deterioration in the cemented joints.

The results of flow angularity measurements taken after the installation of the "one-piece" honeycomb are presented in Table 4. The main point of interest of the latest measurements was whether the "one-piece" honeycomb produced a more random flow angularity picture or a picture devoid of the pattern of framing of the old honeycomb and a more uniform flow. The answer to this question may be seen in Fig. 21, where the flow angularity is presented for a typical operating condition. The flow angularity appears to be mostly random in the upper south corner with a slight outflow in the lower north corner. When the mean upwash and sidewash vectors are subtracted from each of the local upwash and sidewash vectors and the differences are plotted as presented in Fig. 22, the randomness of the flow pattern is fully revealed. Although the mean upwash and sidewash vectors have been reduced to zero algebraically, the same effect can be realized by optimizing the wall porosities, as will be discussed later. Examination of Figs. 21 and 22 reveals that the pattern of the framing of the old honeycomb has been eliminated. The overall quality of the flow with the new honeycomb is demonstrated in Fig. 23, where the averaged flow angles and the standard deviations are plotted against tunnel Mach number. The results of the previous test (during which the built-up honeycomb was installed in the stilling chamber) are included in the figures to demonstrate the beneficial effects of the new honeycomb. As shown in Fig. 23a, the average upwash has remained about the same for all Mach numbers except 1.30. However, the average sidewash has increased somewhat. Figure 23b shows that the standard

deviations have been reduced by a factor of two or better except for the standard deviation in upwash at M = 1.2 or 1.3. If a single number is to be considered representative of the overall nonuniformity of the tunnel in flow angle, it would be the mean standard deviation for both upwash and sidewash over the entire Mach number range. For the latest tests this mean nonuniformity is ±0.0729 deg (at PT = 1,200 psfa) compared to ±0.1544 deg for the previous test with the "built-up" honeycomb (at PT = 2,000 psfa). Further, if the nonuniformity is evaluated only over a 25-in.-diam circle centered on the tunnel centerline, then the present overall mean nonuniformity would drop to only ±0.0584 deg.

Mentioned above was the increase in upwash standard deviation at M = 1.2 and 1.3. Examination of the flow angularity distributions at these two Mach numbers (Figs. 24 and 25) shows relatively uniform perturbation in downwash across the top four inches. The uniformity of these perturbations suggests a compression wave from the top wall or an expansion wave from the lower wall. Reexamination of the flow angularity pattern at M = 1.2 for the earlier test with the built-up honeycomb (Fig. 18) clearly shows that the downwash pattern across the top of the survey region was present before the new honeycomb was installed. It is this perturbation in downwash at these Mach numbers that causes the upturn in the upwash standard deviation curve of Fig. 23. To get some idea of the strength of the wave in terms of Mach number change associated with this wave, the rate of change of expansion angle with Mach number is 24.5 deg at M = 1.2. Dividing the magnitude of the flow angle change attributable to the postulated wave by 24.5 gives a Mach number change of 0.0061 associated with the wave.

The effect of total pressure on the flow angularity parameters is presented in Fig. 26. Both mean flow angle parameters appear to grow in magnitude with increasing total pressure, although there does not seem to be any significant change in the standard deviations with total pressure. The variation in the flow angularity parameters with tunnel station is presented in Fig. 27. The average sidewash appears to remain constant with increasing tunnel station while the upwash appears to decrease. Both standard deviations appear to decrease aft of Station 91.

4.4 ASYMMETRIC POROSITY EFFECTS

Flow angularity measurements have shown that: (1) the mean flow angles may be changed or reduced through the use of asymmetric porosity; (2) asymmetric porosity changes appear to cause the flow angles to change uniformly across the entire test section; and (3) there is very little interaction between porosity changes on one opposing pair of walls and the flow angles in the plane controlled by the other pair of opposing walls. A

demonstration of the effects of asymmetric porosity in the top and bottom walls using test data taken with the framed honeycomb is shown in Fig. 28. These plots show the effects of different or opposing asymmetric porosities. Examination of the upwash angles for the two flow angularity plots in Fig. 28 shows substantial variation in all of the upwash angles but no variation in the sidewash angles. A better indication of the independence of the upwash and sidewash effects is given in Fig. 29. In this figure, the average upwash, average sidewash, and the standard deviations in flow angle are plotted versus the porosity of one of the pairs of walls. The top wall porosity is used as the reference for the horizontal walls and the north wall porosity is the referenced wall for the vertical walls. The porosity for each of the two unreferenced walls was always set equal to 10 percent minus the porosity of the referenced wall. Thus, the mean porosity of the pair was 5 percent. The left-hand plots present the effects of asymmetric horizontal wall porosity variations, while the right-hand plots present the effects of asymmetric vertical wall porosity variations. The upper left-hand plot shows that as the top and bottom walls were varied asymmetrically, the average upwash varied in a linear manner while the average sidewash was hardly affected. When the sidewash porosities were varied asymmetrically (upper right plot), the average sidewash angles changed in a linear fashion, while the average upwash angles showed very little change. In all cases, the standard deviations in both upwash and sidewash angles were hardly affected. The standard deviations in flow angle appear to be independent of the wall porosity configuration and appear to be related to stilling chamber flow quality. When a set of flow angularity measurements is modified by subtracting the mean flow angle from each of the flow angle vectors in the scanned array, the result is the pattern of nonuniformity in flow angles. When this procedure was followed for data taken for various wall porosity configurations, the resulting pattern of nonniformity in upwash and sidewash was always the same (to the degree of experimental accuracy). This result indicated that asymmetric porosity changed the local flow angles uniformly across the entire scanned region and very likely from wall to wall.

The variation in mean flow angles with asymmetric porosity changes for various Mach numbers is presented in Fig. 30. The slopes of these curves, namely the change in flow angle per percent of asymmetric wall porosity defined herein as the flow angle compliance, are plotted in Fig. 31 versus Mach number. The slopes were determined by fitting least-squares lines to the data represented in Fig. 30. The results of the fits are also presented in Table 5. The compliance curves for the vertical and horizontal planes (top and north walls) are in approximate agreement with each other, which indicates that the effective porosities of the pairs of walls are nearly the same. No explanation can be offered at this time as to the functional relationship of the compliances with Mach number.

4.5 EFFECTS OF THE SCHLIEREN PLATE INSTALLATION

The centerline Mach number distributions at selected Mach numbers with and without the schlieren plate installed are presented in Figs. 32a-f. At subsonic Mach numbers, the schlieren plate had no effect on the Mach number distribution. The locations at the tunnel centerline of the bow shock from the leading edge of the plate, and the expansion wave generated by the step at the rear of the plate at MA > 1 were estimated using Mach angles. The estimated location of the schlieren plate bow shock is identified in Figs. 32d, e, and f by 1 while the estimated location of the expansion wave from the end of the plate is identified by 2. A small variation in Mach number distribution can be detected at Mach numbers above 1.05 at the predicted centerline location of the bow wave from the schlieren plate. A larger variation in Mach number distribution at the predicted centerline expansion wave location at M = 1.05 was detected. At higher Mach numbers, the centerline location of the expansion wave is aft of the instrumented section of the centerline pipe. The disturbance produced by the bow shock at the tunnel cneterline is less than the normal axial centerline Mach number variations, and the expansion fan is aft of the calibrated region of the test section. Therefore, it is concluded that the schlieren plate had no significant effects on either the tunnel calibration or the flow quality at any Mach number tested.

5.0 CONCLUSIONS

The current centerline Mach number distributions have confirmed the high quality distributions that were demonstrated in earlier calibrations. The centerline Mach number gradients are very small, as are the spatial nonuniformities in Mach number. One unexplained phenomenon noted in the data was that around Mach number 1.0, the flow on the centerline appears to become more uniform. Future calibrations of transonic wind tunnels should be concerned with further substantiation of this characteristic.

The present honeycomb provides very low nonuniformity in flow angularity. The very low standard deviations in flow angularity and the low standard deviations in Mach number demonstrate that the Tunnel 4T test section air flow is an excellent environment for all types of aerodynamic teting, including captive trajectory testing.
Testing

The flow angularity measurements that have been presented appear to be the most detailed and most accurate measurements of this type available in the open literature. The high sensitivity and fast response of the 3-in.-span flow angularity probe make it one of the best operational instruments available. Other facilities should be encouraged to use it (or duplicate it) so that meaningful comparisons with the flow angularity of other wind tunnels may be made.

The effects of the schlieren plate on the centerline Mach number distributions have been shown to be negligible.

The effects of tunnel total pressure on the centerline Mach number distributions have also been shown to be negligible. The effect of total pressure on the tunnel calibration parameter, DM, was not adequately defined by the data. Generally, there appeared to be no effect above Mach number of 0.60, and below Mach number 0.60, the data were too scattered to define a meaningful relationship.

The effect of the diffuser flap position on the centerline Mach number distributions was not evident over the normal test section length; therefore, none of this data was presented. There was a small effect of flap position on the centerline Mach number distributions aft of the test section at Mach numbers from 0.80 to 1.0.

REFERENCES

1. Hartley, M.S and Jacocks, J. L. "Initial Calibration Results from the AEDC-PWT 4-Foot Transonic Tunnel." AEDC-TR-68-141 (AD837078), August 1968.

2. Jacocks, J. L. and Hartley, M. S. "Calibration of the AEDC-PWT 4-Ft Transonic Tunnel with Modified Walls." AEDC-TR-69-134 (AD853841), June 1969.

3. Gunn, J. A. "Calibration of the AEDC-PWT Aerodynamic Wind Tunnel (4T) Using Diffuser Flap Plenum Suction." AEDC-TR-70-74 (AD867975), April 1970.

4. Gunn, J. A. and Maxwell, H. "Calibration of the AEDC-PWT Aerodynamic Wind Tunnel (4T) Mach Numbers 1.6 and 2.0 Nozzle Blocks." AEDC-TR-72-111 (AD749513), September 1972.

5. Jackson, F. M. "Calibration of the AEDC-PWT 16-Ft Transonic Tunnel with the Propulsion Test Section at Various Reynolds Numbers." AEDC-TR-77-121 (AD-A057877), August 1978.

6. *Test Facilities Handbook* (Eleventh Edition). "Propulsion Wind Tunnel Facility, Vol. 4." Arnold Engineering Development Center, June 1979.

7. Maxwell, H., and Luchuk, W. "Evaluation of a Wedge on a Force Balance as a Flow Angle Probe." AEDC-TR-74-110 (AD-A004765), February 1975.

8. Reed, T. D., Pope, T. C., and Cooksey, J. M. "Calibration of Transonic and Supersonic Wind Tunnels." NASA Contractor Report 2920, Vought Corporation, Dallas, TX, November 1977.

9. Abernethy, R. B. and Thompson, J. W., Jr. "Handbook — Uncertainty in Gas Turbine Measurements." AEDC-TR-73-5 (AD755356), February 1973.

10. Stein, Robert E., Jr. "Multiple Regression Analysis Program for the Aerodynamic Coefficient Analysis System." MSC Program No. 6097, prepared by Lockheed Electronics Company, Inc., Houston Aerospace Systems Division, Houston, TX, for NASA Manned Spacecraft Center, Houston, TX, January 1973.

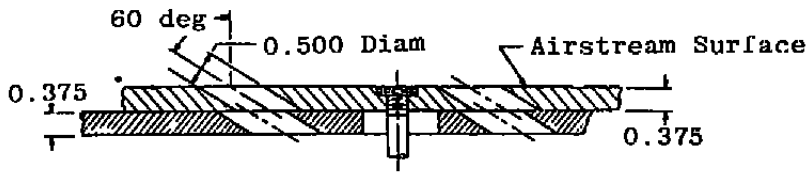

Typical Perforated Wall Cross Section

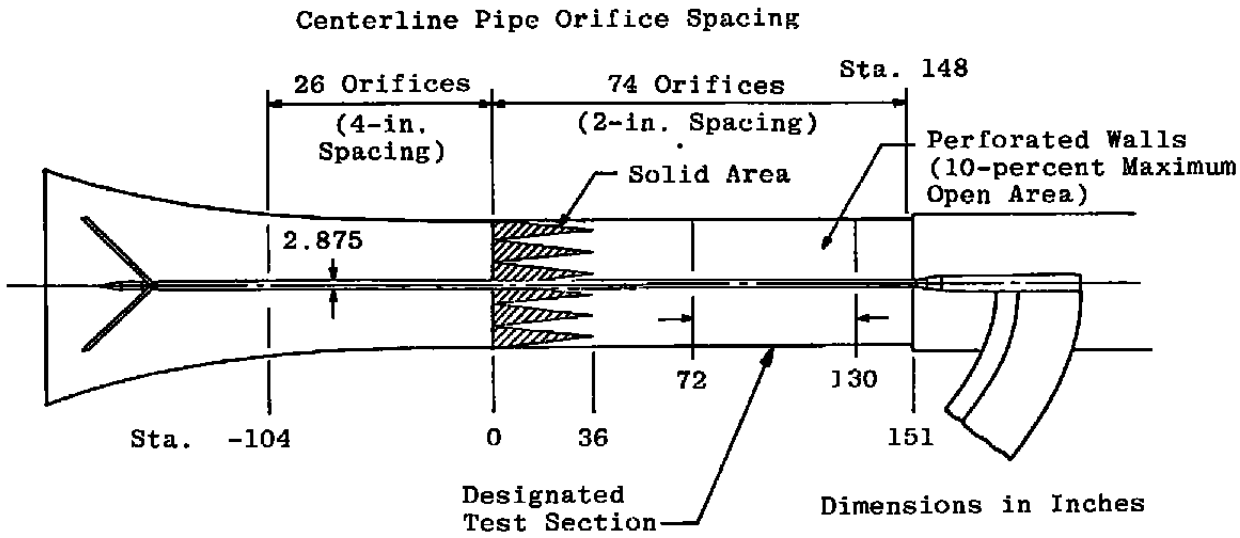

Figure 1. Tunnel installation of the centerline calibration pipe.

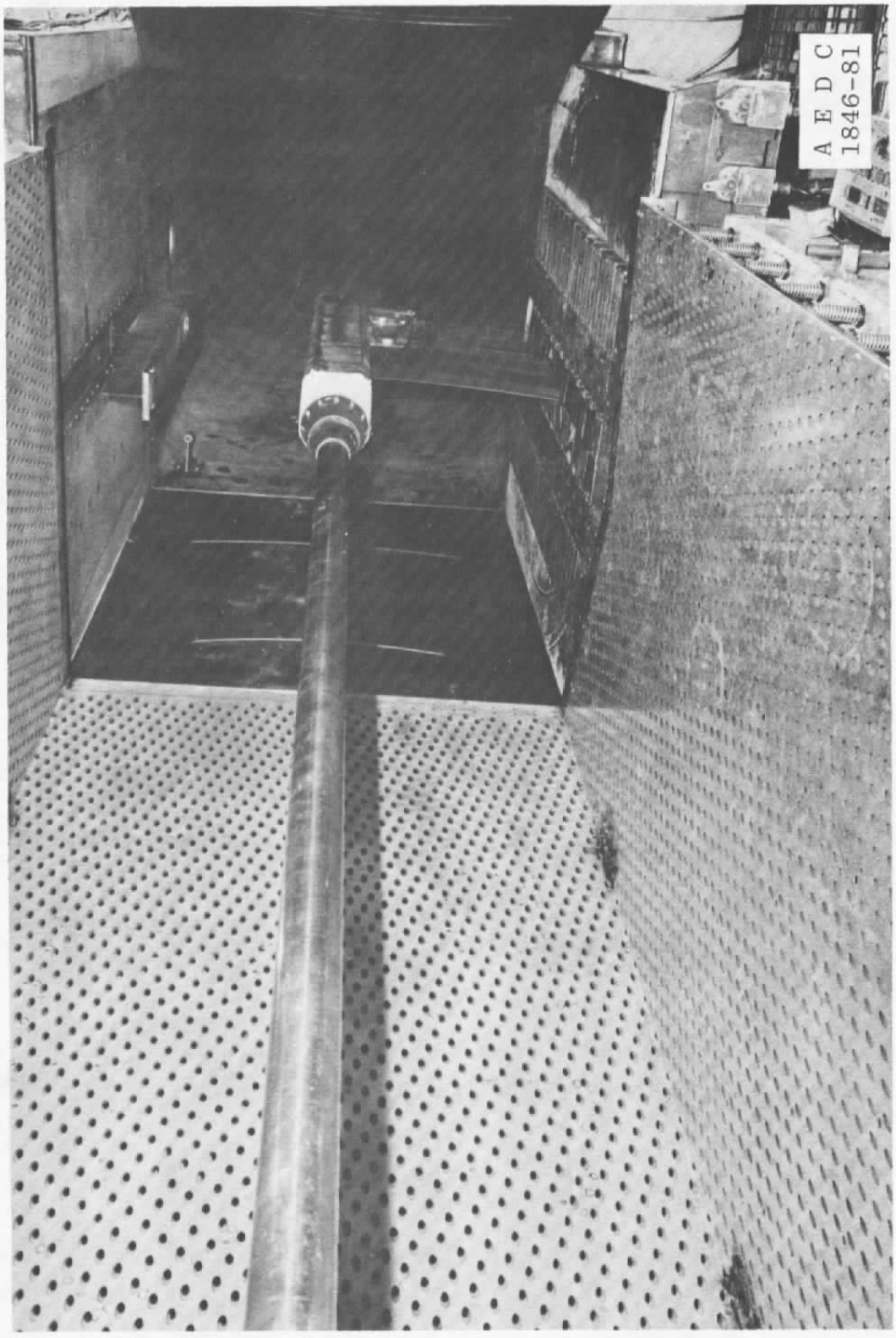

a. Test section view

Figure 2. Photographs of the centerline calibration pipe.

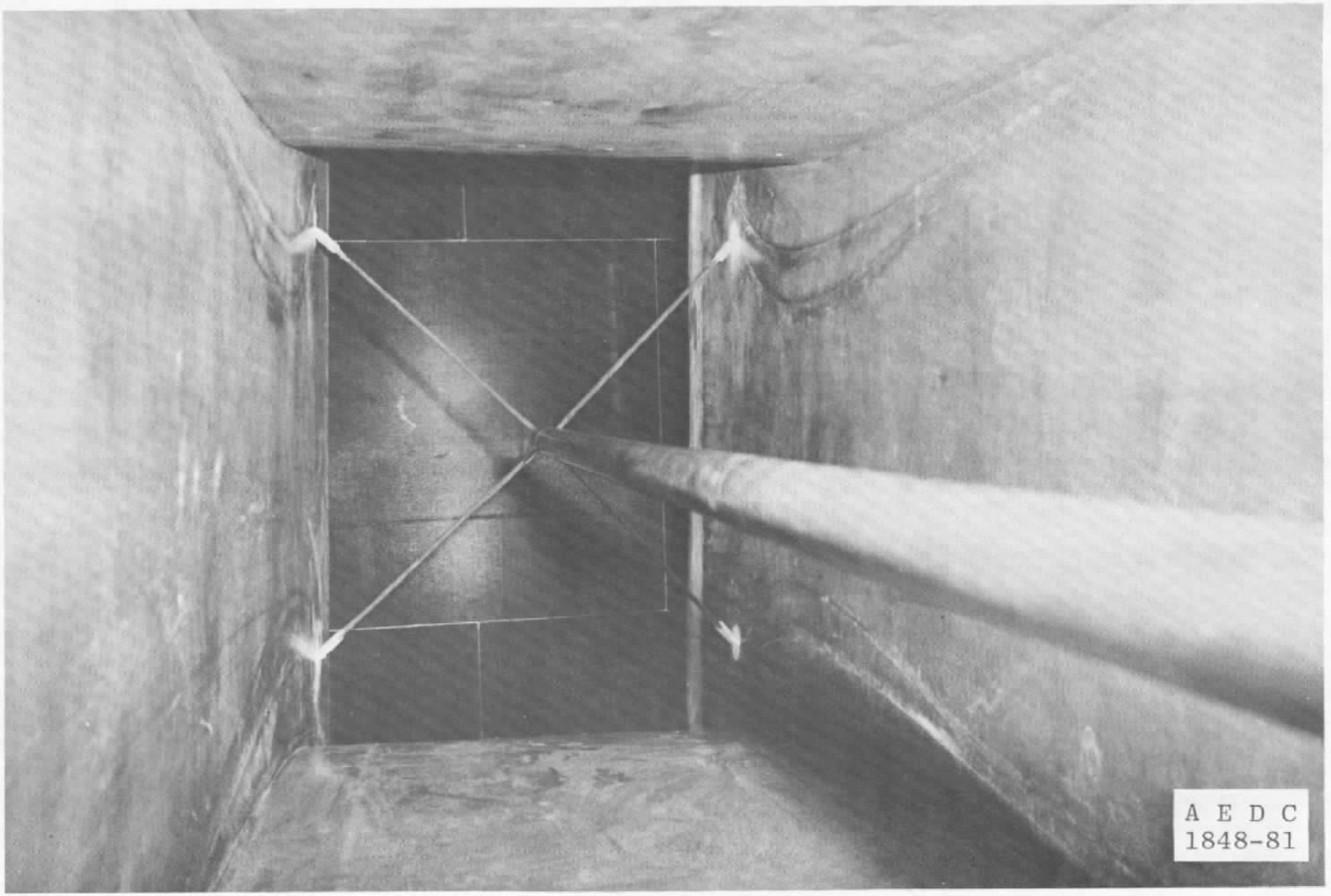

b. Upstream view
Figure 2. Concluded.

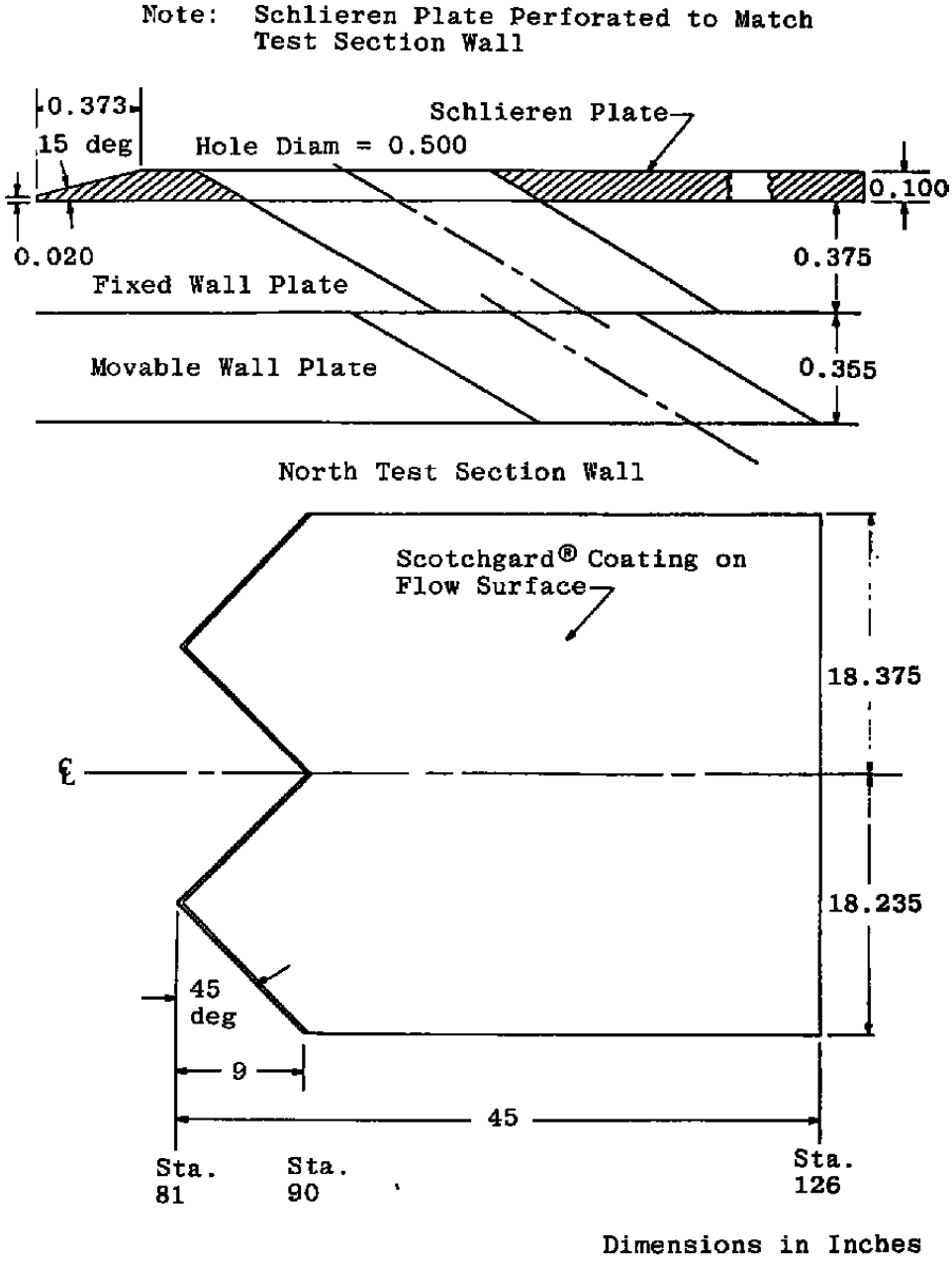

Figure 3. Schlieren plate details.

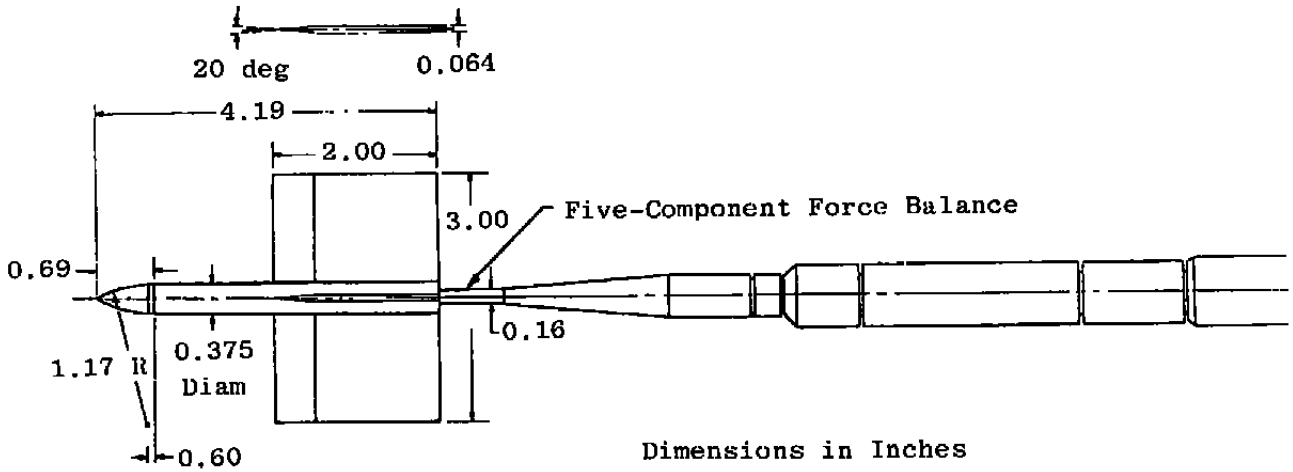

Figure 4. 3-in.-span flow angularity probe.

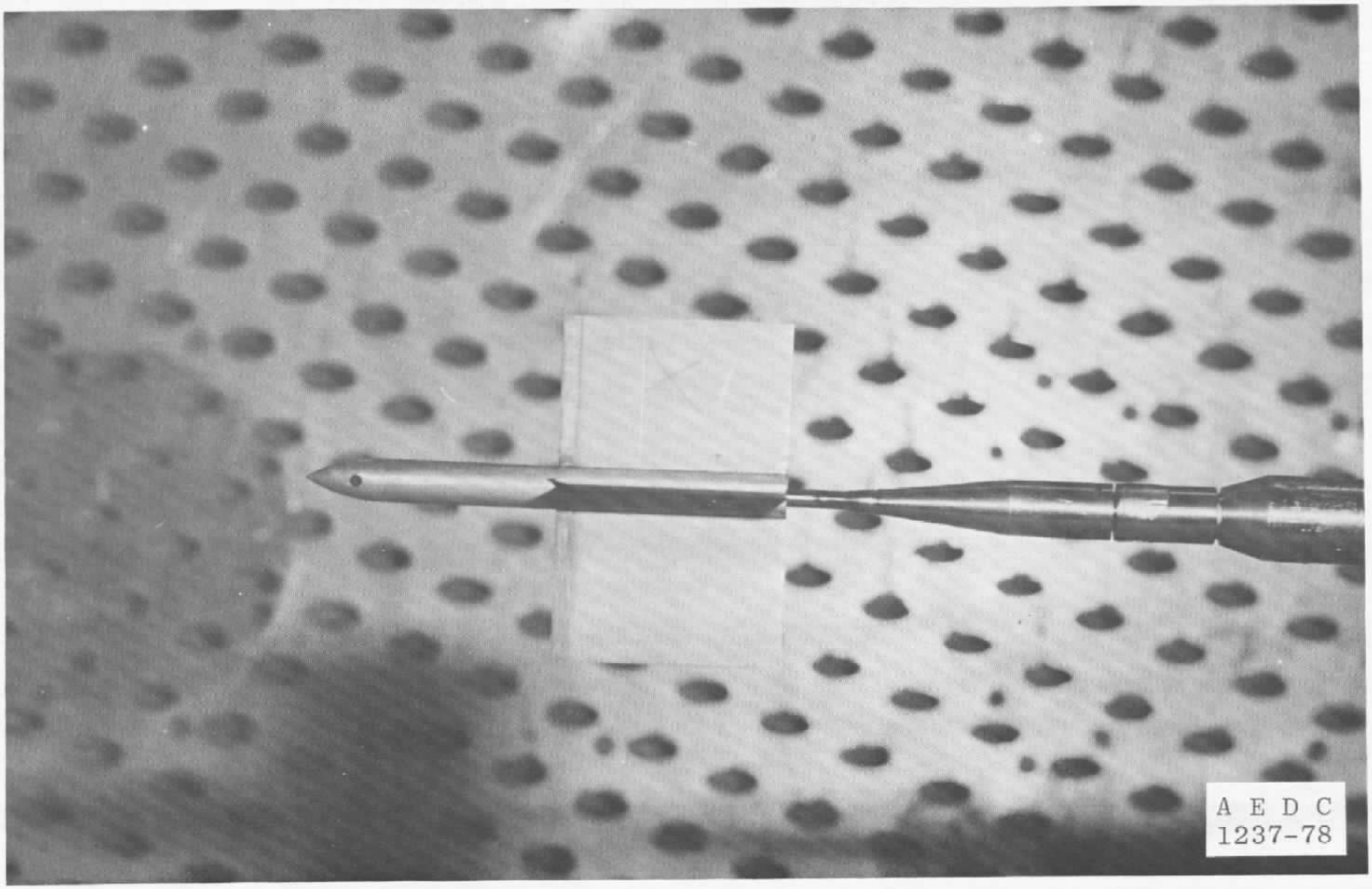

Figure 5. Photograph of flow angularity probe.

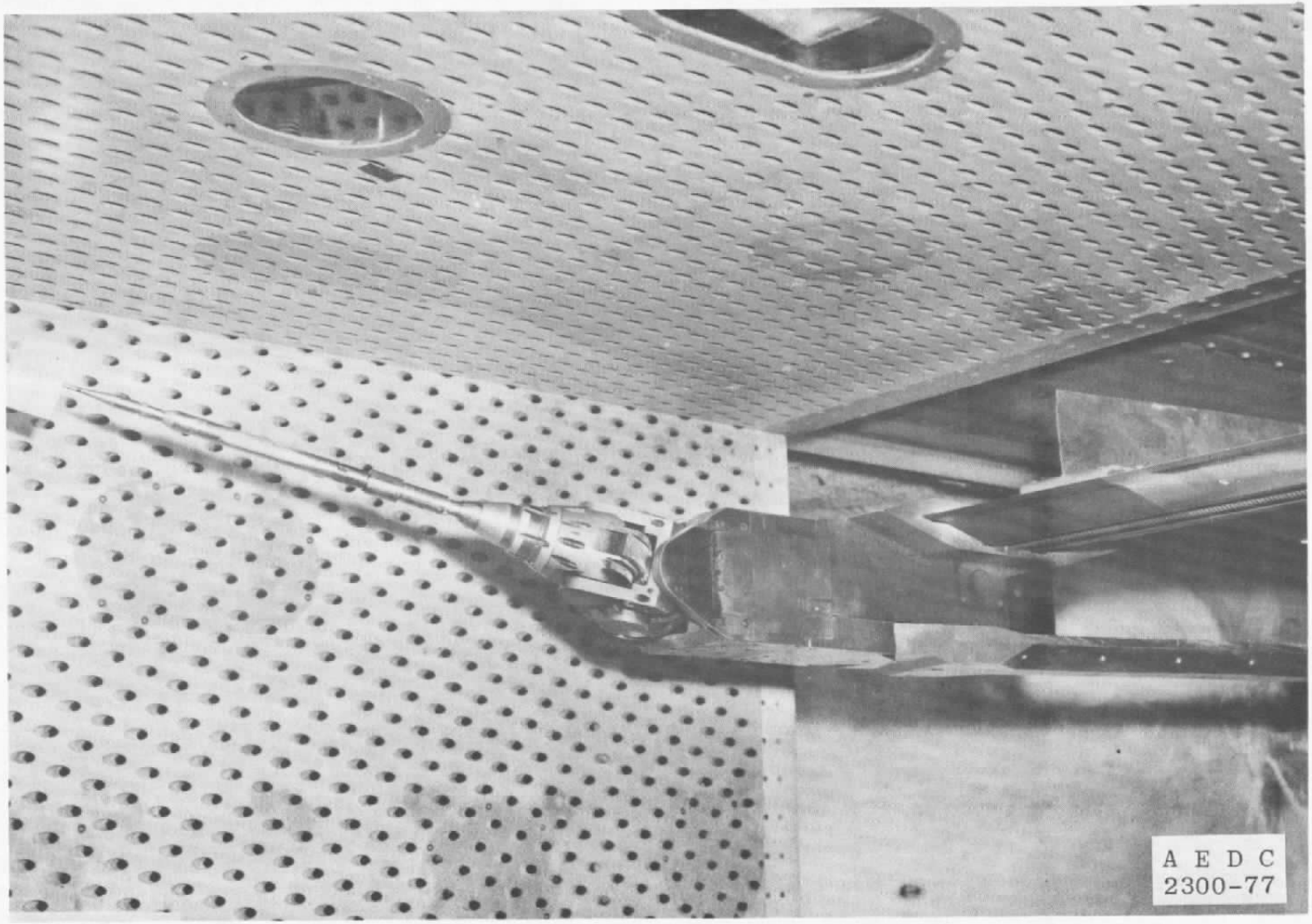

Figure 6. Photograph of the flow angularity probe installed on the CTS.

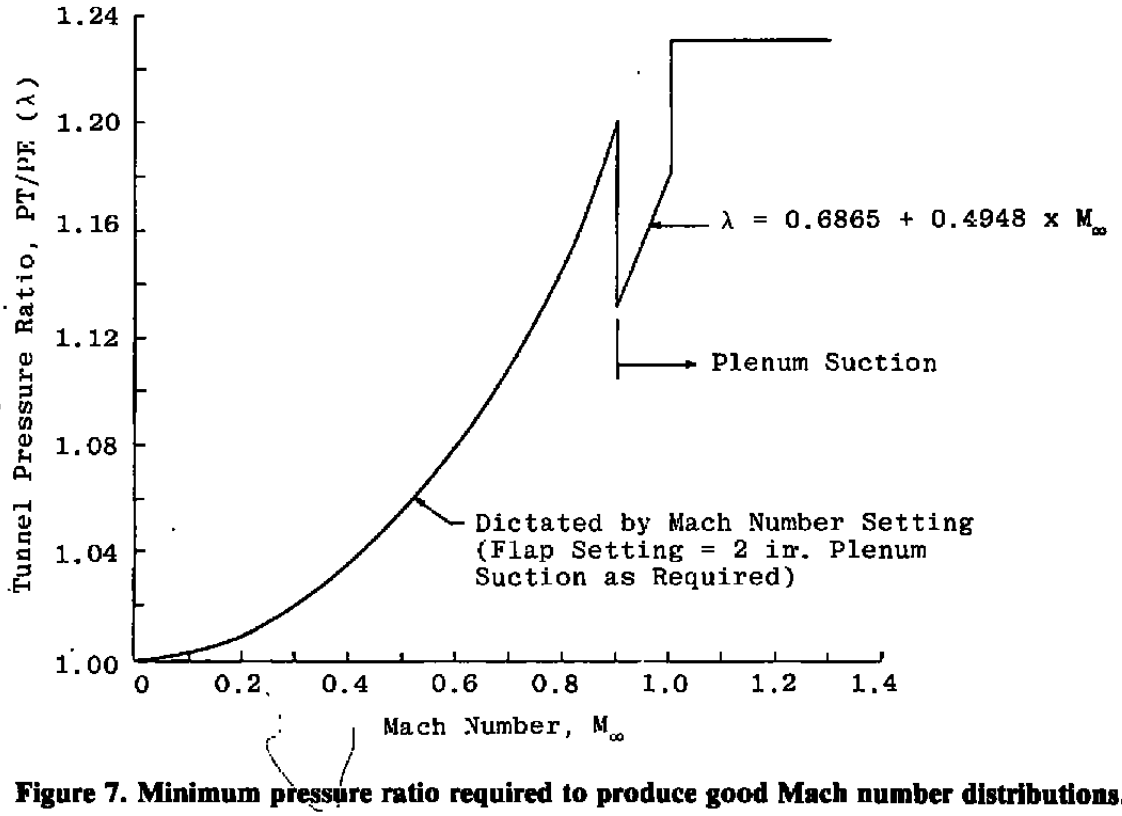

Figure 7. Minimum pressure ratio required to produce good Mach number distributions.

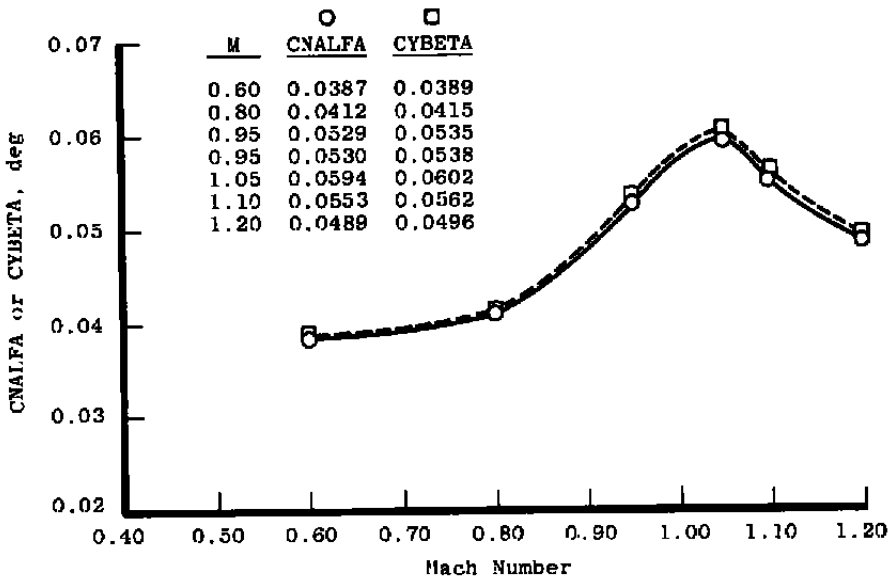

a.

M	$RMS_{0'}$ deg	$RMS_{180'}$ deg	$RMS_{90'}$ deg	$RMS_{-90'}$ deg	Avg, deg	Std. Dev., deg
0.60	±0.0098	±0.0120	±0.0110	±0.0098	±0.0106	±0.0011
0.80	0.0090	0.0090	0.0098	0.0072	0.0088	0.0011
0.95	0.0079	0.0030	0.0094	0.0052	0.0064	0.0028
0.95	0.0125	0.0110	0.0089	0.0058	0.0095	0.0039
1.05	0.0014	0.0107	0.0085	0.0040	0.0061	0.0042
1.10	0.0007	0.0054	0.0039	0.0083	0.0046	0.0032
1.20	0.0080	0.0120	0.0114	0.0094	0.0102	0.0018
				Avg.	0.0080	0.0024

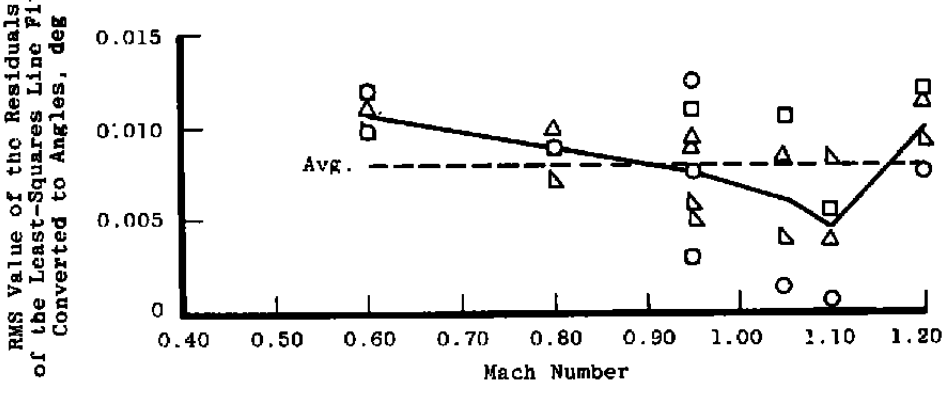

b.

Figure 8. 3-in.-span flow angularity probe calibration results.

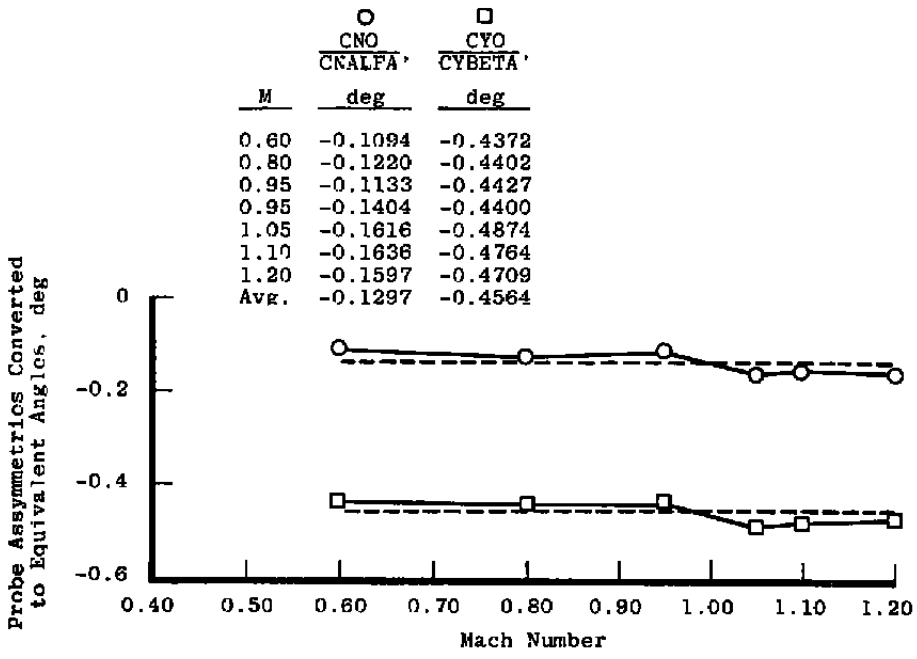

c.

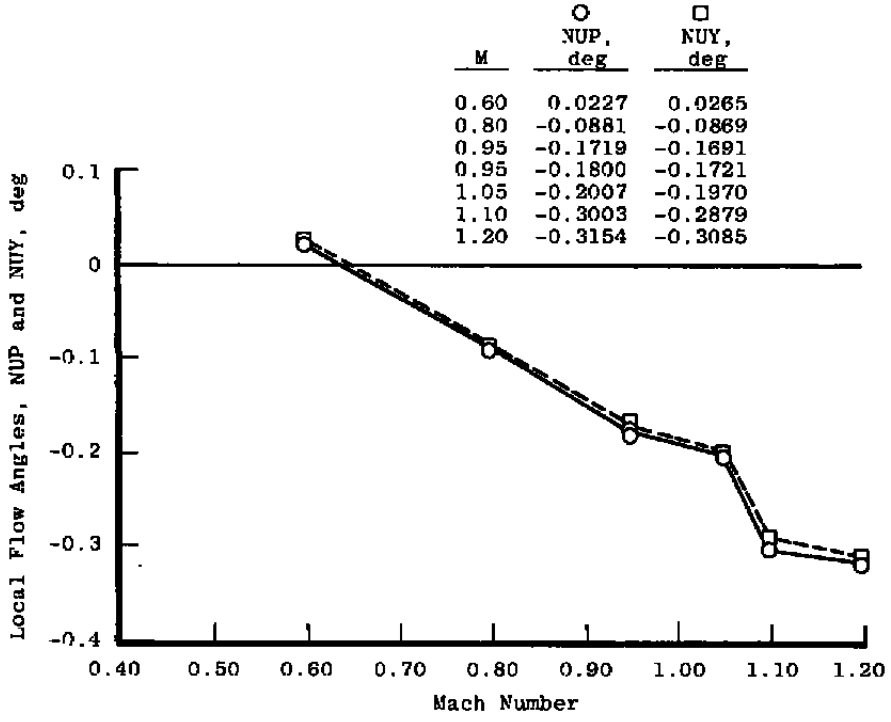

d.

Figure 8. Concluded.

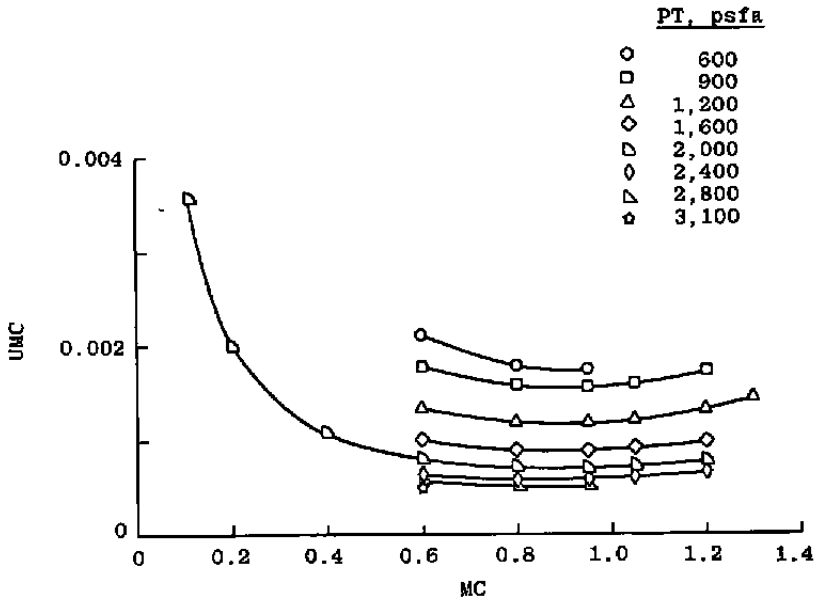

a. Plenum Mach number

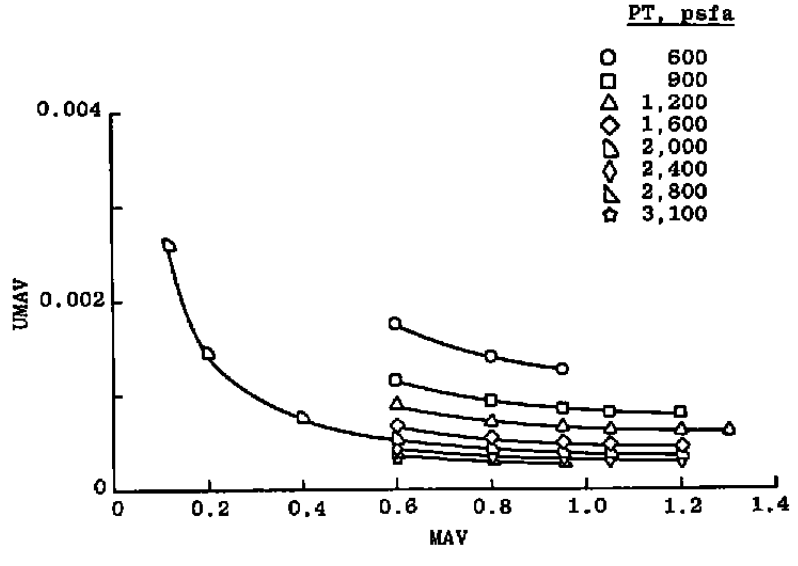

b. Average centerline Mach number

Figure 9. Estimated Mach number uncertainties.

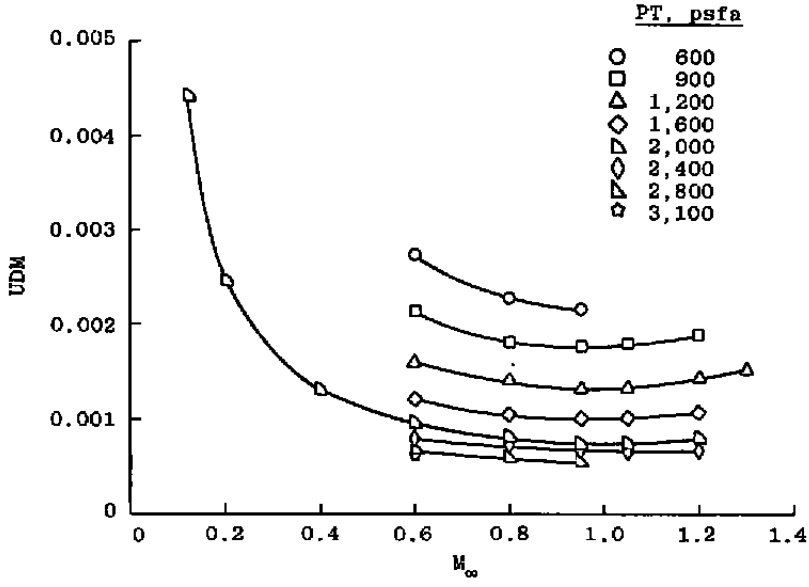

c. Calibration factor
Figure 9. Concluded.

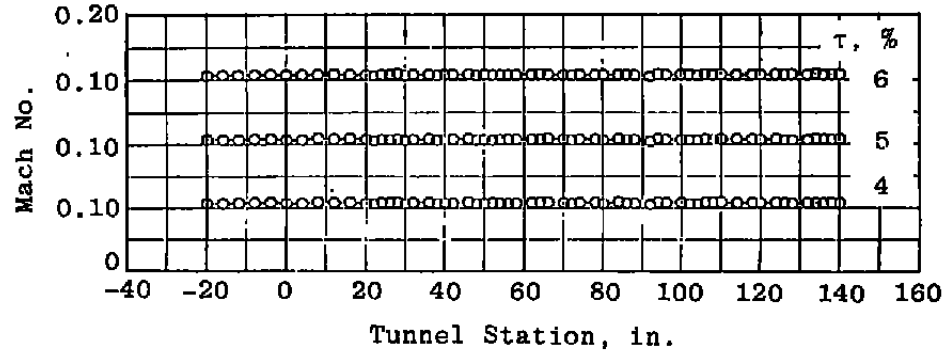

a. M = 0.11 (nom.), PT = 2,000 psfa

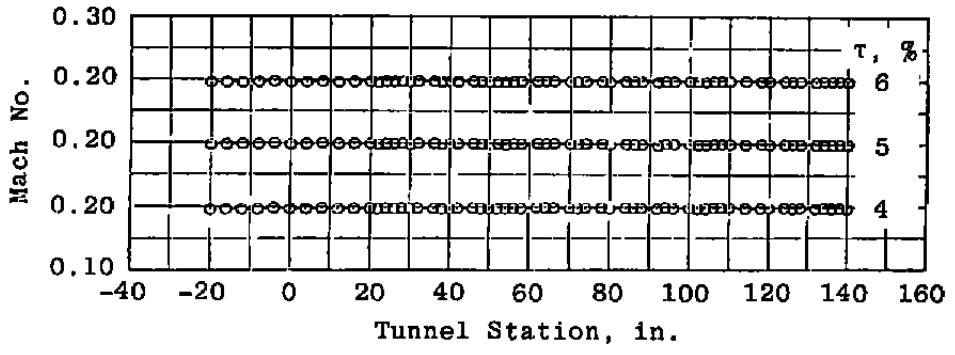

b. M = 0.20 (nom.), PT = 2,000 psfa

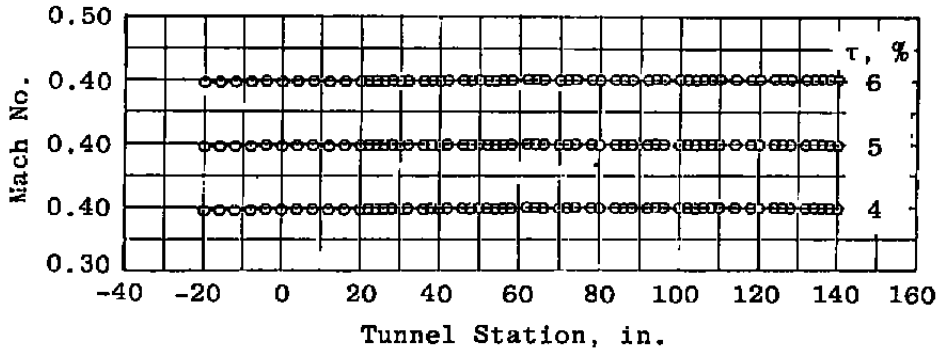

c. M = 0.40 (nom.), PT = 2,000 psfa

Figure 10. Effects of porosity on the centerline Mach number distributions.

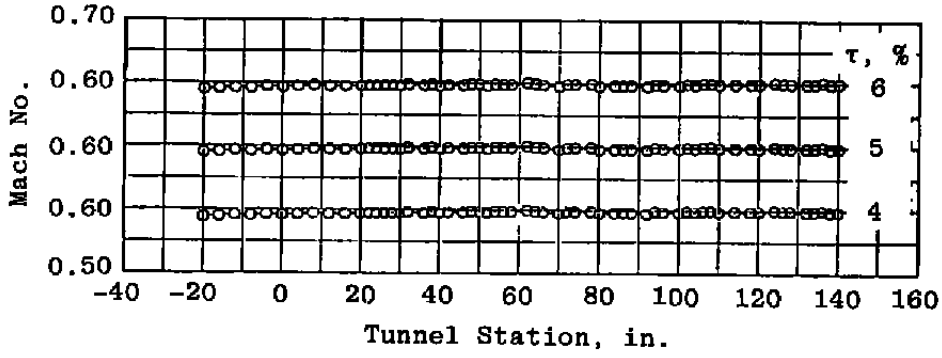

d. M = 0.60 (nom.), PT = 1,200 psfa

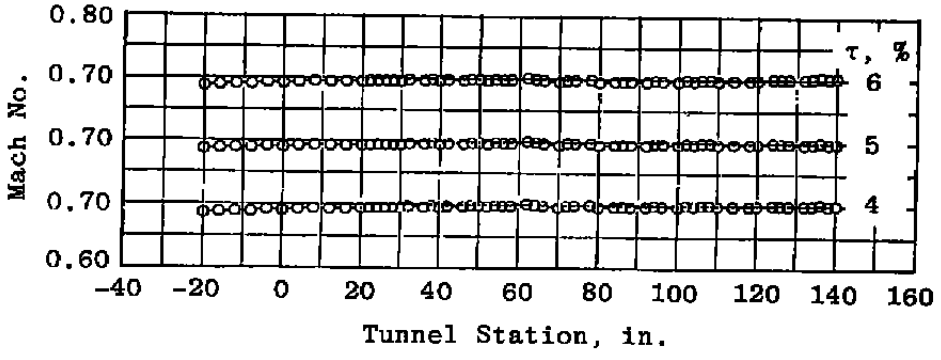

e. M = 0.70 (nom.), PT = 1,200 psfa

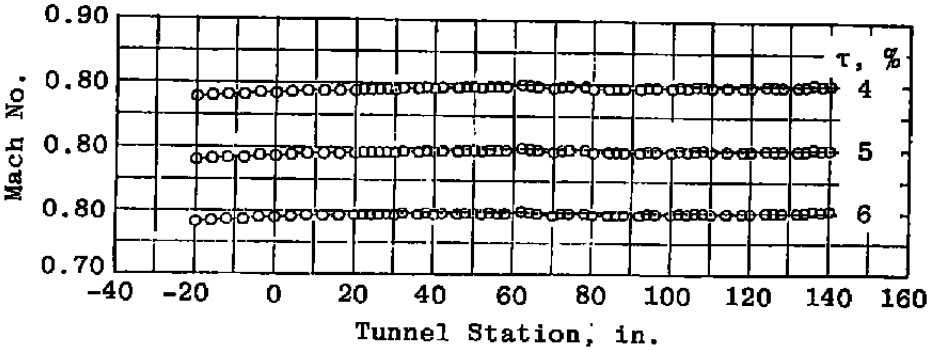

f. M = 0.80 (nom.), PT = 1,200 psfa
Figure 10. Continued.

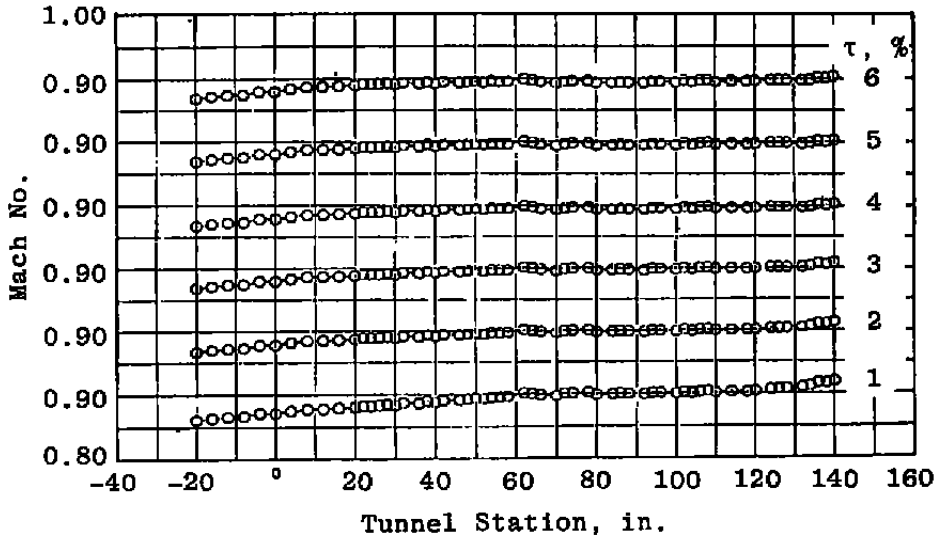

g. M = 0.90 (nom.), PT = 1,200 psfa

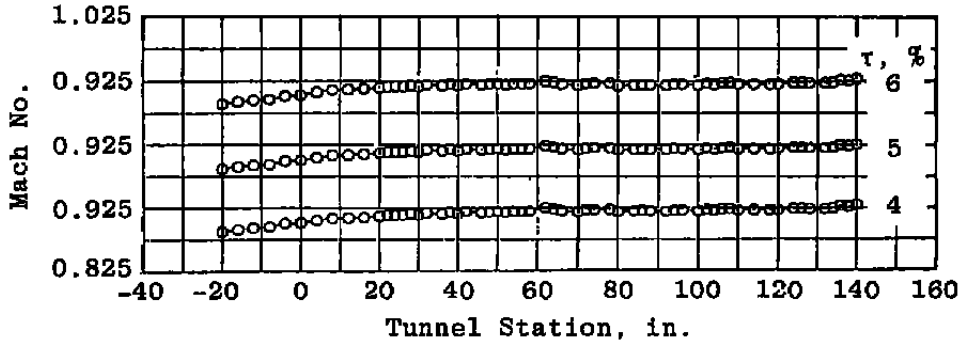

h. M = 0.925 (nom.), PT = 1,200 psfa

Figure 10. Continued.

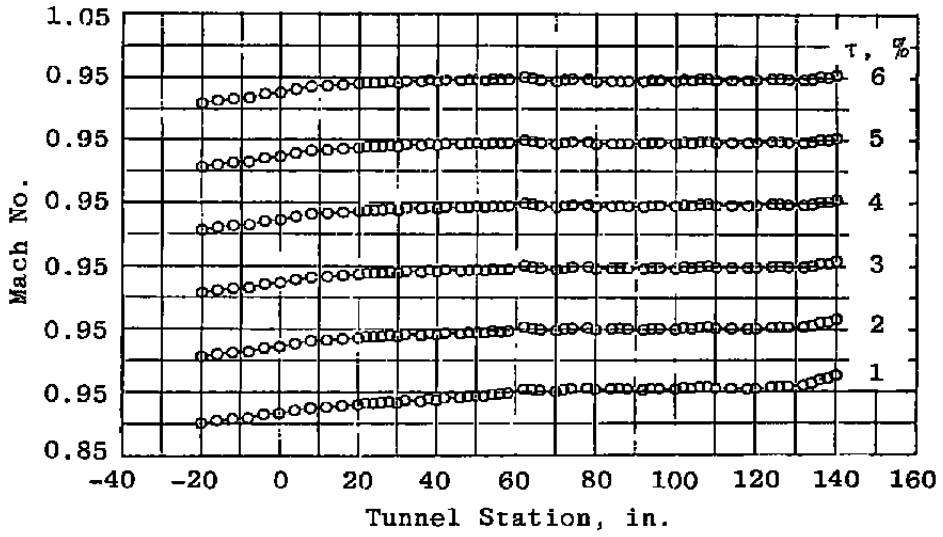

i. M = 0.95 (nom.), PT = 1,200 psfa

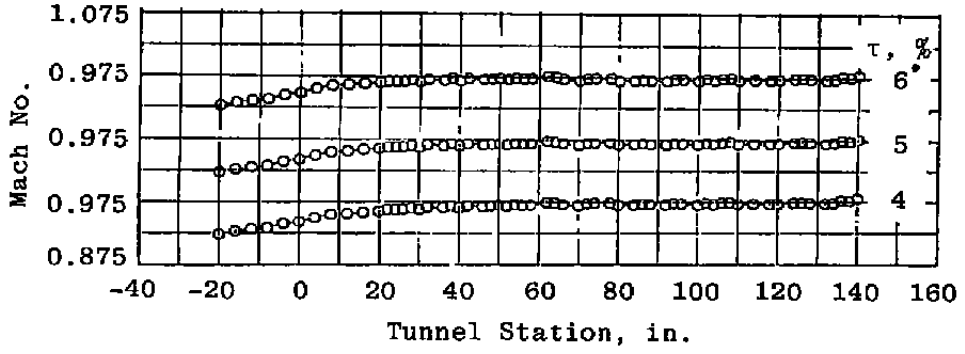

j. M = 0.974 (nom.), PT = 1,200 psfa

Figure 10. Continued.

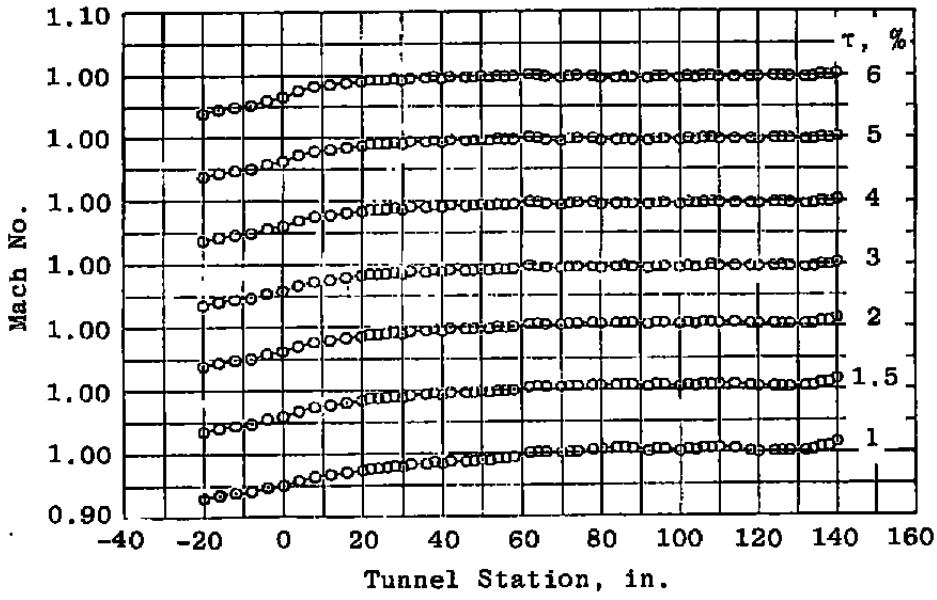

k. M = 1.0 (nom.), PT = 1,200 psfa

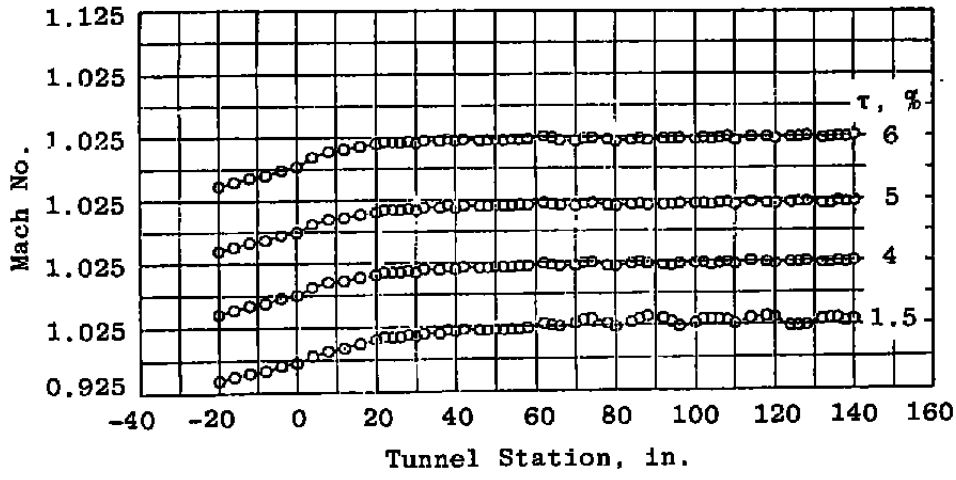

l. M = 1.025 (nom.), PT = 1,200 psfa
Figure 10. Continued.

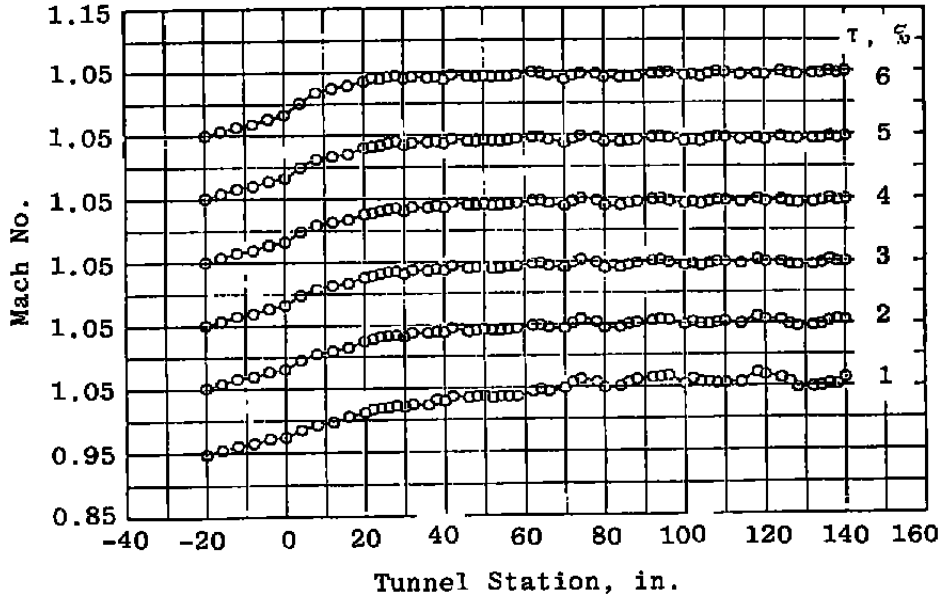

m. M = 1.05 (nom.), PT = 1,200 psfa

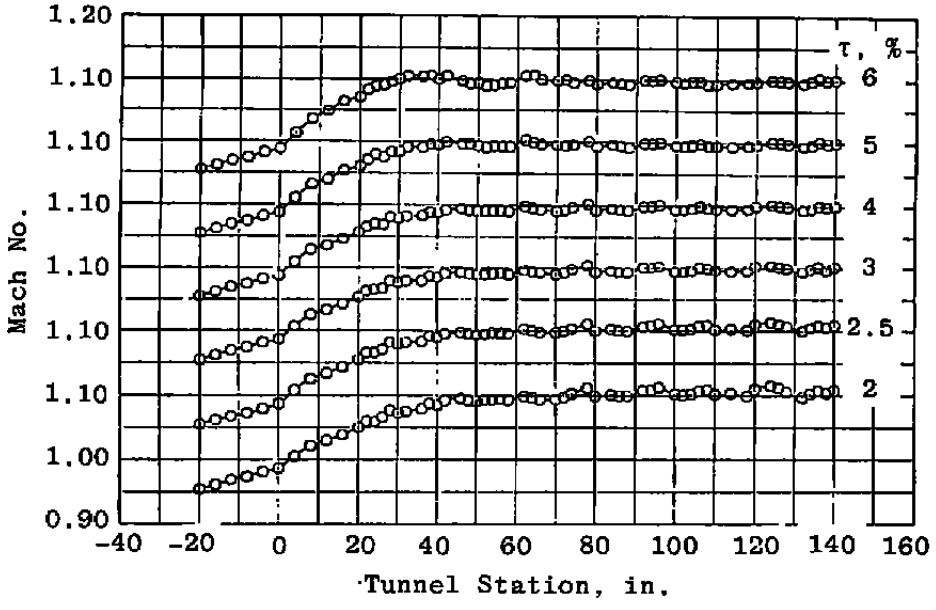

n. M = 1.10 (nom.), PT = 1,200 psfa
Figure 10. Continued.

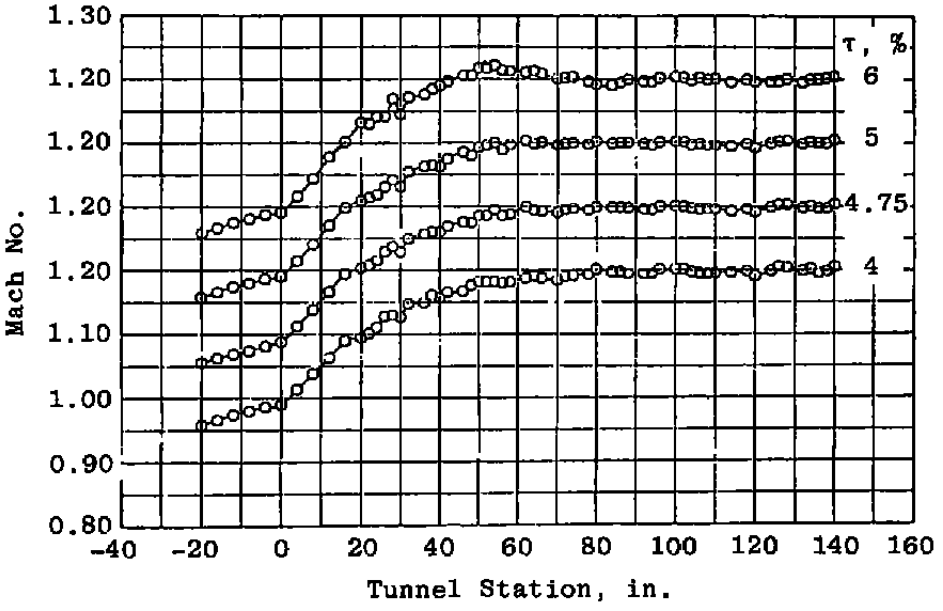

o. M = 1.20 (nom.), PT = 1,200 psfa

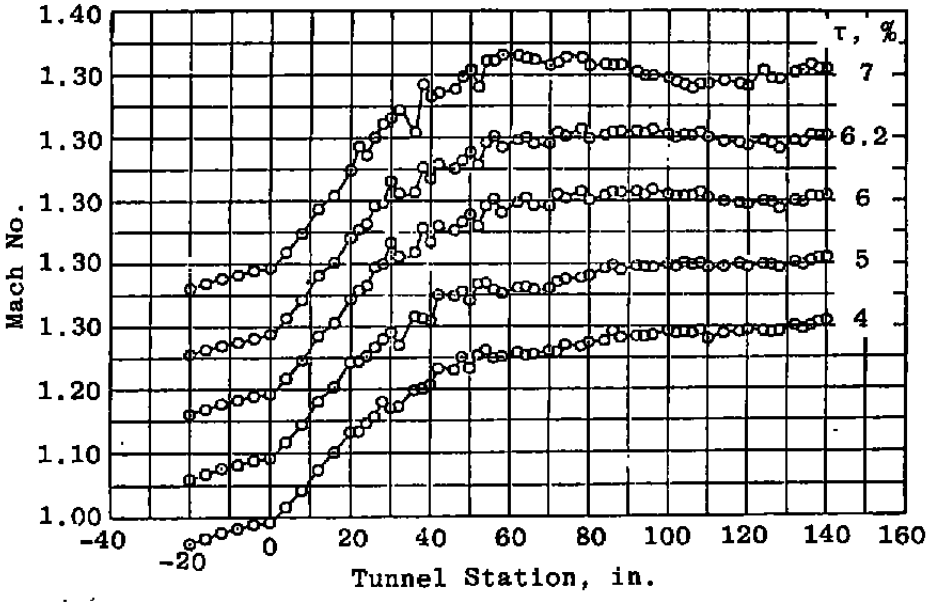

p. M = 1.30 (nom.), PT = 1,200 psfa

Figure 10. Concluded.

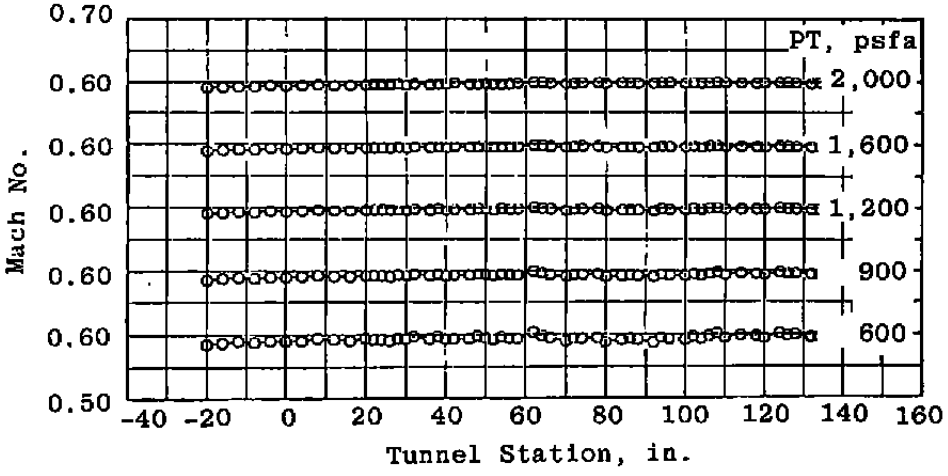

a. M = 0.60 (nom.) τ = 5 percent

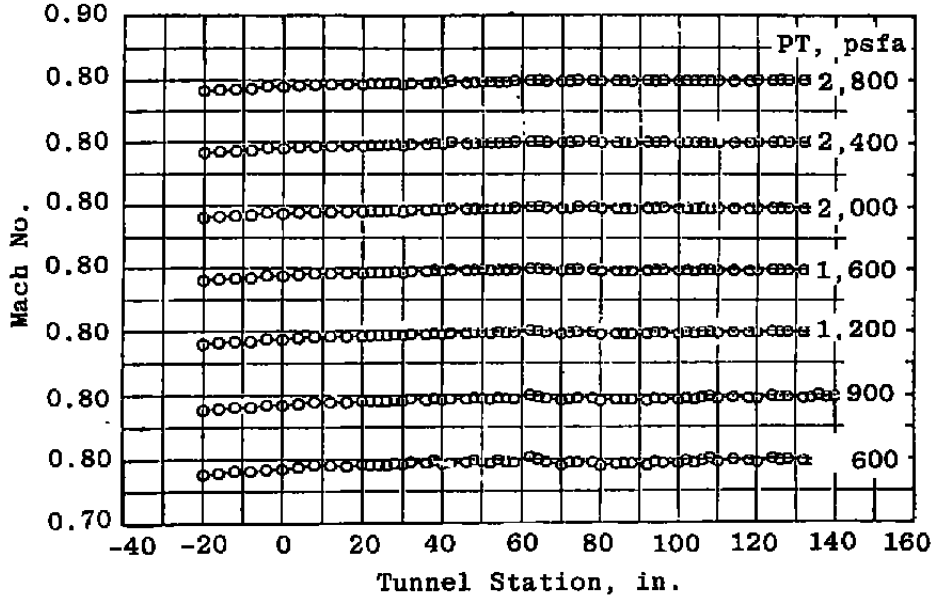

b. M = 0.80 (nom.) τ = 5 percent

Figure 11. Effect of PT on the centerline Mach number distributions.

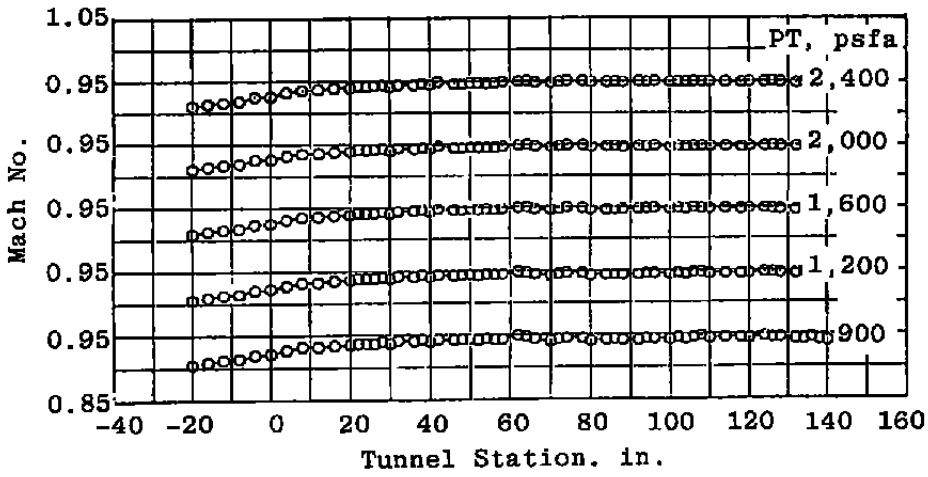

c. M = 0.925 (nom.) PT = 1,200 psfa

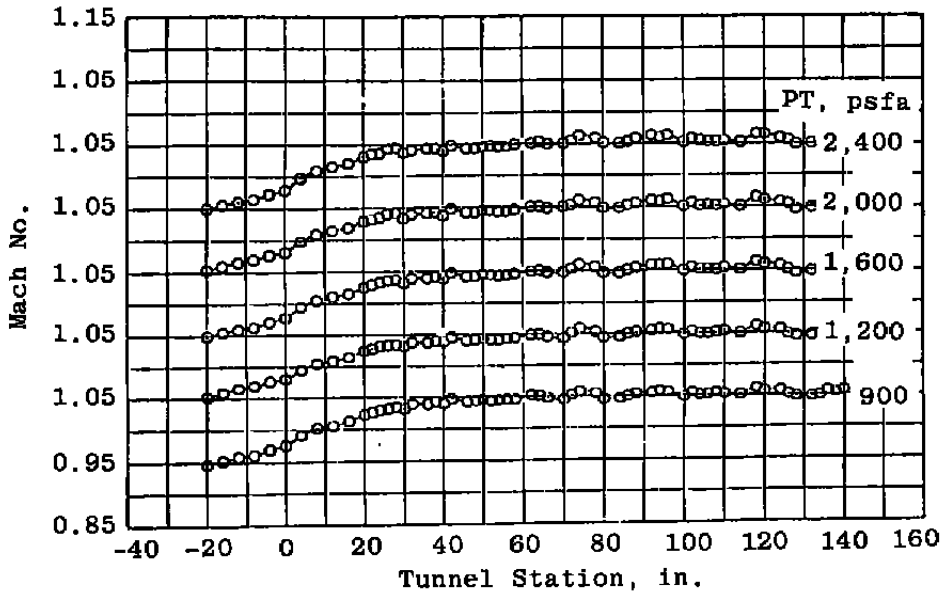

d. M = 1.05 (nom.) τ = 2 percent

Figure 11. Continued.

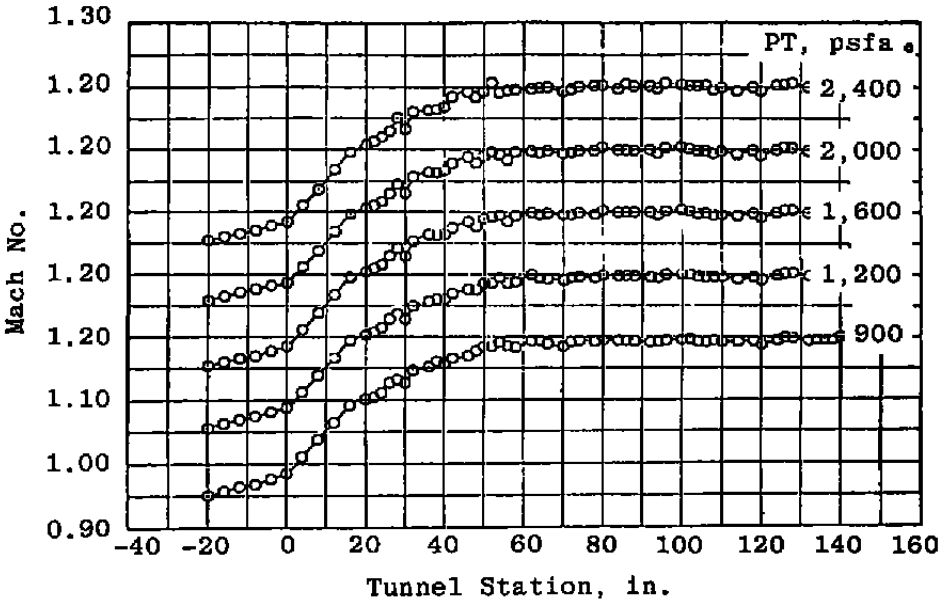

e. M = 1.20 (nom.) τ = 4.75

Figure 11. Concluded.

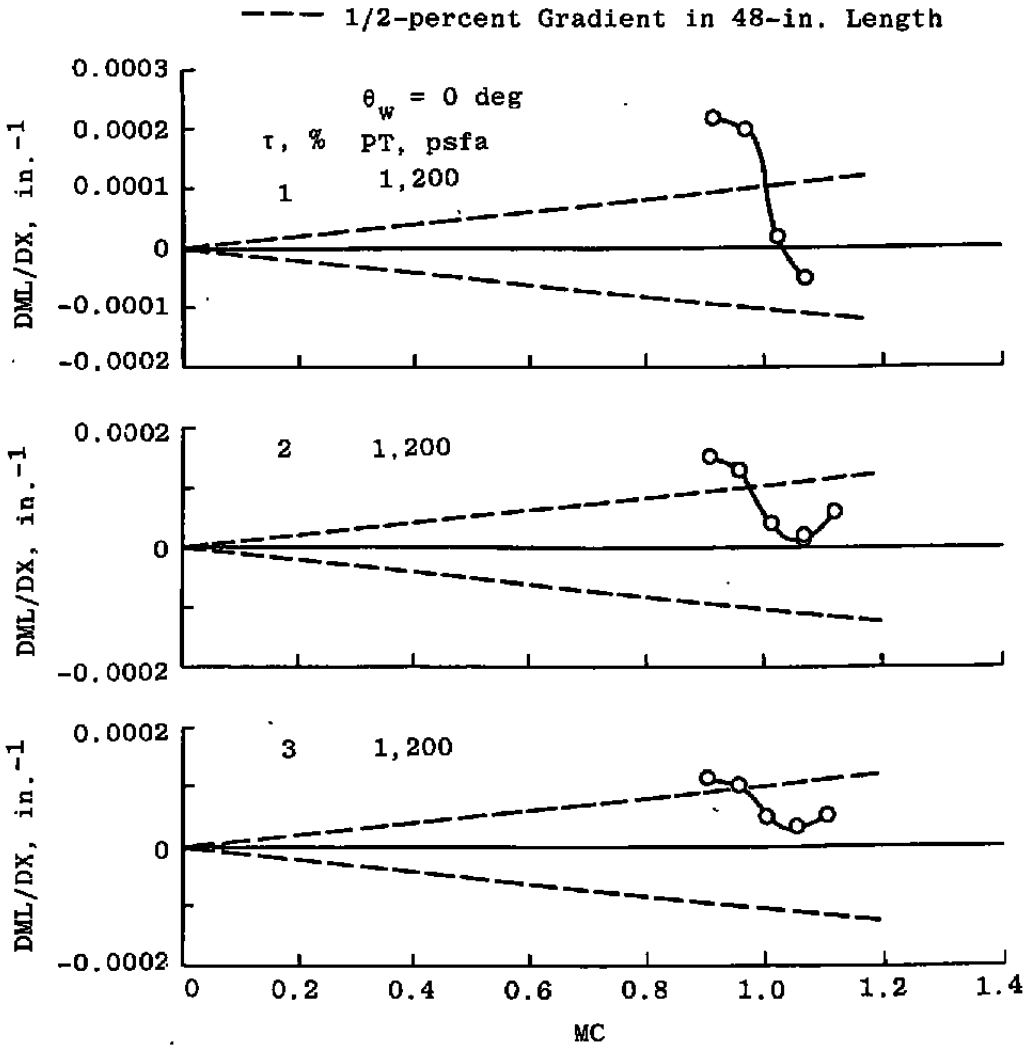

Figure 12. Effect of Mach number on the centerline Mach number gradient, porosity as a parameter.

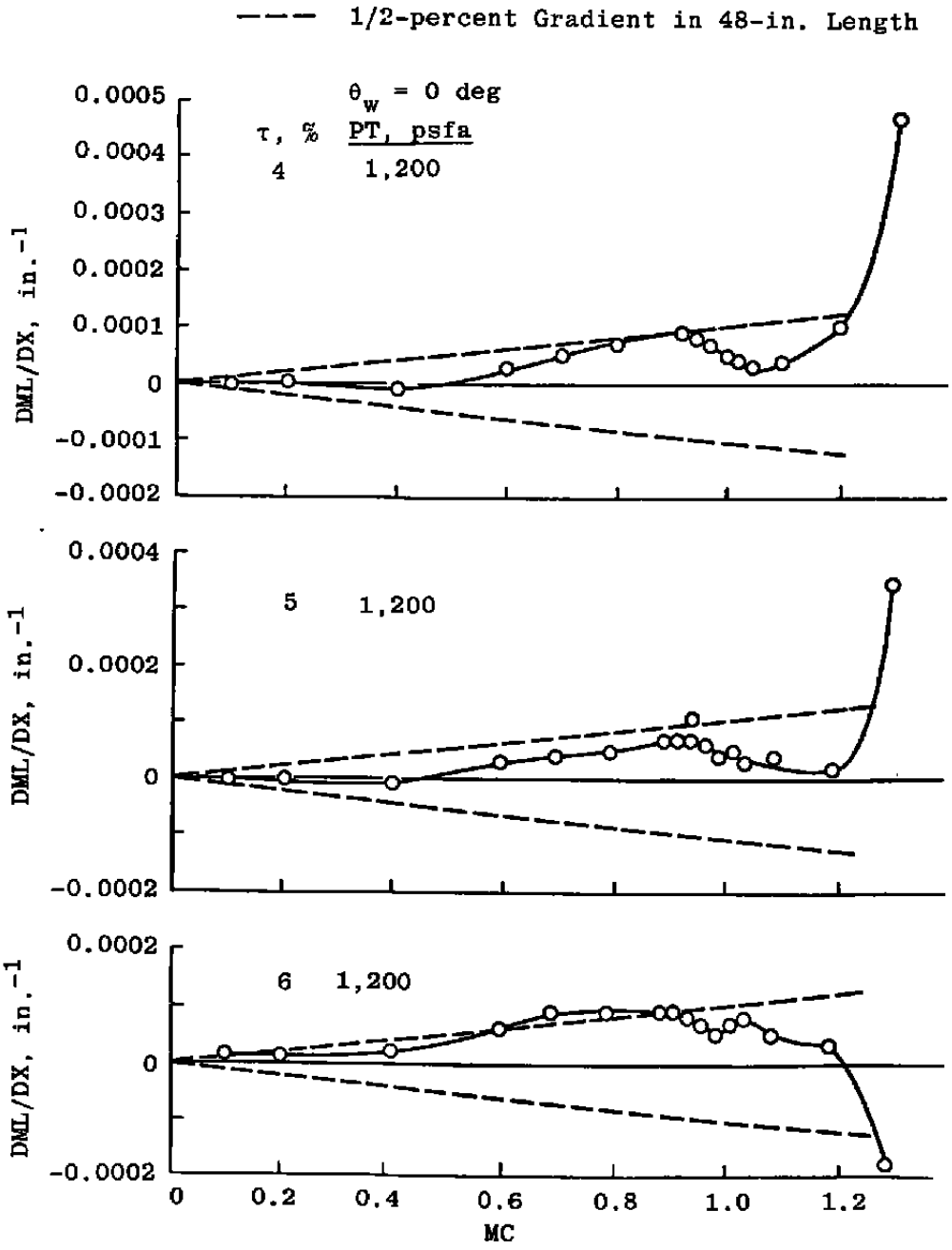

Figure 12. Concluded.

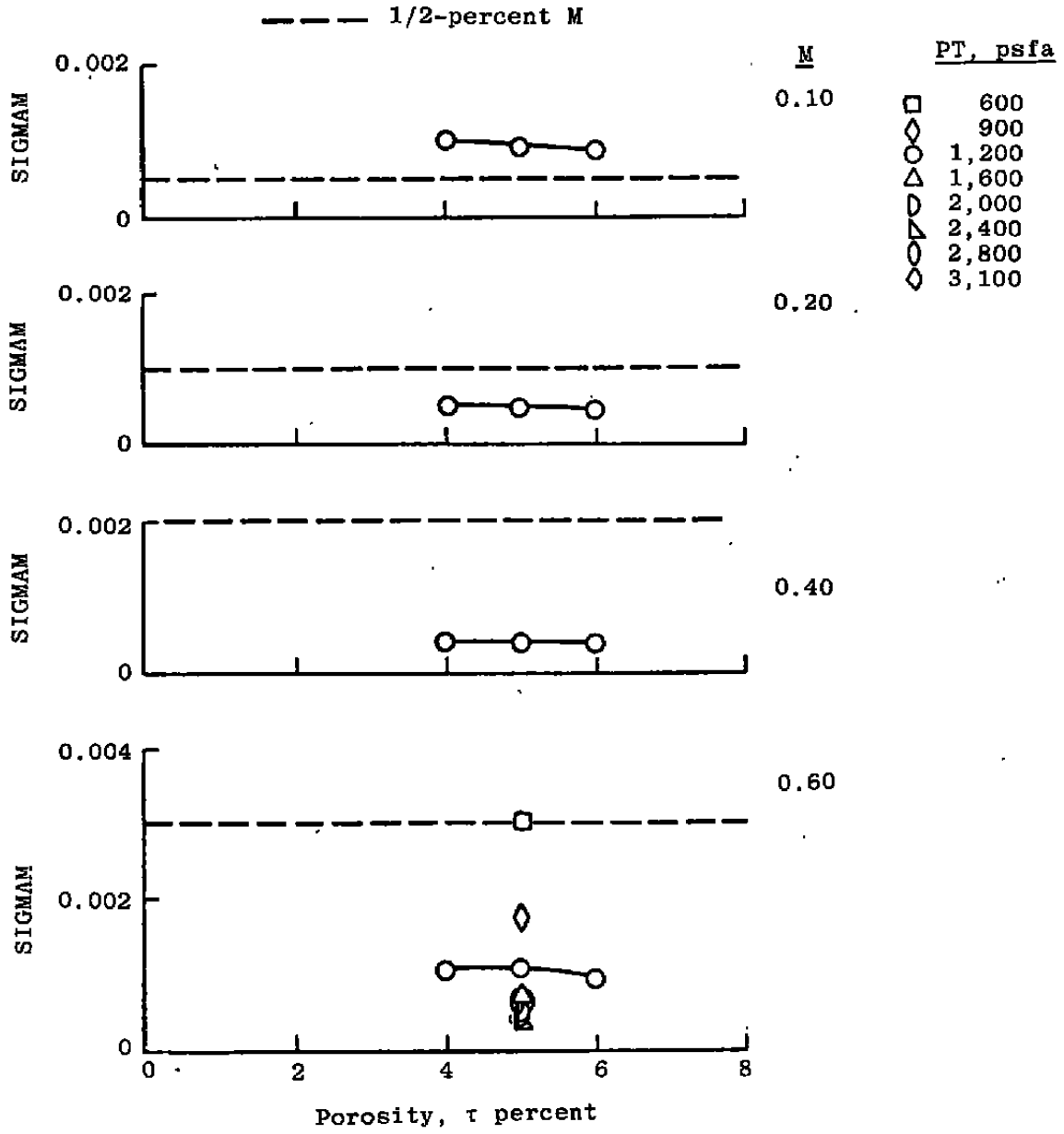

Figure 13. Effect of porosity on SIGMAM, Mach number as a parameter.

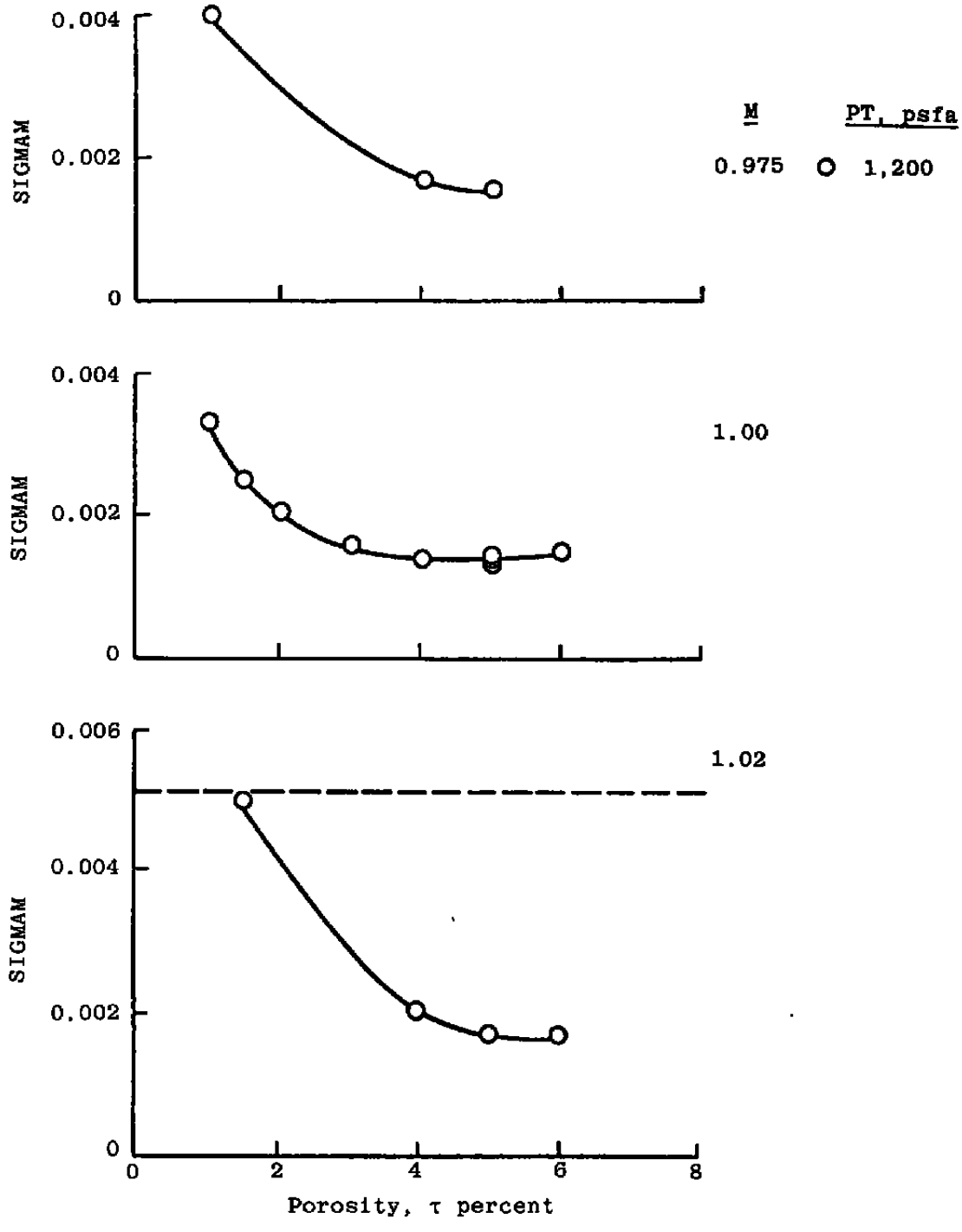

Figure 13. Continued.

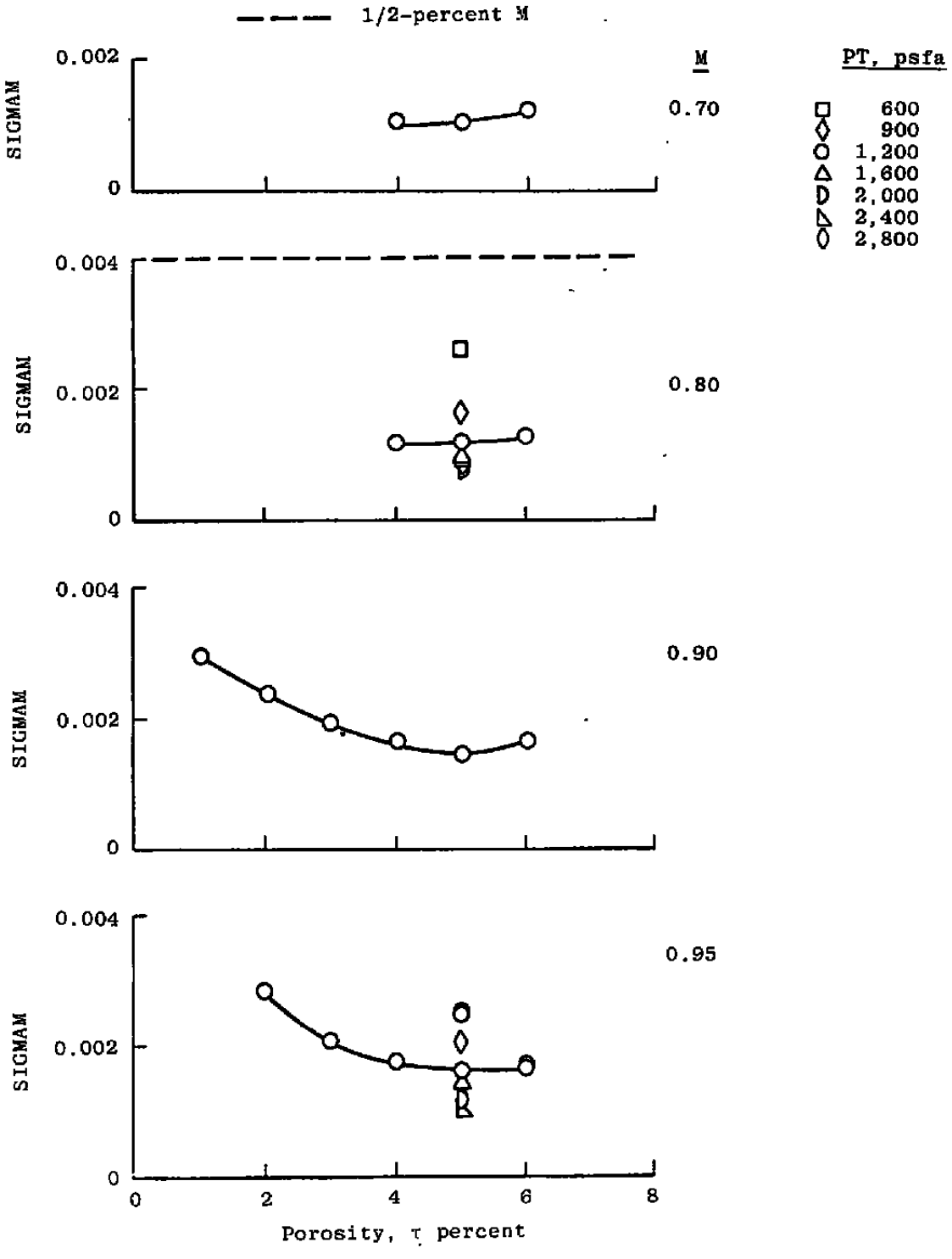

Figure 13. Continued.

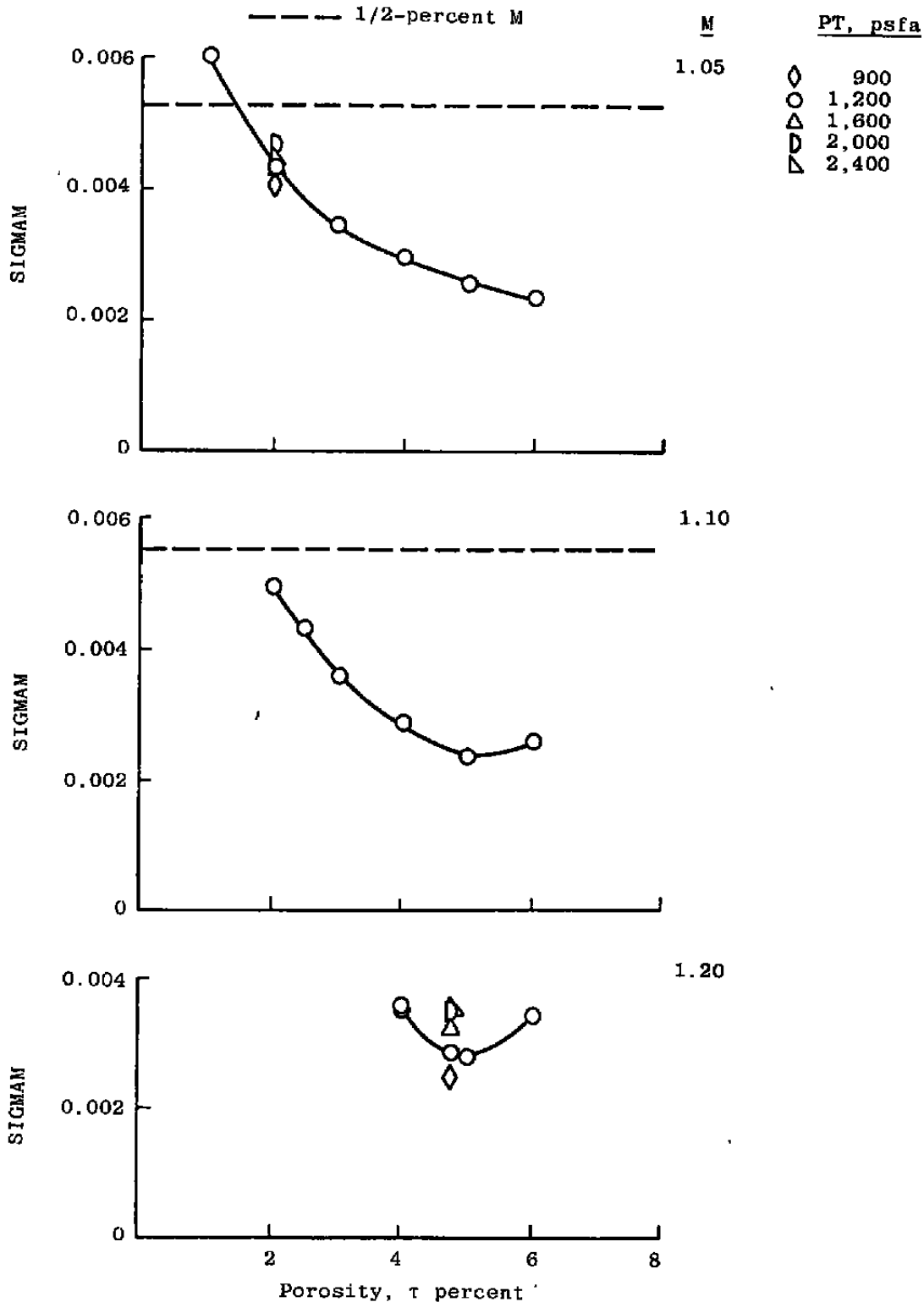

Figure 13. Continued.

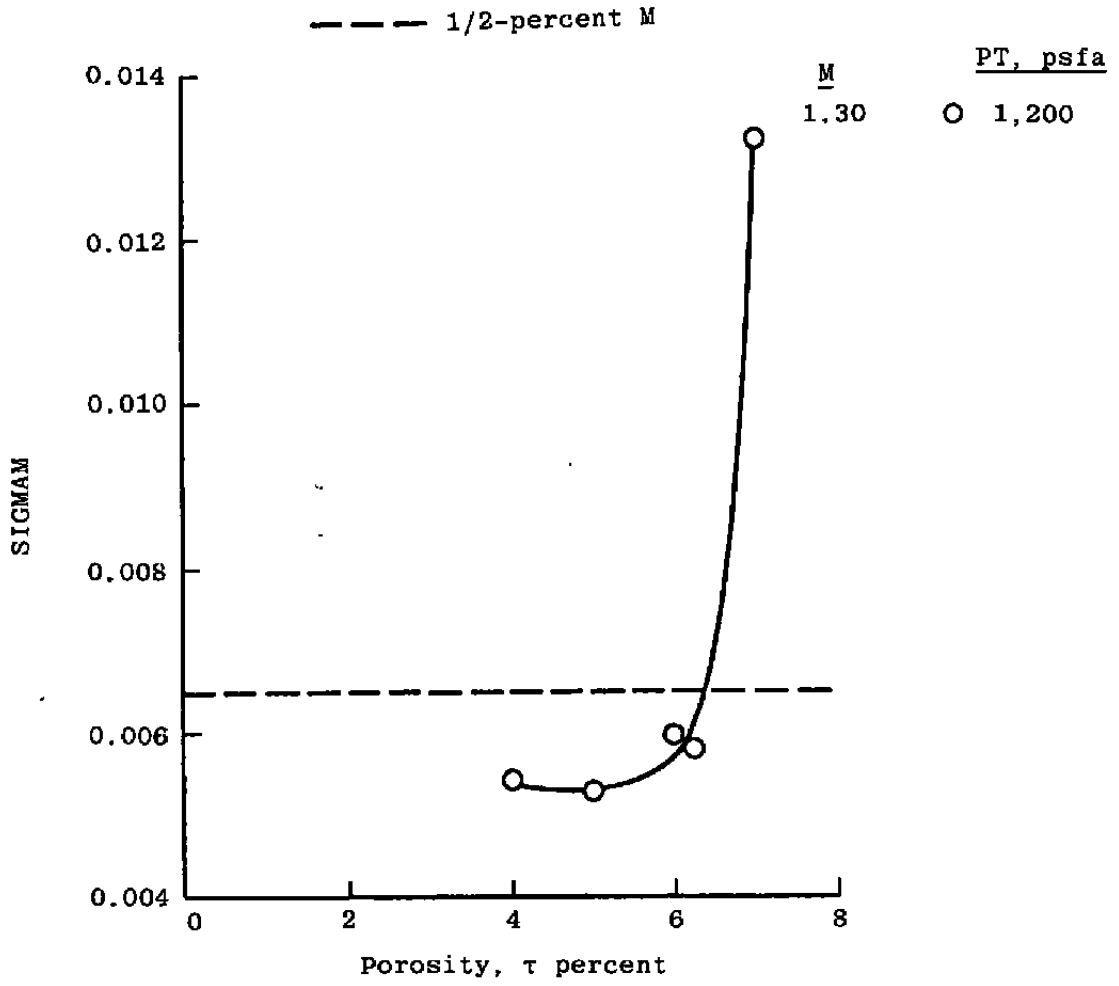

Figure 13. Concluded.

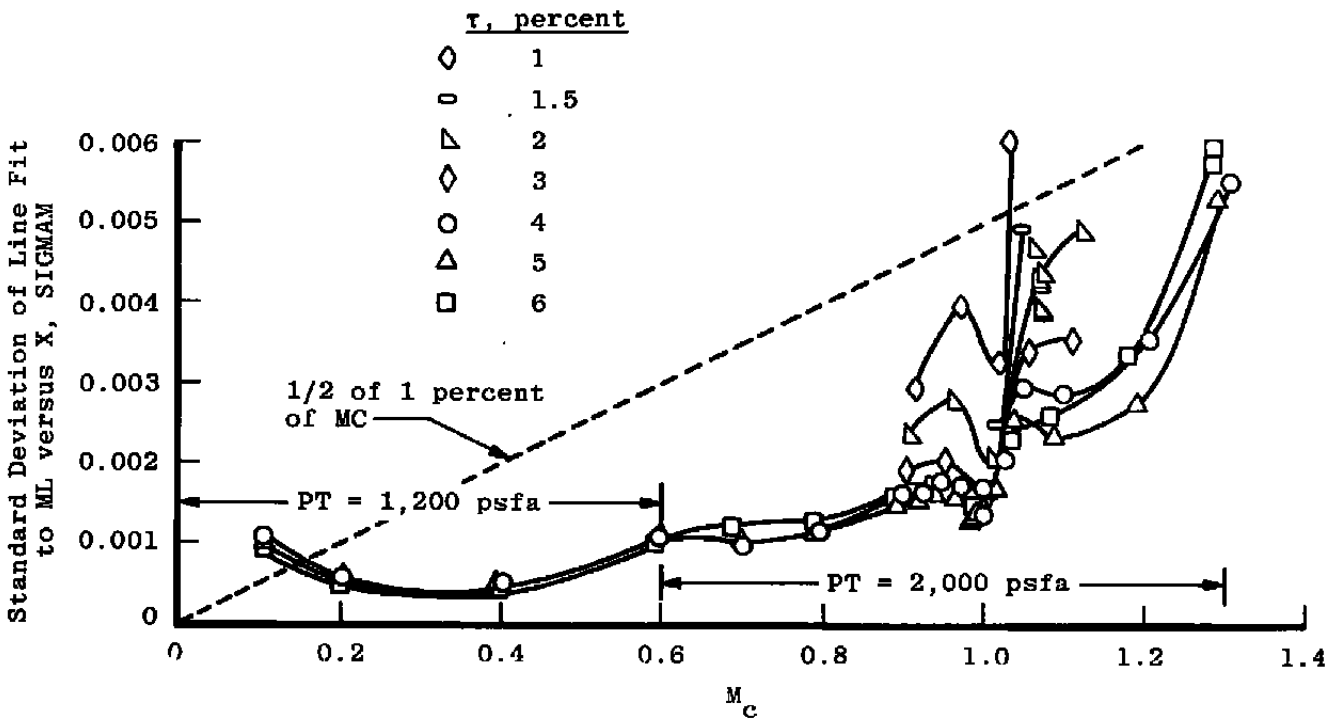

Figure 14. Effect of Mach number on SIGMAM, porosity as a parameter.

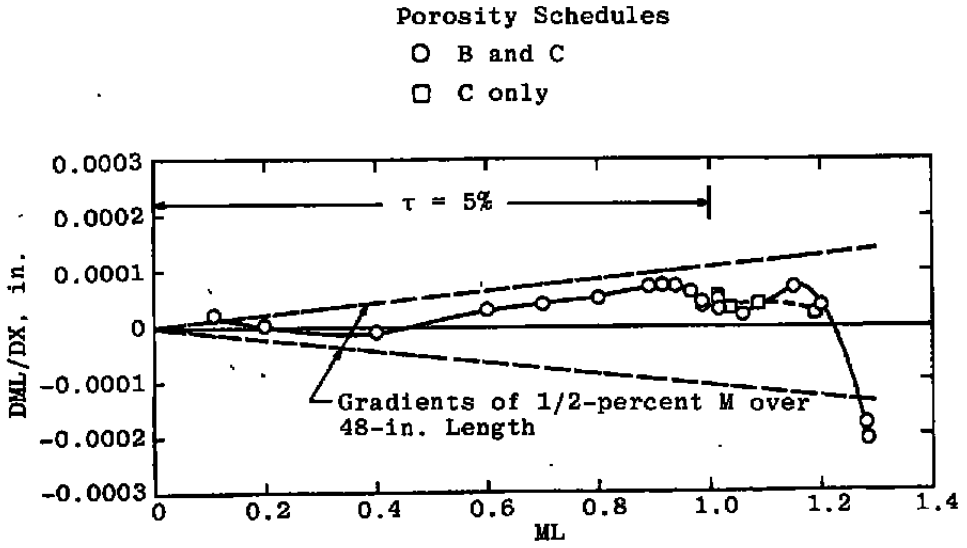

Figure 15. Mach number gradients versus Mach number for Tunnel 4T operating porosity schedules.

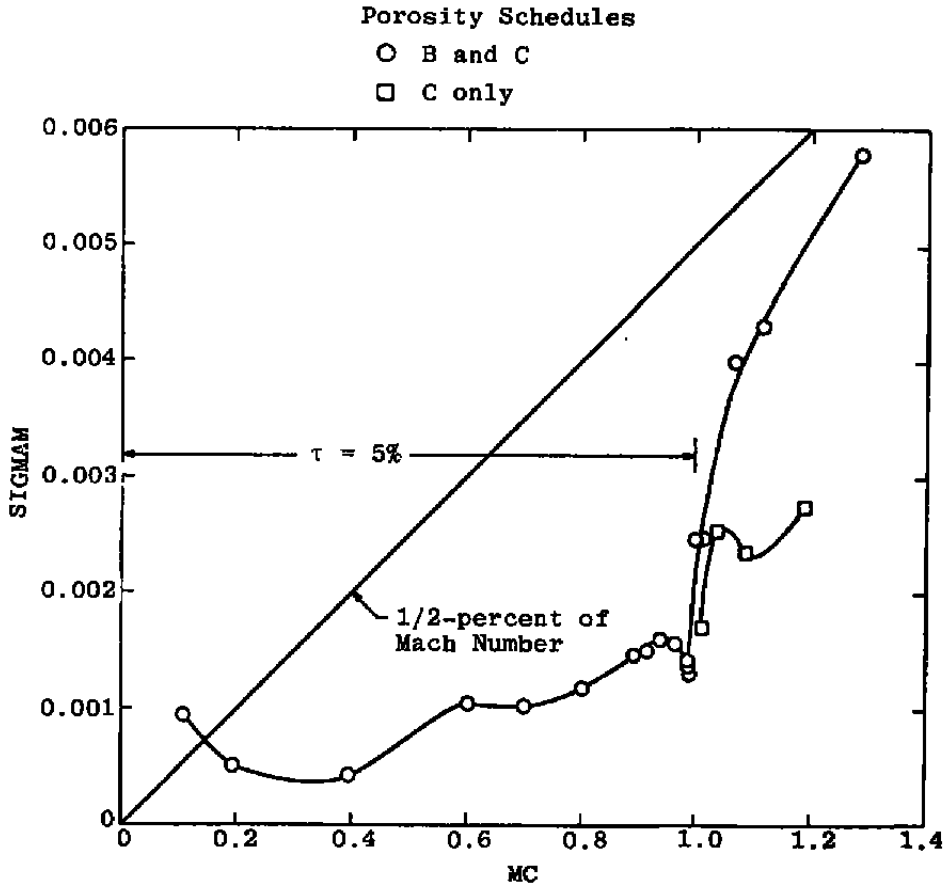

Figure 16. Standard deviations in Mach number for Tunnel 4T operating porosity schedules.

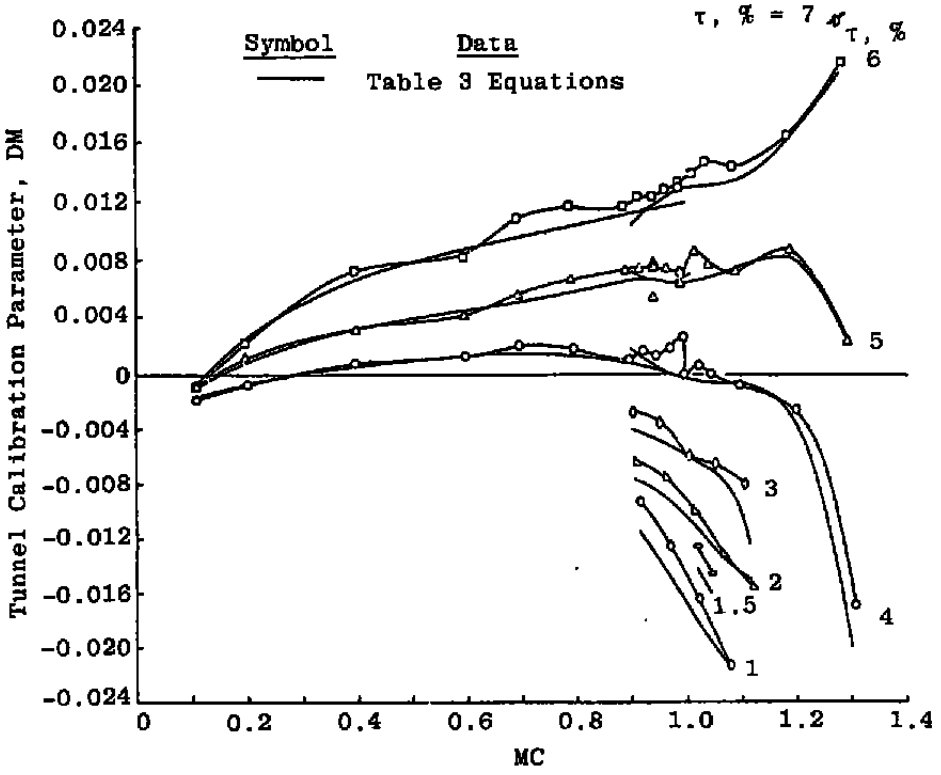

Figure 17. Tunnel calibration factor, DM, versus MC, porosity as a parameter.

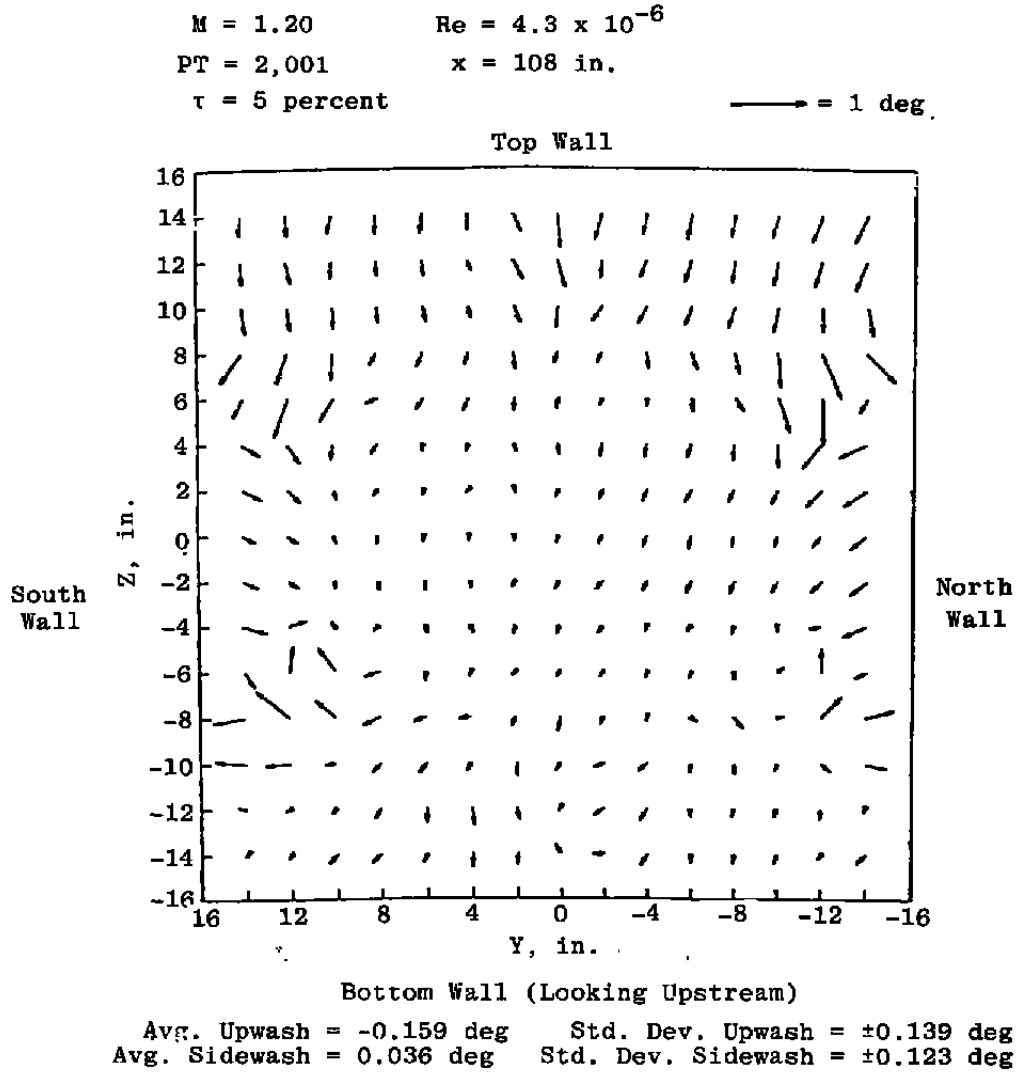

Figure 18. Typical flow angularity measurements with the built-up honeycomb in the stilling chamber.

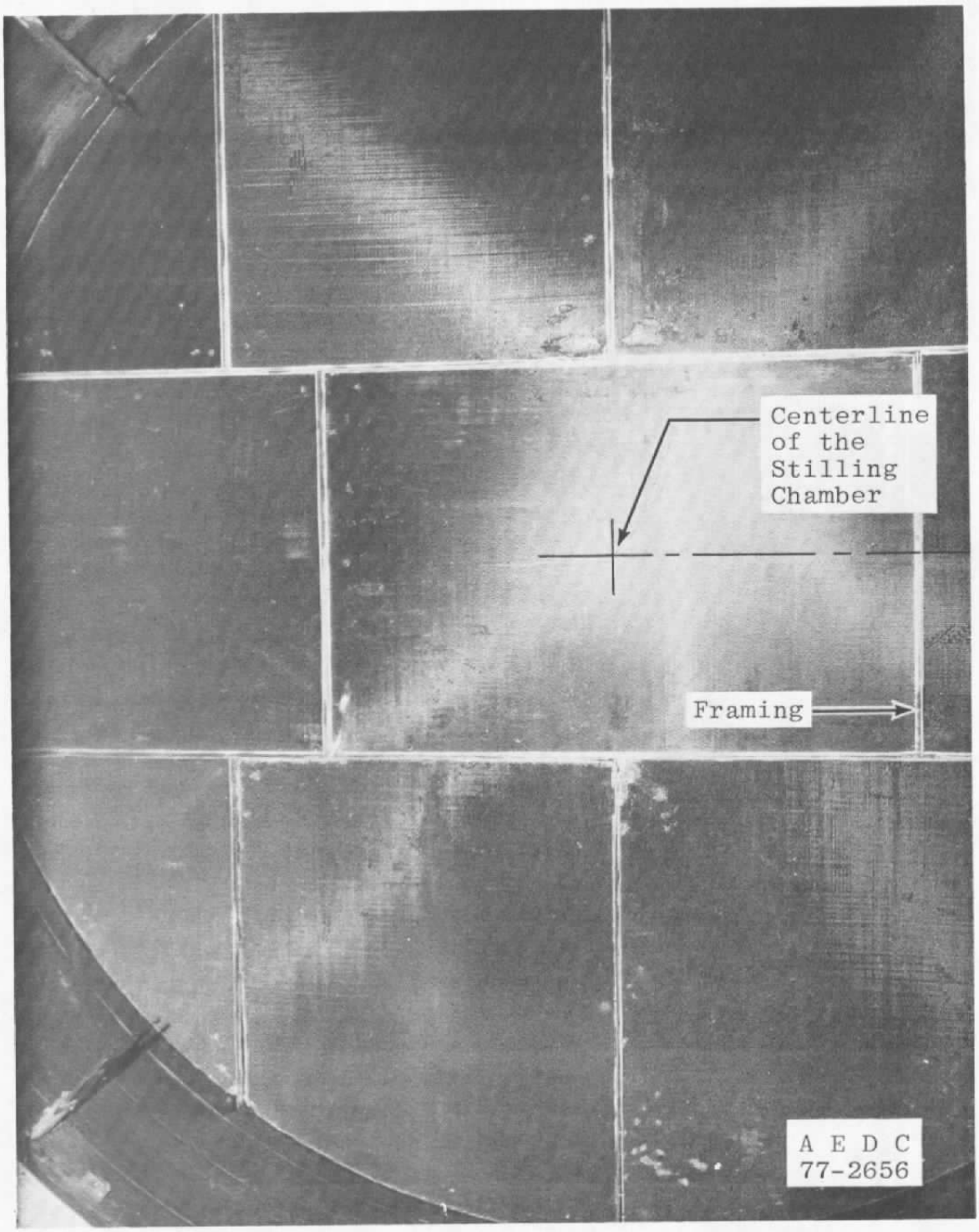

Figure 19. Photograph of the built-up honeycomb.

Figure 20. "One-piece" honeycomb under construction.

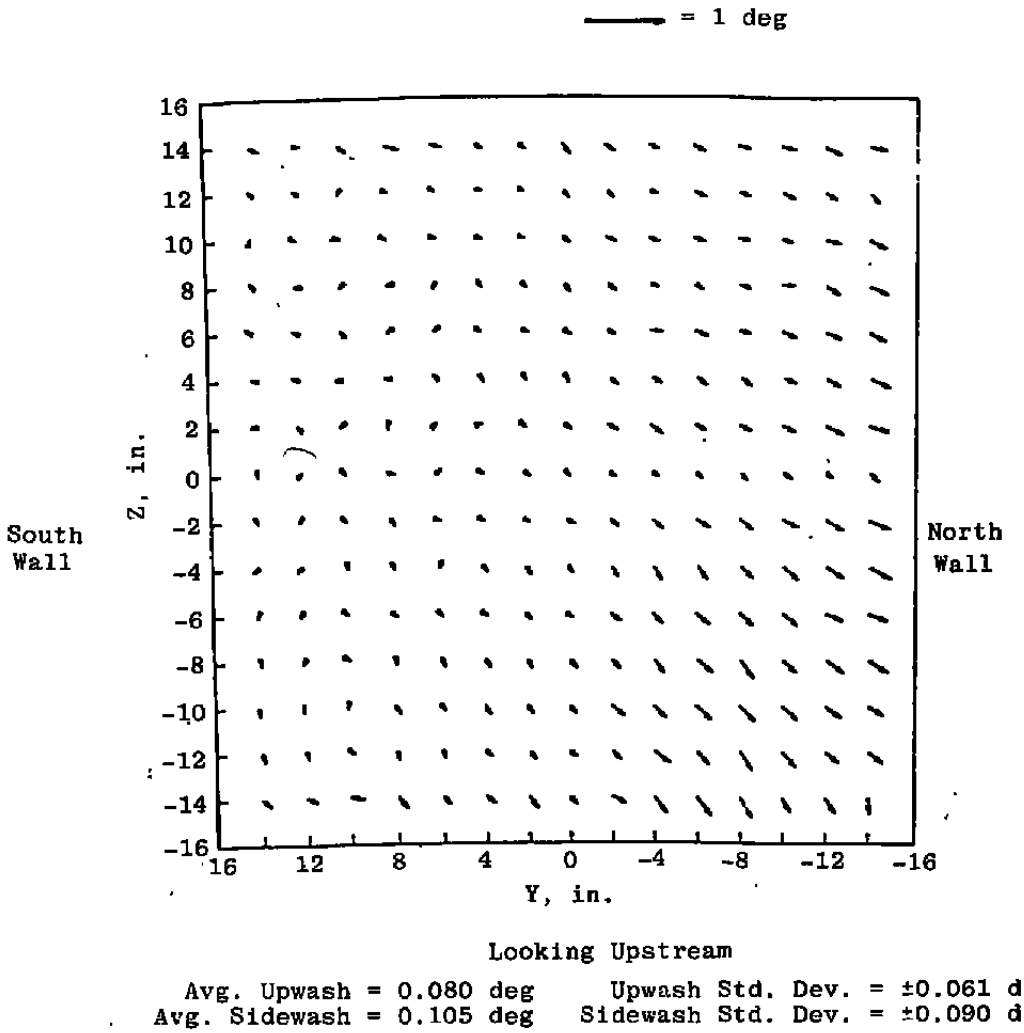

Figure 21. Flow angularity distributions at M = 0.80, PT = 1,200 psfa, T_T = 5 percent (all walls), and X = 108 in.

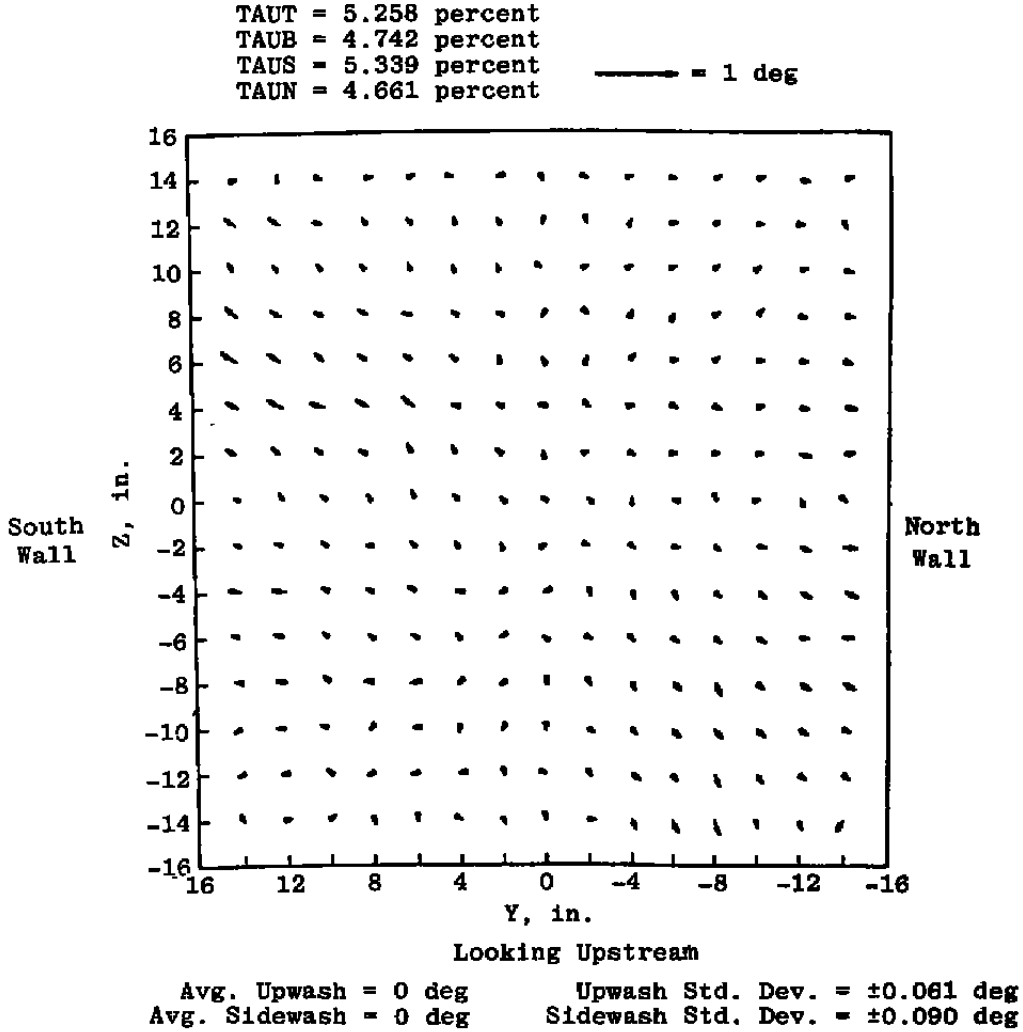

Figure 22. Randomness of the flow angularity distributions for M = 0.80, PT = 1,200 psfa, τ = 5 percent (all walls), and X = 108 in.

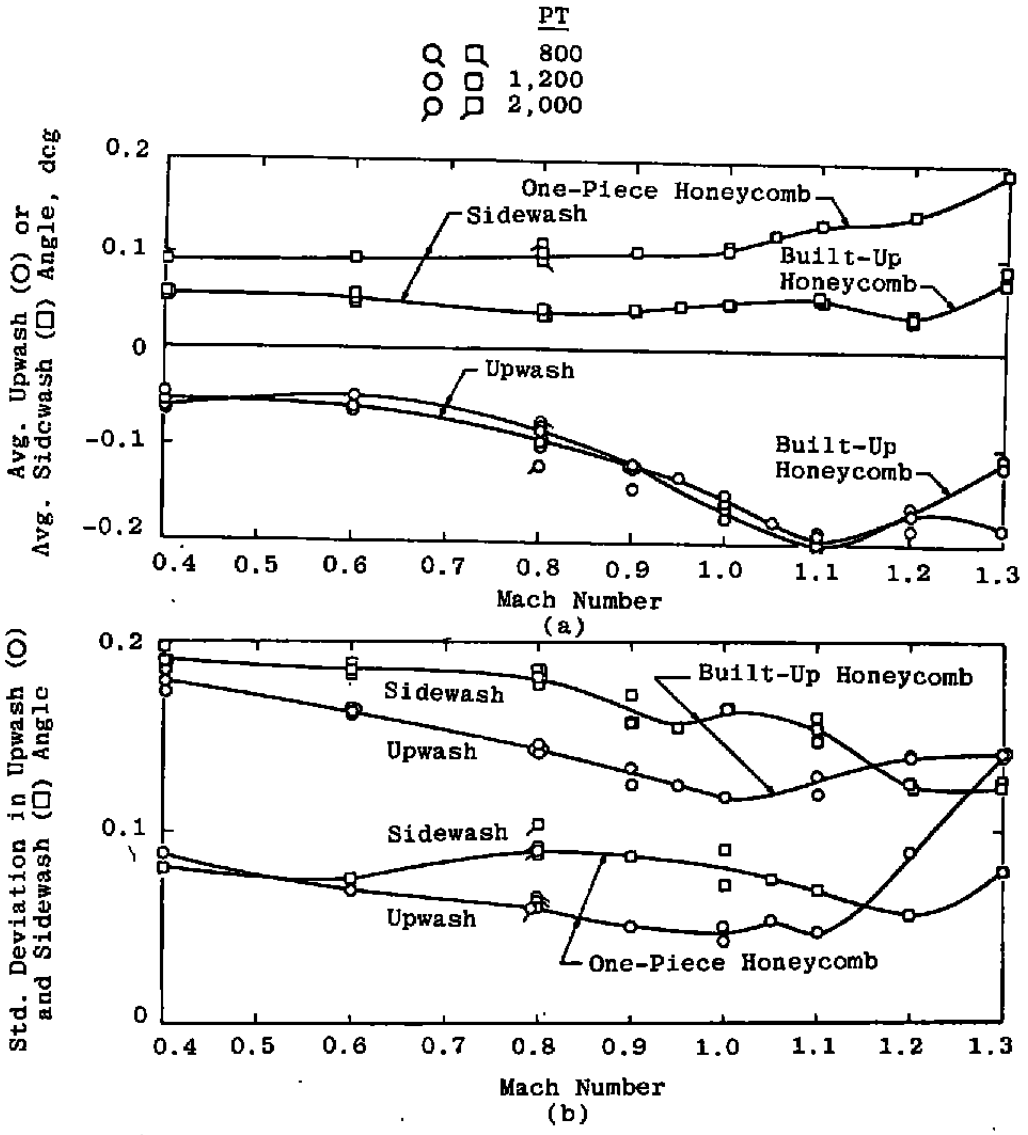

Figure 23. Averaged flow angles and standard deviations in flow angle versus Mach number for the two honeycomb configurations.

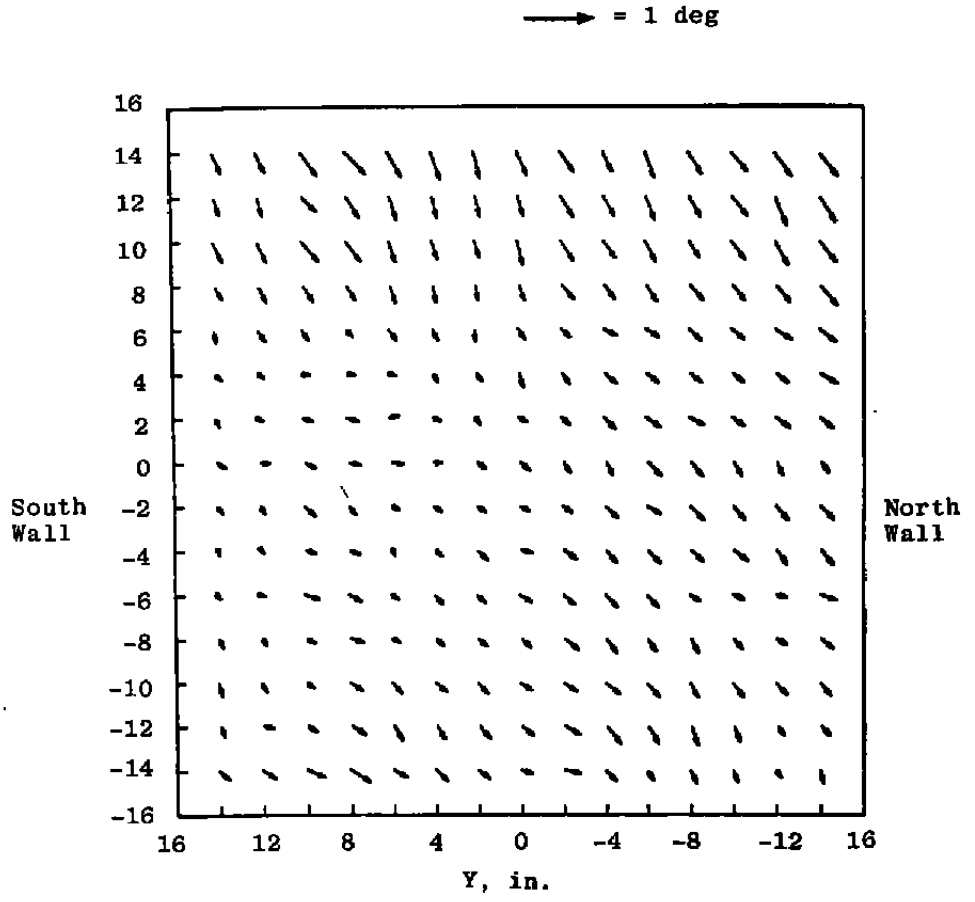

Figure 24. Flow angularity distribution at M = 1.20, PT = 1,200 psfa, τ = 5 percent (all ~~wheels~~), and X = 108 in.

WALLS

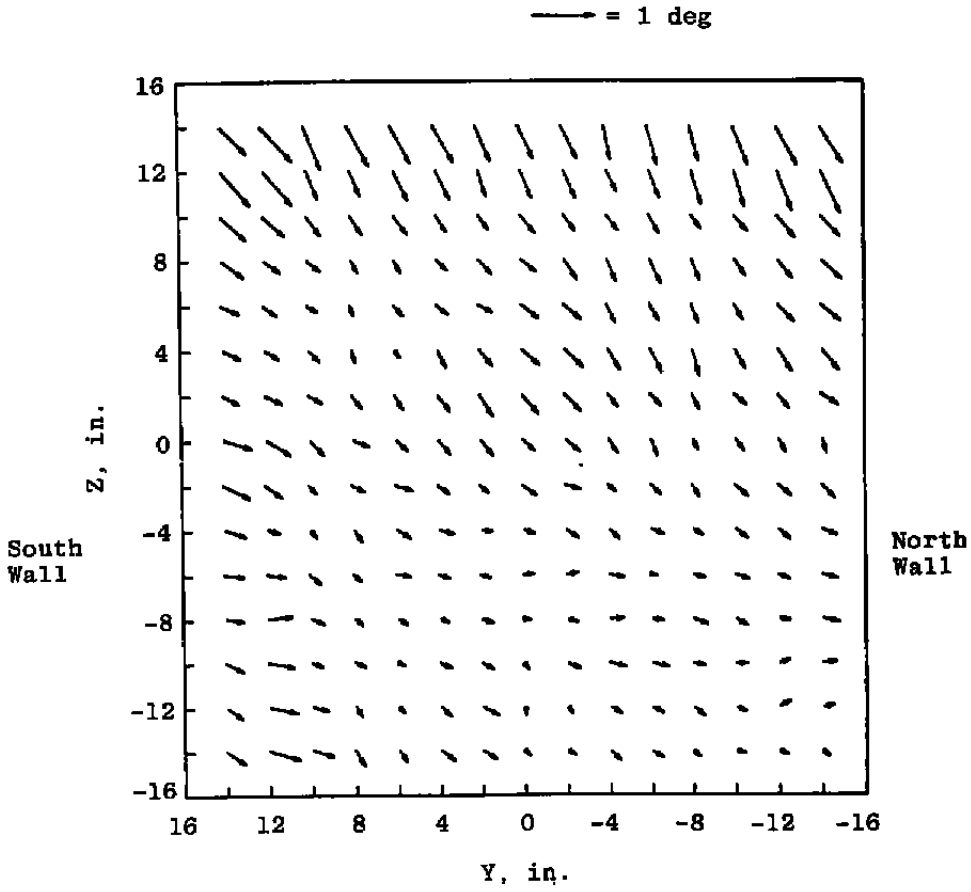

Figure 25. Flow angularity distributions at M = 1.30, PT = 1,200 psfa, τ = 6.2 percent (all walls), and X = 108 in.

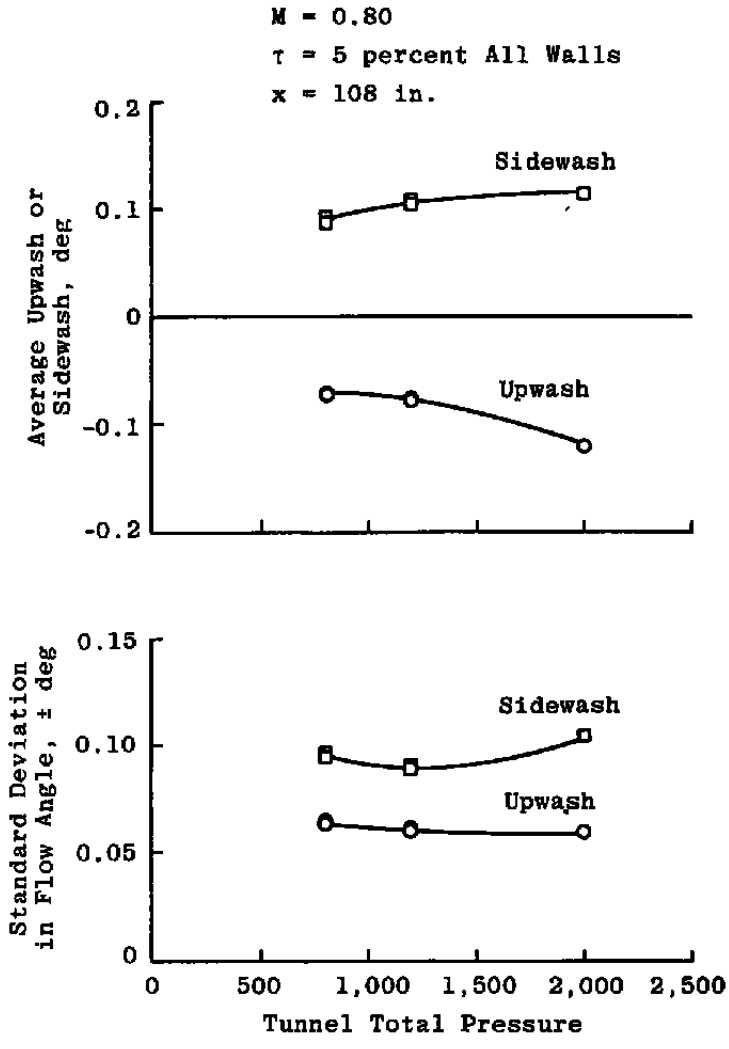

Figure 26. Variation of the flow angularity parameters with total pressure.

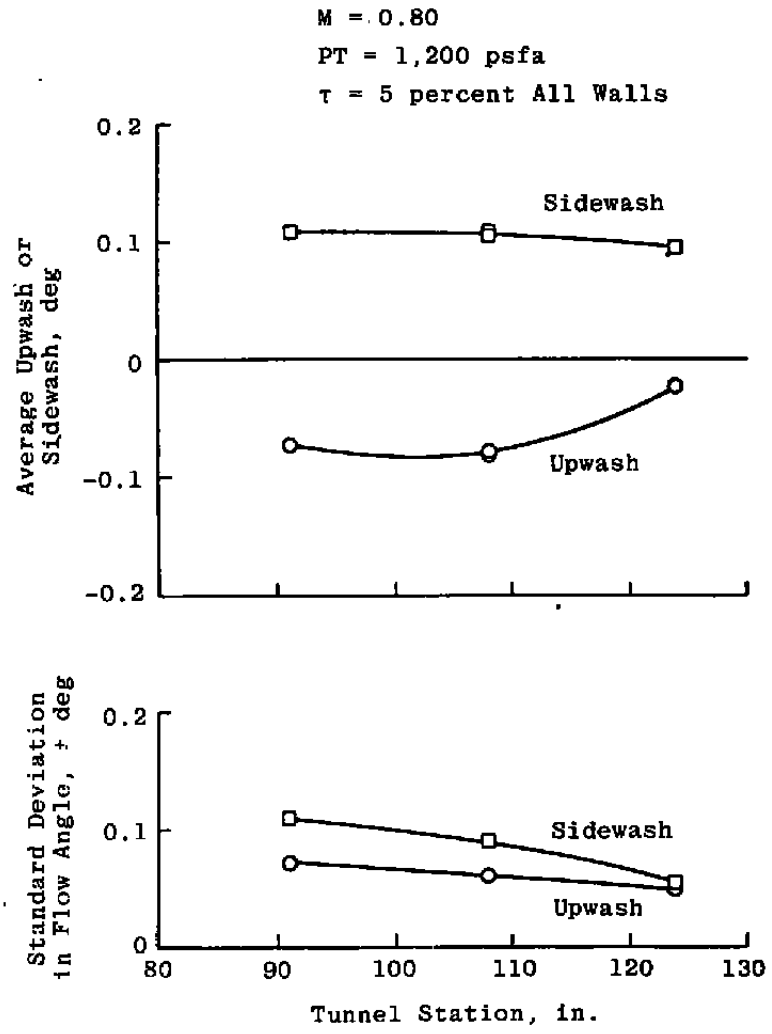

Figure 27. Variation of the flow angularity parameters with tunnel station.

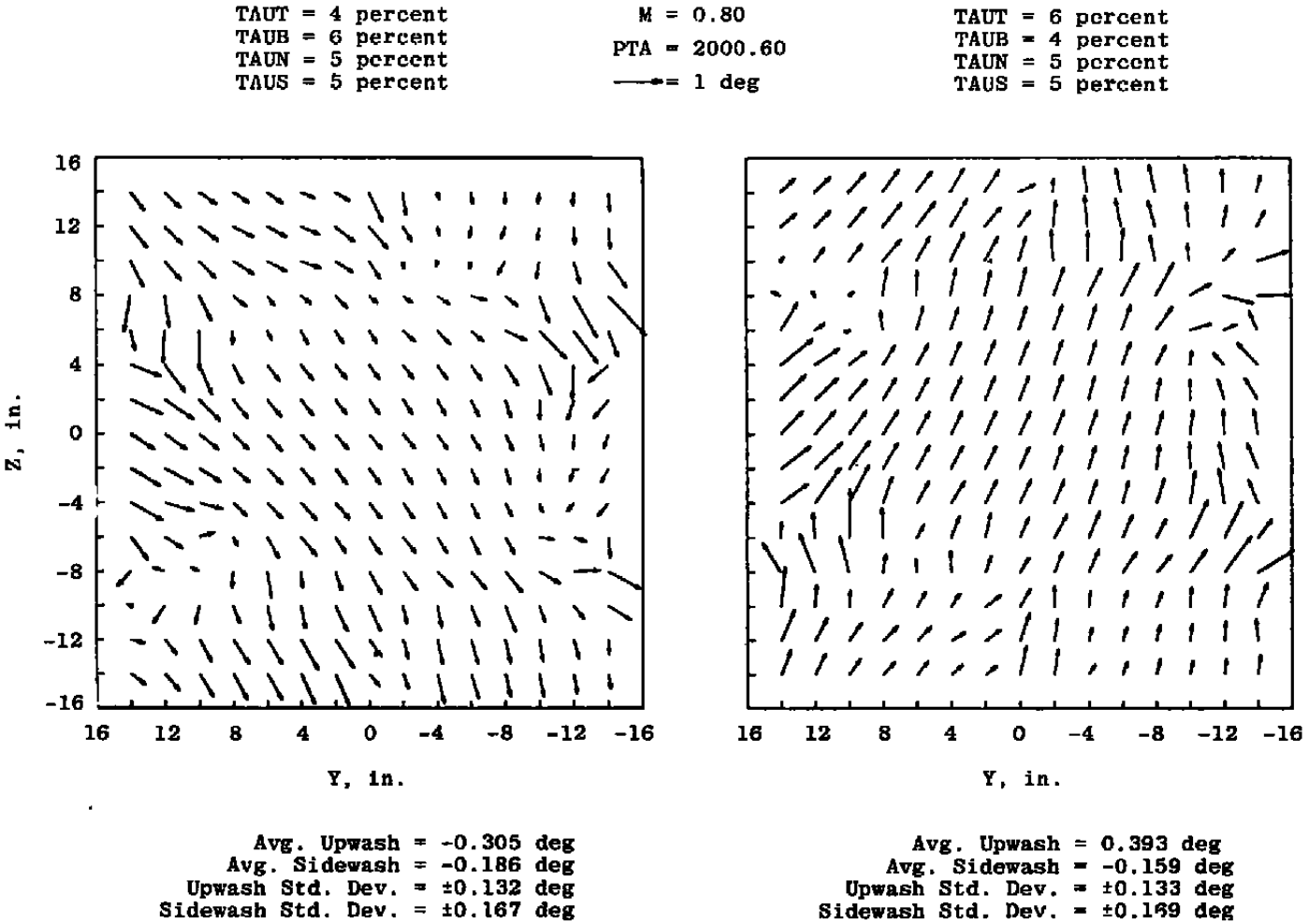

Figure 28. Effects of asymmetric top and bottom wall porosities.

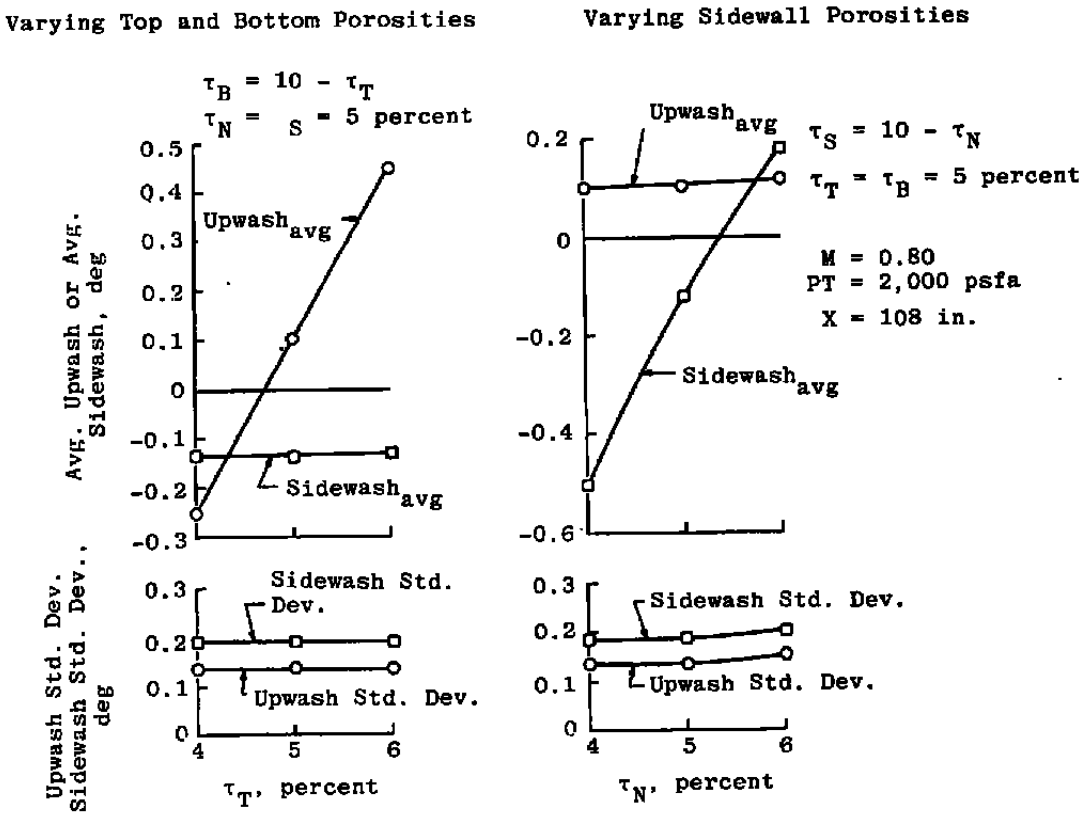

Figure 29. Effect of asymmetric porosities on the average flow angles and the standard deviations in flow angle.

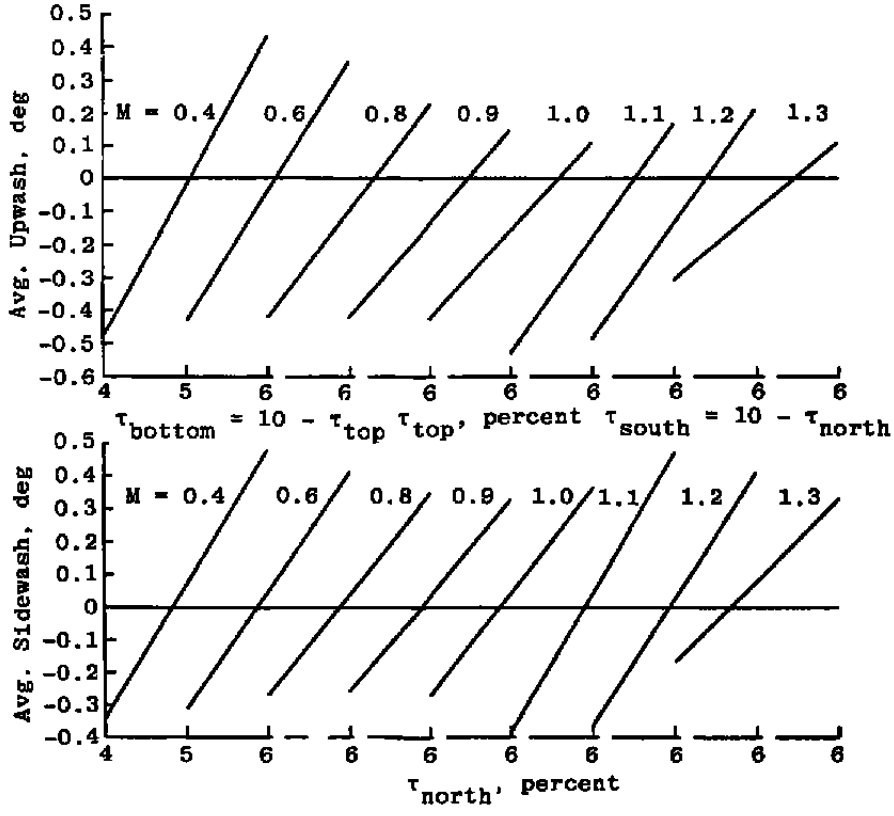

Figure 30. Effect of asymmetric porosity on the mean upwash and sidewash angles (Mach number as a parameter).

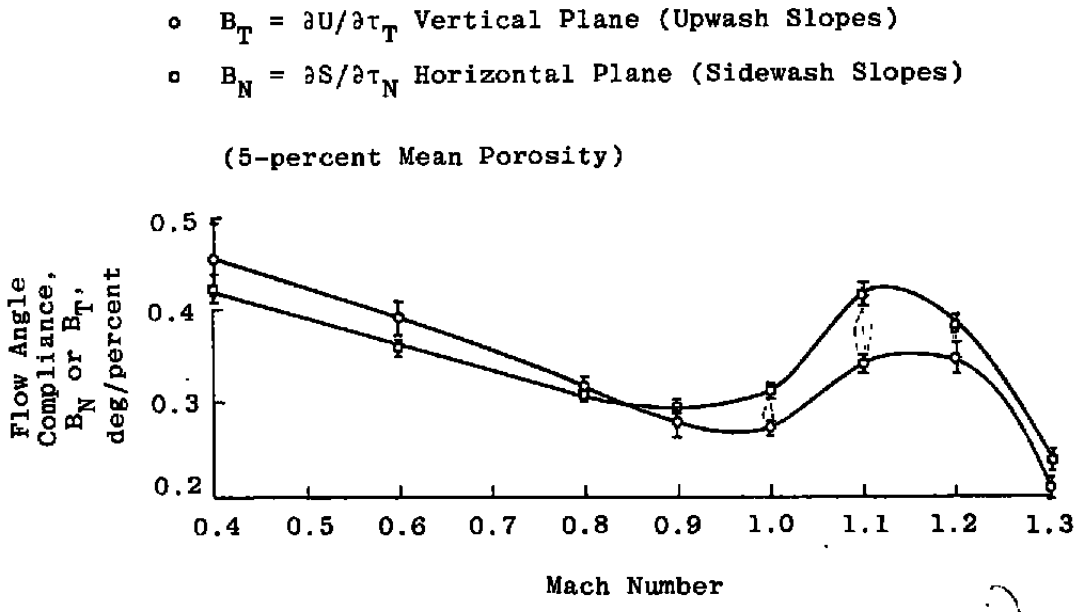

Figure 31. Flow angle compliance versus Mach number.

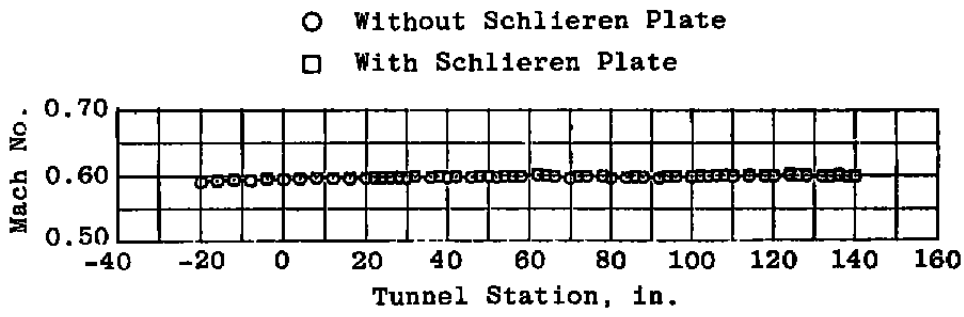

a. M = 0.60 (nom.), τ = 5 percent, PT = 1,200 psfa

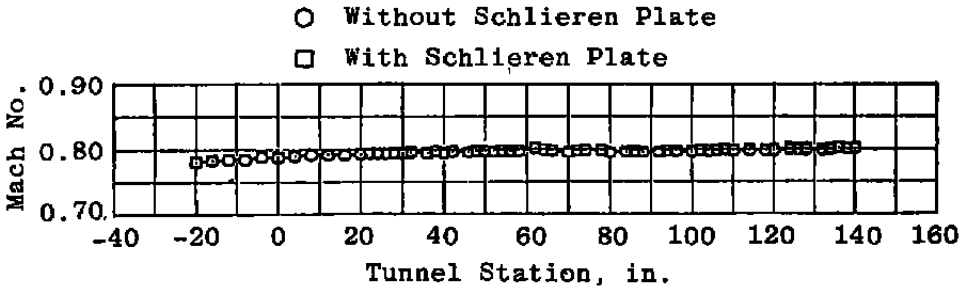

b. M = 0.80 (nom.), τ = 5 percent, PT = 1,200 psfa

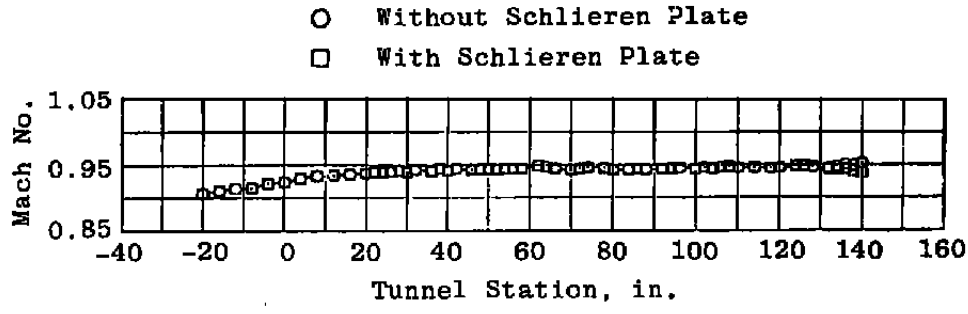

c. M = 0.95 (nom.), τ = 5 percent, PT = 1,200 psfa

Figure 32. Effect of the schlieren plate on the centerline Mach number distributions.

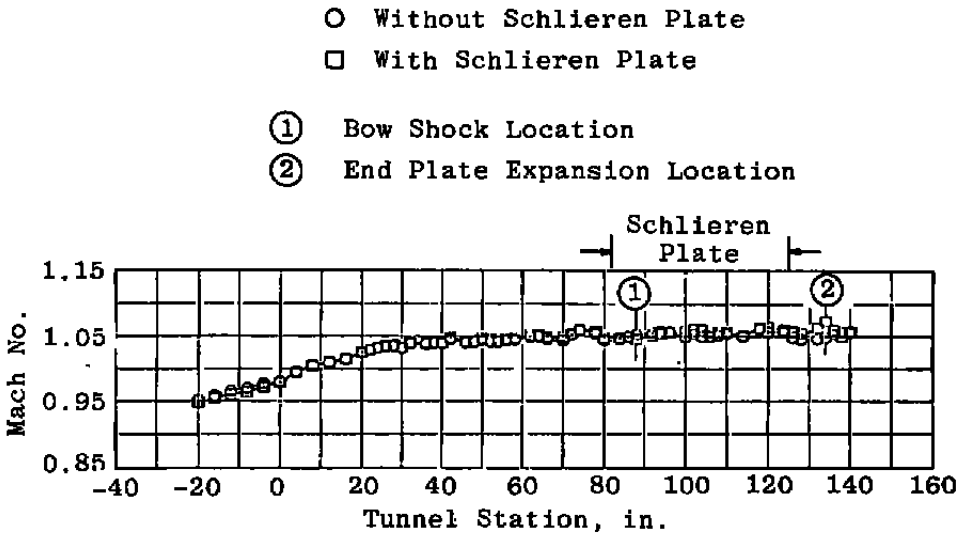

d. M = 1.05 (nom.), τ = 5 percent, PT = 1,200 psfa

Figure 32. Continued.

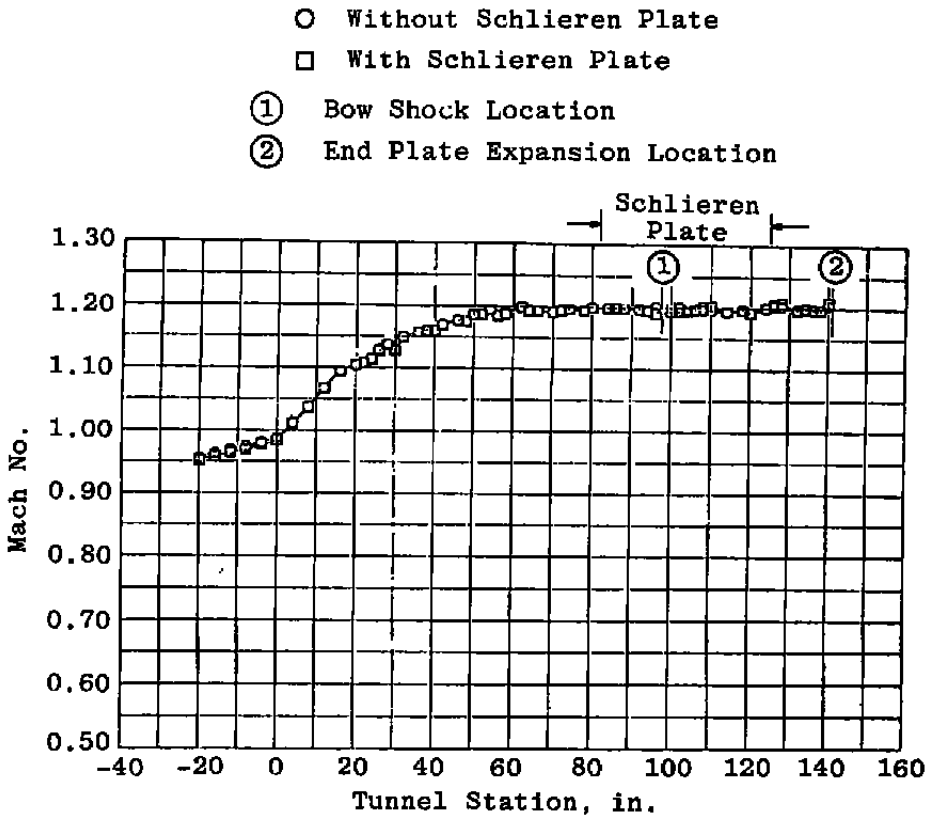

e. M = 1.20 (nom.), τ = 5 percent, PT = 1,200 psfa
Figure 32. Continued.

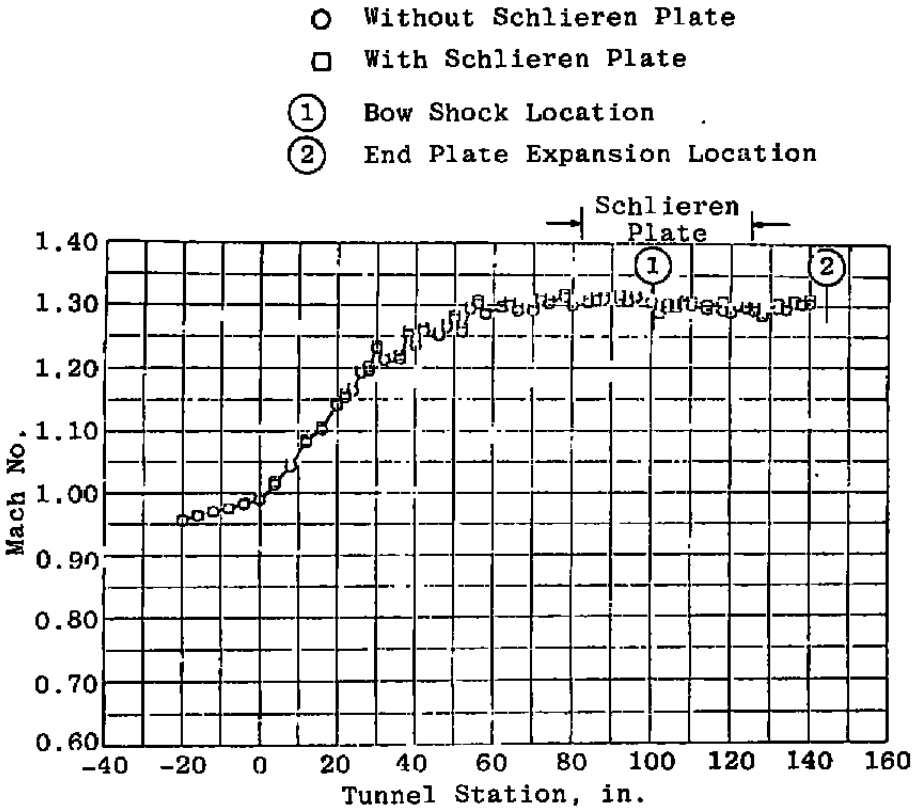

f. M = 1.30 (nom.), τ = 5 percent, PT = 1,200 psfa

Figure 32. Concluded.

Table 1. Centerline Pipe Orifice Locations

Orifice No.	Location	Orifice No.	Location
1	−20.0	35	72.0
2	−16.0	36	74.0
3	−12.0	37	76.0
4	−8.0	38	78.0
5	−4.0	39	80.0
6	0.0	40	84.0
7	4.0	41	86.0
8	8.0	42	88.0
9	12.0	43	90.0
10	16.0	44	92.0
11	20.0	45	94.0
12	22.0	46	96.0
13	24.0	47	100.0
14	26.0	48	102.0
15	28.0	49	104.0
16	30.0	50	106.0
17	32.0	51	108.0
18	36.0	52	110.0
19	38.0	53	112.0
20	40.0	54	114.0
21	42.0	55	116.0
22	44.0	56	118.0
23	46.0	57	120.0
24	48.0	58	122.0
25	50.0	59	124.0
26	52.0	60	126.0
27	54.0	61	128.0
28	56.0	62	130.0
29	58.0	63	132.0
30	60.0	64	134.0
31	62.0	65	136.0
32	64.0	66	138.0
33	66.0	67	140.0
34	70.0		

Table 2. Results of the Least-Squares Line Fits to the Centerline Mach Number Distributions

Mach No. (Avg.)	PT (Avg.), psf	t (Avg.), percent	ML × O (Avg.), Intercept	DML/DX, $in.^{-1}$ (Avg.), Slope	SIGMAM (Avg.), Std. Dev.
0.109	1999.6	4	0.10724	0.00000	0.00103
0.109	1999.1	5	0.10751	0.00000	0.00095
0.109	2001.6	6	0.10609	0.00002	0.00089
0.199	2002.9	4	0.19874	0.00000	0.00052
0.197	2001.8	5	0.19893	0.00000	0.00052
0.196	2001.3	6	0.19663	0.00001	0.00049
0.399	2001.8	4	0.40095	−0.00001	0.00049
0.396	2001.8	5	0.40033	−0.00001	0.00043
0.394	2001.1	6	0.39965	0.00002	0.00040
0.597	1203.2	4	0.59502	0.00003	0.00104
0.594	1201.9	5	0.59529	0.00003	0.00105
0.594	600.0	5	0.58254	0.00011	0.00302
0.593	901.4	5	0.58963	0.00005	0.00173
0.594	1599.8	5	0.59703	0.00001	0.00070
0.594	2001.0	5	0.59866	0.00000	0.00052
0.593	2003.4	5	0.59777	0.00001	0.00049
0.594	2399.7	5	0.59929	−0.00001	0.00049
0.594	2800.6	5	0.60206	−0.00003	0.00067
0.594	3100.9	5	0.60187	−0.00003	0.00063
0.591	1201.7	6	0.59324	0.00006	0.00097
0.697	1200.0	4	0.69352	0.00005	0.00101
0.693	1198.7	5	0.69409	0.00004	0.00101
0.688	1200.0	6	0.68949	0.00009	0.00121
0.796	1200.2	4	0.79041	0.00007	0.00117
0.791	1199.6	5	0.79249	0.00005	0.00118
0.792	601.0	5	0.78174	0.00013	0.00260
0.791	902.1	5	0.78745	0.00008	0.00163
0.791	1600.4	5	0.79325	0.00004	0.00092
0.791	2000.1	5	0.79536	0.00002	0.00078
0.791	2401.6	5	0.79626	0.00002	0.00083
0.791	2799.5	5	0.79691	0.00002	0.00082
0.787	1200.1	6	0.78879	0.00009	0.00128

Table 2. Continued

Mach No. (Avg.)	PT (Avg.), psf	t (Avg.), percent	ML × O (Avg.), Intercept	DML/DX, in.$^{-1}$ (Avg.), Slope	SIGMAM (Avg.), Std. Dev.
0.896	1199.9	4	0.88789	0.00009	0.00163
0.890	1199.6	5	0.88954	0.00007	0.00146
0.886	1201.5	6	0.88799	0.00009	0.00163
0.915	1200.1	1	0.88218	0.00022	0.00292
0.909	1200.6	2	0.88633	0.00015	0.00235
0.902	1199.8	3	0.88797	0.00011	0.00189
0.960	1200.0	2	0.93892	0.00013	0.00280
0.953	1199.7	3	0.93889	0.00010	0.00204
0.945	1199.6	4	0.93824	0.00008	0.00176
0.939	1199.6	5	0.93866	0.00007	0.00160
0.939	898.8	5	0.94384	0.00000	0.00201
0.940	1197.5	5	0.93589	0.00011	0.00249
0.940	1200.8	5	0.93580	0.00011	0.00244
0.939	1599.8	5	0.94979	−0.00003	0.00140
0.939	2000.5	5	0.94291	0.00004	0.00114
0.940	2401.8	5	0.95044	−0.00003	−0.00099
0.935	1199.6	6	0.93886	0.00008	0.00176
0.959	1199.8	6	0.96513	0.00007	0.00168
0.969	1200.2	1	0.93564	0.00020	0.00397
0.970	1199.3	4	0.96444	0.00007	0.00171
0.964	1200.4	5	0.96504	0.00006	0.00156
1.023	1200.9	1	1.00292	0.00002	0.00328
1.017	1200.7	1.5	1.00102	0.00003	0.00247
1.013	1200.1	2	0.99894	0.00004	0.00202
1.004	1198.6	3	0.99284	0.00005	0.00158
0.996	1201.5	4	0.99062	0.00005	0.00138
0.990	1197.9	5	0.99178	0.00004	0.00131
0.989	1200.2	5	0.99188	0.00004	0.00142
0.990	1201.4	5	0.99279	0.00004	0.00137
0.985	1199.3	6	0.99327	0.00005	0.00149
0.985	1202.5	6	0.99289	0.00005	0.00147
1.045	1200.2	1.5	1.03161	−0.00001	0.00494
1.021	1199.5	4	1.01707	0.00004	0.00204
1.013	1199.6	5	1.01584	0.00005	0.00171
1.009	1199.8	6	1.01622	0.00007	0.00170

Table 2. Concluded

Mach No. (Avg.)	PT (Avg.), psf	t (Avg.), percent	ML × O (Avg.), Intercept	DML/DX, $in.^{-1}$ (Avg.), Slope	SIGMAM (Avg.), Std. Dev.
1.079	1200.2	1	1.06275	−0.00005	0.00601
1.065	1199.9	2	1.05097	0.00003	0.00400
1.065	899.9	2	1.04997	0.00001	0.00430
1.067	1598.9	2	1.05411	0.00001	0.00430
1.067	1999.9	2	1.05528	−0.00001	0.00464
1.067	2398.0	2	1.05771	−0.00002	0.00441
1.053	1200.5	3	1.04391	0.00003	0.00342
1.046	1200.0	4	1.04205	0.00003	0.00296
1.038	1199.8	5	1.04196	0.00003	0.00254
1.033	1199.9	6	1.03899	0.00008	0.00233
1.120	1200.2	2	1.09814	0.00006	0.00491
1.115	1200.0	2.5	1.09619	0.00007	0.00430
1.106	1199.4	3	1.09268	0.00005	0.00357
1.097	1200.4	4	1.09150	0.00004	0.00287
1.089	1200.3	5	1.09165	0.00004	0.00234
1.082	1199.5	6	1.09083	0.00005	0.00260
1.201	1199.3	4	1.18783	0.00010	0.00353
1.201	1200.1	4	1.18813	0.00010	0.00355
1.191	898.5	4.76	1.18926	0.00006	0.00248
1.193	1202.0	4.75	1.19445	0.00004	0.00281
1.192	1598.8	4.76	1.19811	0.00002	0.00319
1.192	1999.6	4.76	1.19874	0.00001	0.00347
1.193	2401.0	4.77	1.20029	0.00000	0.00349
1.190	1200.0	5	1.19690	0.00002	0.00274
1.182	1200.9	6	1.19545	0.00003	0.00338
1.305	1199.0	4	1.23750	0.00047	0.00542
1.292	1203.3	5	1.25732	0.00035	0.00529
1.283	1201.8	6	1.32480	−0.00018	0.00594
1.182	1200.1	6.2	1.32597	−0.00021	0.00581
1.274	1202.2	7	1.32474	−0.00024	0.01322

Table 3. Results of the Least-Squares Fits of DM as a Function of MC and τ

$$DM = a_1M_c + a_2\tau + a_3M_c^2 + a_4M_c\tau + a_5\tau^2 + a_6M_c^3 + a_7M_c^2\tau + a_8M_c\tau^2 + a_9\tau^3 + a_{10}M_c^4 + a_{11}M_c^3\tau + a_{12}M_c^2\tau^2 + a_{13}M_c\tau^3 + a_{14}\tau^4 + a_{15}M_c^5 + a_{16}M_c^4\tau + a_{17}M_c^3\tau^2 + a_{18}M_c^2\tau^3 + a_{19}M_c\tau^4 + a_{20}\tau^5 + a_{21}$$

	For Mach Numbers up to 0.95	For Mach Numbers over 0.95
a_1	0.43656 − 01	0
a_2	−0.96929 − 01	0.2918929 + 01
a_3	0	0.2054313 + 02
a_4	0.96697 − 01	−0.9482121 + 01
a_5	0.58549 − 01	−0.2034162 + 00
a_6	−0.76084 − 01	−0.3517751 + 02
a_7	0	0.1019544 + 02
a_8	−0.68507 − 01	0.8374222 + 00
a_9	−0.11684 − 01	0.2179888 − 01
a_{10}	0	0.2155684 + 02
a_{11}	0.29182 − 01	−0.3619460 + 01
a_{12}	0	−0.1069151 + 01
a_{13}	0.14349 − 01	0.4446489 − 01
a_{14}	0.76421 − 03	0
a_{15}	0	−0.4382189 + 01
a_{16}	−0.53873 − 02	0
a_{17}	0	0.4316988 + 00
a_{18}	−0.52757 − 03	−0.2213520 − 01
a_{19}	−0.91871 − 03	0
a_{20}	0	−0.3555843 − 05
a_{21}	0.35020 − 06	−0.2566878 + 01
Standard Error of Estimate	±0.78934 − 03	±0.86297 − 03

Note: 0.55555 − 03 = .00055555

Table 4. Flow Angularity Results over 28- by 28-in. Cross Sections

	Mach No.	PT, psfa	Average Upwash, deg	Average Sidewash, deg	Upwash Std. Dev., deg	Sidewash Std. Dev., deg	Wall Porosity, percent, τ	Comments
Mach No. Effects	0.40	1,200	−0.063	0.093	0.088	0.081	5 All	
	0.60	↓	−0.048	0.096	0.069	0.075	↓	
	0.80		−0.080	0.105	0.061	0.090		
	0.80		−0.077	0.108	0.060	0.088		Repeat Run
	0.90		−0.120	0.105	0.048	0.087		
	0.95		−0.164	0.112	0.049	0.071		
	1.00		−0.174	0.108	0.042	0.091		
	1.05		−0.177	0.126	0.052	0.074		
	1.10		−0.200	0.138	0.046	0.068		
	1.20		−0.171	0.149	0.089	0.055		
	1.30		−0.184	0.194	0.141	0.078		
Total Pressure Effects	0.80	800	−0.076	0.095	0.063	0.092	5 All	
	0.80	800	−0.074	0.088	0.064	0.090	↓	
	0.80	1,200	−0.080	0.105	0.061	0.090		
	0.80	1,200	−0.077	0.108	0.060	0.088		
	0.80	2,000	−0.121	0.115	0.059	0.104		
Asymmetric Porosity Effects	0.80	1,200	+0.208	+0.377	0.058	0.105		$\tau_T = \tau_n = 6\%$; $\tau_B = \tau_s = 4\%$
	0.80	↓	−0.080	0.105	0.061	0.090	τ = 5 All	
	0.80		−0.077	0.108	0.060	0.088	τ = 5 All	
	0.80		−0.381	−0.198	0.076	0.073		$\tau_T = \tau_N = 4\%$; $\tau_B = \tau_s = 6\%$
Tunnel Station Effects	0.80	1,200	−0.071	0.108	0.072	0.112	5 All	XSTA = 91
	0.80	↓	−0.080	0.105	0.061	0.090	↓	XSTA = 108
	0.80		−0.077	0.108	0.060	0.088		XSTA = 108
	0.80		−0.020	0.097	0.049	0.055		XSTA = 124

Table 5. Summary of the Least-Squares Line Fits of Average Flow Angles as a Function of Asymmetric wall Porosities

Avg. Upwash = $U = A_T + B_T T_T$

Avg. Sidewash = $S = A_N + B_N T_N$

(Mean Porosity = 5 percent)

$$T_{T0} = -\frac{A_T}{B_T}$$

$$\tau_{N_o} = -\frac{A_N}{B_N}$$

Mach No.	Compliance		Porosity for Zero Flow Angle		Residuals of the Fits	
	Upwash Slopes $B_T = (\partial U/\partial \tau_T)$	Sidewash Slopes $B_N = (\partial S/\partial \tau_N)$	Upwash Zero τ_{T_o}(%)	Sidewash Zero τ_{N_o}(%)	Upwash RMS (deg)	Sidewash RMS (deg)
0.4	0.4557	0.4240	5.065	4.850	±0.0383	±0.0158
0.6	0.3925	0.3625	5.116	4.861	±0.0186	±0.0045
0.8	0.3185	0.3090	5.292	4.866	±0.0044	±0.0053
0.9	0.2798	0.2955	5.501	4.863	±0.0167	±0.0065
1.0	0.2732	0.3140	5.567	4.839	±0.0087	±0.0084
1.1	0.3432	0.4190	5.564	4.854	±0.0104	±0.0129
1.2	0.3495	0.3865	5.450	4.921	±0.0172	±0.0091
1.3	0.2058	0.2422	5.515	4.671	±0.0060	±0.0110

Note: The bottom wall porosity for zero upwash angle is 10-t_{to}. The south wall porosity for zero sidewash angle is 10-t_{No}

APPENDIX A
SIGN CONVENTION FOR TUNNEL 4T FLOW ANGULARITY MEASUREMENTS

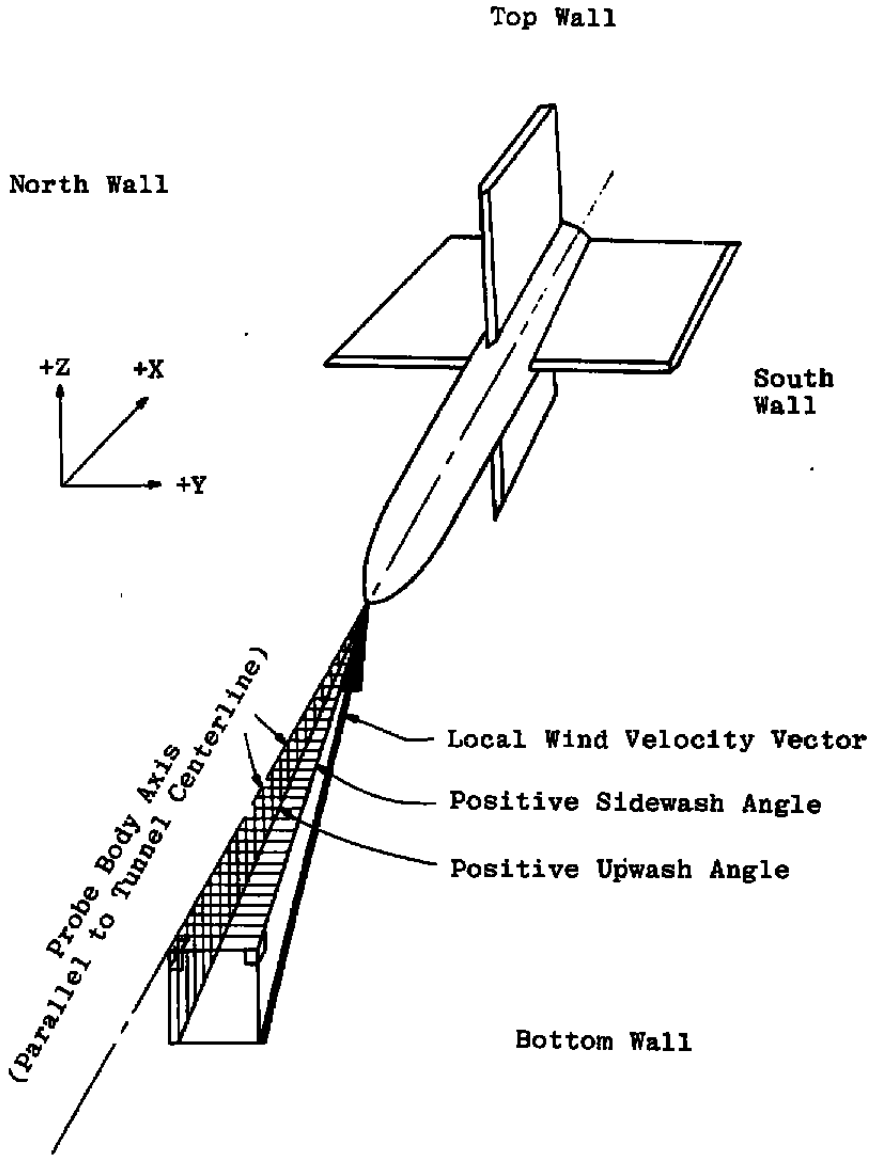

APPENDIX B
TUNNEL 4T TEST SECTION WALL POROSITY SCHEDULES

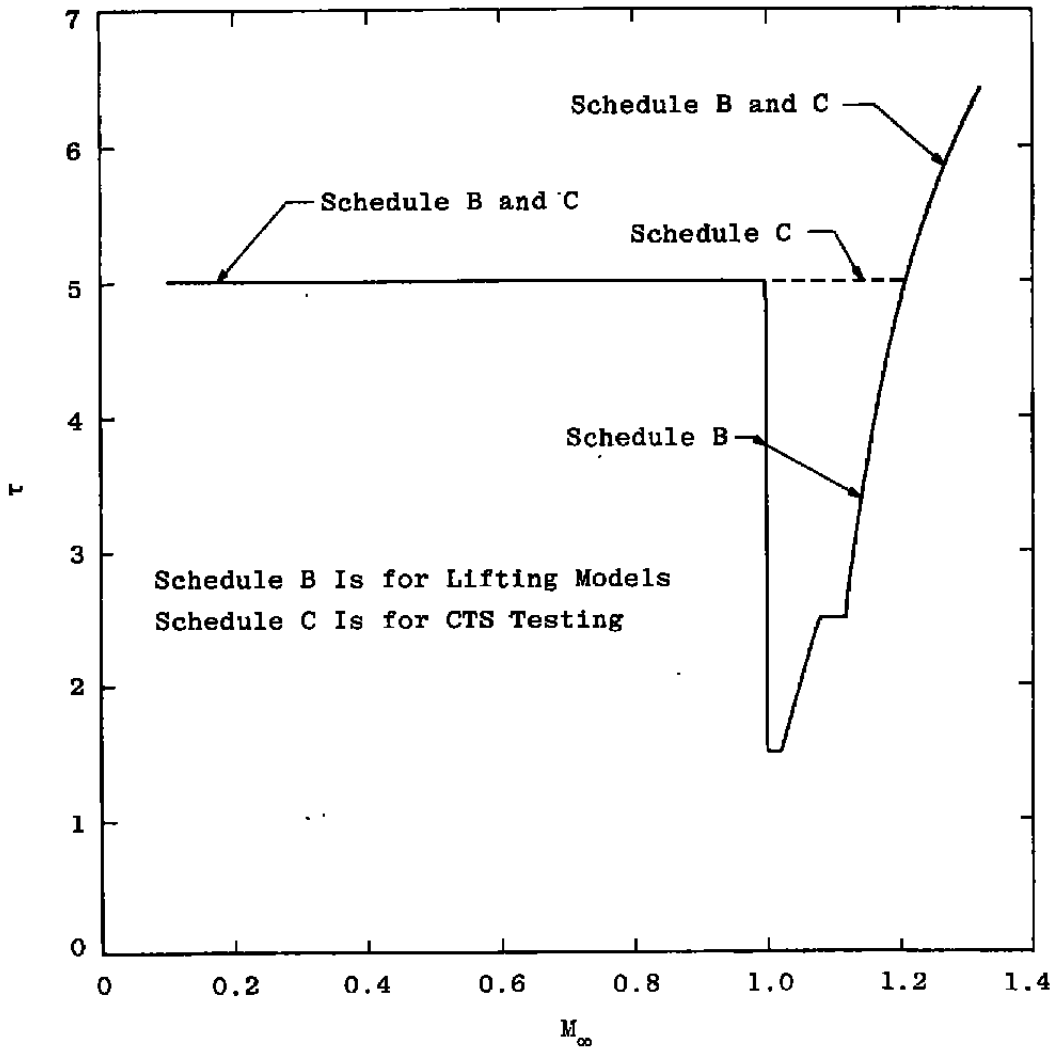

APPENDIX C
METHOD FOR CALIBRATING THE FLOW ANGULARITY PROBE

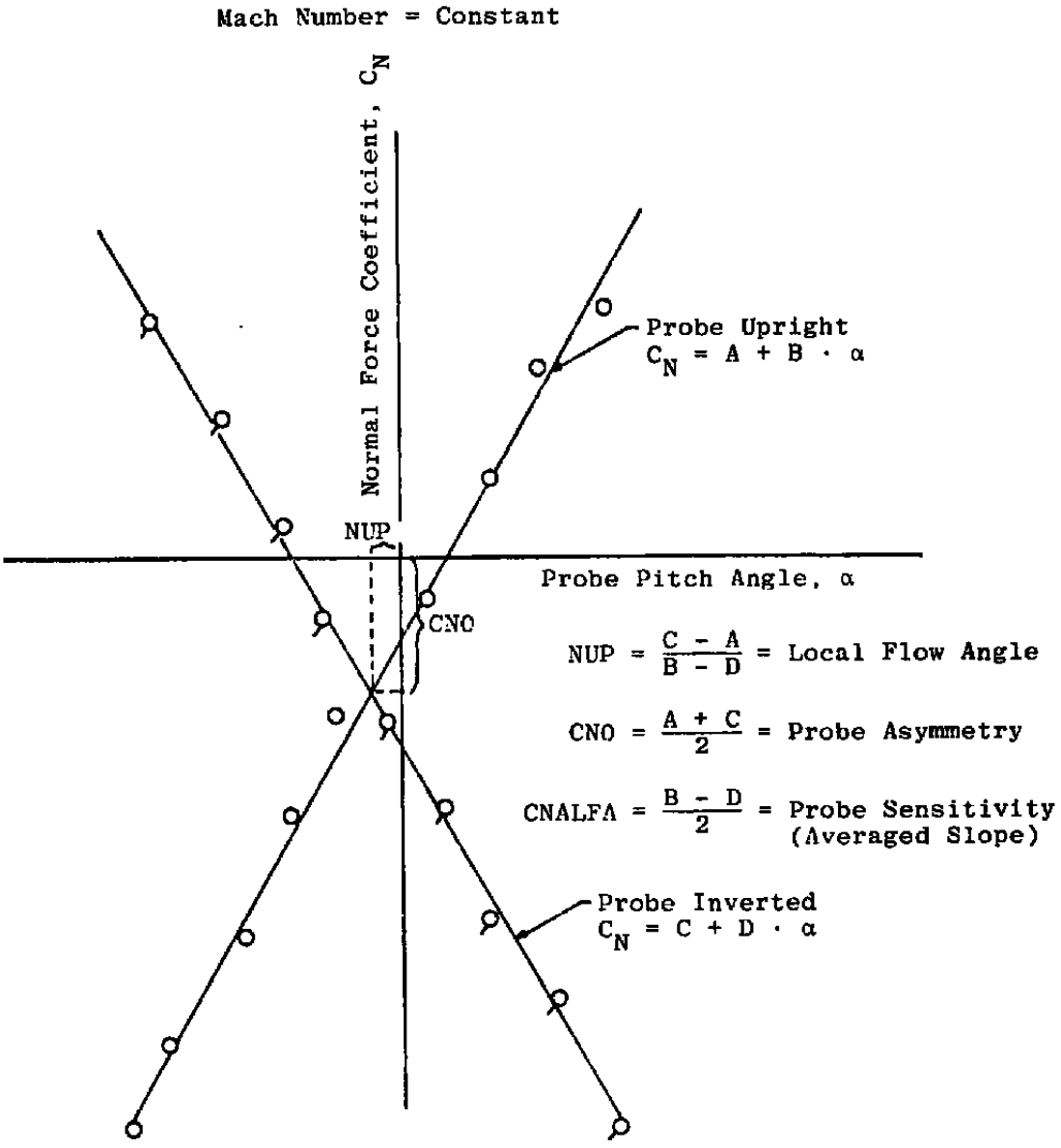

NOMENCLATURE

$B_{N,T}$	Flow angle compliance, change in sidewash (upwash) angle with north (top) wall porosity
C_N	Normal-force coefficient
CNALFA	Normal-force coefficient slope (dCN/dα), deg^{-1}
CNO	Normal-force coefficient intercept at $\alpha_i = 0$ deg
CY	Side force coefficient
CYBETA	Side force coefficient slope (dCY/dβ), deg^{-1}
CYO	Side force coefficient intercept at $\beta = 0$ deg
DM	Tunnel calibration parameter, MA - MC
DML/DX	Mach number gradient, in.$^{-1}$
MA	Averaged calibration pipe Mach number over test section length
MC	Plenum chamber Mach number (Fictitious) see Section 3.4.1
MBX,ML	Local Mach number
MLXO	Least-squares line fit intercept
NUP	Local upwash angle determined from calibration of the pitch section of the flow angularity probe, deg
NUY	Local upwash angle determined from calibration of the yaw section of the flow angularity probe, deg
PC	Plenum chamber pressure, psfa
PE	Diffuser exit static pressure, psfa
PLX	Local pressure on calibration pipe, psfa
PT	Tunnel total pressure, psfa
P	Averaged calibration pipe pressure over test section, psfa
S	Average sidewash angle, deg
SIGMAM	Standard deviation in centerline Mach number (Spatial)

TAU-T,B,N,S	Porosity of the top, bottom, north, and south test section walls, respectively, percent
U	Average upwash angle, deg
UMC	Uncertainty in plenum Mach number
UMAV	Uncertainty in average centerline Mach number
UDM	Uncertainty in calibration parameter, DM
X	Tunnel axial station, in.
Y	Lateral distance from tunnel centerline, in.
Z	Vertical distance from tunnel centerline
α_l	Flow angle probe indicated angle of attack
β_l	Flow angle probe indicated angle of yaw
τ	Tunnel wall porosity, percent (average of 4 walls)